PHASE DIAGRAMS OF THE TITANIUM-ALUMINUM, TITANIUM-CHROMIUM-IRON, AND TITANIUM-OXYGEN ALLOY SYSTEMS

R. J. VAN THYNE
E. S. BUMPS
H. D. KESSLER
M. HANSEN

ARMOUR RESEARCH FOUNDATION
ILLINOIS INSTITUTE OF TECHNOLOGY

DECEMBER 1952

WRIGHT AIR DEVELOPMENT CENTER

NOTICES

When Government drawings, specifications, or other data are used for any purpose other than in connection with a definitely related Government procurement operation, the United States Government thereby incurs no responsibility nor any obligation whatsoever; and the fact that the Government may have formulated, furnished, or in any way supplied the said drawings, specifications, or other data, is not to be regarded by implication or otherwise as in any manner licensing the holder or any other person or corporation, or conveying any rights or permission to manufacture, use, or sell any patented invention that may in any way be related thereto.

The information furnished herewith is made available for study upon the understanding that the Government's proprietary interests in and relating thereto shall not be impaired. It is desired that the Judge Advocate (WCJ), Wright Air Development Center, Wright-Patterson Air Force Base, Ohio, be promptly notified of any apparent conflict between the Government's proprietary interests and those of others.

PHASE DIAGRAMS OF THE TITANIUM-ALUMINUM, TITANIUM-CHROMIUM-IRON, AND TITANIUM-OXYGEN ALLOY SYSTEMS

R. J. Van Thyne
E. S. Bumps
H. D. Kessler
M. Hansen

Armour Research Foundation
Illinois Institute of Technology

December 1952

Wright Air Development Center
Air Research and Development Command
United States Air Force
Wright-Patterson Air Force Base, Ohio

The binary equilibrium diagrams of titanium and its alloying elements can be considered as an absolute prerequisite for the understanding of the behavior of all titanium base alloys.

In the course of the alloy development work, which the Materials Laboratory has been sponsoring for several years at Battelle Memorial Institute, the first preliminary knowledge of the phase relationships at the titanium-rich end of various alloy systems was obtained. This investigation has also furnished a broader knowledge of the applicability of the different alloying elements to the production of practical titanium alloys.

In view of the aforementioned necessity for a knowledge of the binary equilibrium diagrams, and the paucity of information on this subject in the literature, it was decided to start a broader research project on binary diagrams of titanium and the most promising alloying elements. Investigation was started on ten alloy systems, the work being divided among five research institutions. More recently, additional binary and ternary systems were included in this program.

After the first year of research, a summary report was prepared by each contractor and these reports are being published as Air Force Technical Reports. The following list gives a compilation of the contractors, systems investigated, and technical report numbers concerned. Since, in some cases, the investigations are not yet finished, the reports concerned are designated as Part 1. Part 2 will follow as soon as the investigations are completed, and will disclose the final shape of the equilibrium diagrams.

Contractor	Systems Investigated	Report No.
Armour Research Foundation	Ti-Si, Ti-Cb, Ti-Mo	AFTR 6225
	Ti-O, Ti-Al, Ti-Fe-Cr	WADC TR 52-16
Battelle Memorial Institute	Ti-Mn, Ti-Ta, Ti-W	AFTR 6516 Pt 1
Massachusetts Institute of Technology	Ti-Cr, Ti-Cu	AFTR 6595 Pt 1
		AFTR 6595 Pt 2
	Ti-Cr-O	WADC TR 52-255
New York University	Ti-Ni	AFTR 6569 Pt 1
		AFTR 6569 Pt 2
University of Notre Dame	Ti-Fe	AFTR 6597 Pt 1
		AFTR 6597 Pt 2

This report was prepared by the Armour Research Foundation, Chicago, Illinois, under USAF Contract No. AF 33(038)-8708. The contract was initiated under Research and Development Order No. 615-11, "Titanium Metal and Alloys" and was administered under the direction of the Materials Laboratory, Directorate of Research, Wright Air Development Center, with Lt W. R. Freeman, Jr., acting as project engineer.
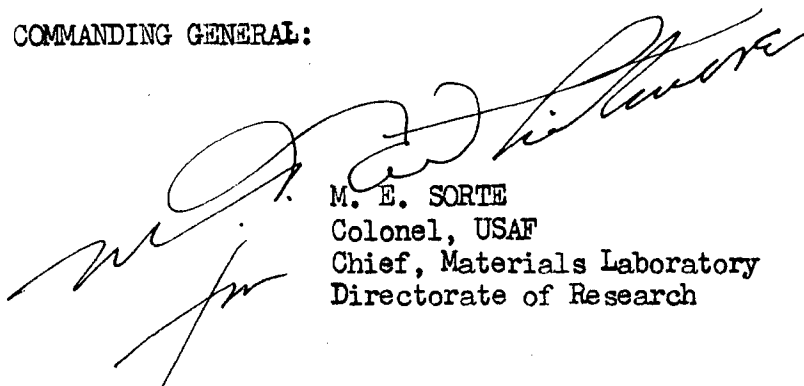
ABSTRACT

Partial phase diagrams are presented for the systems titanium-aluminum, titanium-chromium, titanium-iron, titanium-chromium-iron, and titanium-oxygen. All studies are completed except for the titanium-chromium-iron system, which requires further confirmatory work in certain areas. The results are outlined in Section IV of this report (page 78).

PUBLICATION REVIEW

This report has been reviewed and is approved.

FOR THE COMMANDING GENERAL:

M. E. SORTE
Colonel, USAF
Chief, Materials Laboratory
Directorate of Research

WADC TR 52-16

TABLE OF CONTENTS

LIST OF ILLUSTRATIONS

LIST OF TABLES

PHASE DIAGRAMS OF THE TITANIUM-ALUMINUM,

TITANIUM-CHROMIUM-IRON, AND TITANIUM-OXYGEN ALLOY SYSTEMS

I.   INTRODUCTION

This is a Summary Report of the second year's work on the extension
of Contract No. AF 33(038)-8708. The object of the extension was the
determination of phase diagrams of the systems titanium-aluminum, titanium-
chromium-iron, and titanium-oxygen.

Micrographic analysis of annealed arc melted alloys was the principal
method used for the determination of the subject systems. Thermal analy-
sis, incipient melting studies, and X-ray diffraction analysis were also
used to obtain data on certain portions of the systems.

II.   EXPERIMENTAL PROCEDURE

The alloys were prepared by arc melting on a copper block in a helium
atmosphere, using a water-cooled tungsten electrode. As this method was
detailed in the Final Report of last year's work*, no further description
need be given here. Where somewhat special techniques were used, they
are presented in the section of this report where they apply.

Sample preparation methods, annealing procedures, incipient melting
and thermal analysis techniques, metallographic procedures, and X-ray
diffraction methods were essentially identical to those used in last
year's studies. Therefore, the reader is referred to the previous report
for the procedural details. Variations in the techniques were required
in some cases; these changes are presented in the appropriate sections
of this report.

A.   Materials

Iodide titanium obtained from the New Jersey Zinc Company through
Wright Air Development Center was used for the preparation of most of the
alloys. This metal had a purity of 99.9+% with minor quantities of Fe,
Al, Mn, Mg, Si, O, and N.

A special lot of high purity magnesium reduced sponge titanium was
used to prepare a limited number of alloys for the titanium-chromium and
titanium-iron binary studies. This material had an as-cast hardness of
105 DPN and the analysis was as follows:

---

*Air Force Technical Report No. 6225

Iron	0.02%
Magnesium	0.045
Silicon	0.005
Nickel	0.003
Chlorine	0.06

The aluminum was obtained from the Aluminum Company of America in the form of sheet. The given analysis was:

Silicon	0.0006%
Iron	0.0005
Copper	0.0022
Magnesium	0.0003
Calcium	<0.0006
Sodium	<0.0005
Aluminum	99.99

Vacuum melted iron and chromium were purchased from the National Research Corporation. The impurities in the iron were:

Silicon	0.0093%
Nickel	0.012
Phosphorus	0.0023
Sulfur	0.013
Carbon	0.011

Two heats of chromium were used for these studies; Heat No. 591 for the titanium-chromium system, and No. 590 for the titanium-chromium-iron system:

Impurity	Heat No. 591	Heat No. 590
Carbon	0.102%	0.015%
Oxygen	0.019	0.066
Nitrogen	0.0017	0.0022

High purity titanium dioxide purchased from the National Lead Company was used in the preparation of the arc melted titanium-oxygen alloys. The spectrographic analysis of this material is as follows:

SiO_2	0.07%	Pb	<0.002%
Fe_2O_3	0.002	Mn	<0.00005
Al_2O_3	<0.001	W	<0.01
Sb_2O_3	<0.002	V	<0.002
SnO_3	<0.001	Cr	<0.002
Mg	0.001	Ni	<0.001
Nb	<0.01	Mo	<0.002
Cu	0.0004		

B. Analytical Methods

As weight losses during melting were of minor proportions for all systems studied, nominal compositions were used in plotting the data. To further substantiate the use of nominal values, chemical analysis was applied to a limited number of representative alloys in each system. The analytical methods used for the titanium alloys are summarized below:

1. Aluminum

Dissolve appropriate sample in 1-3 H_2SO_4;

Dilute so that H_2SO_4 concentration is 5-10%;

Separate Ti with cupferron (chloroform extraction);

Evaporate aqueous material;

Dilute, precipitate $Al(OH)_3$ with NH_4OH, use methyl orange indicator, filter, ignite and weigh Al_2O_3.

2. Iron

Dissolve appropriate sample in 1-3 H_2SO_4;

Dilute to 150 ml, add 5 gm tartaric acid;

Add excess ammonia and some $(NH_4)_2S_X$;

Heat to coagulate FeS;

Filter off FeS and wash well with hot water;

Return filter to original beaker;

Dissolve in $HNO_3 \cdot H_2SO_4$, remove all NO_3 by fuming, dilute to 150 ml;

Reduce by usual procedures ($ZnCl_2$, $PbCl_2$, $SnCl_2$);

Titrate iron with standard $K_2Cr_2O_7$ or $KMnO_4$.

3. Chromium

Dissolve sample in 1-3 H_2SO_4;

Dilute to 200 ml, heat to boiling;

Add $AgNO_3$ and oxidize chromium with $(NH_4)_2S_2O_8$;

Precipitate $AgNO_3$ with dilute HCl, boil to coagulate;

Cool and add excess of standard ferrous ammonia sulfate;

Titrate with standard $K_2Cr_2O_7$ or $KMnO_4$.

(This method is essentially the same as is used in all ferrous laboratories.)

4. Oxygen

The liquid amalgam reduction method developed by the National Lead Company was used. It is briefly as follows:

Dissolve sample in $H_2SO_4-(NH_4)_2SO_4$;

Dilute to 150 ml, cool, and transfer to separating funnel;

~ Add liquid zinc-amalgam;

After 5 min of shaking, add 5 ml CCl_4, draw off amalgam;

Titrate with standard $KMnO_4$ to faint pink.

III. RESULTS AND DISCUSSION

A. The Titanium-Aluminum System

Included in the available information concerning the phase relationships in titanium-rich titanium-aluminum alloys is a brief statement by Brown (1) that "aluminum raises the transformation temperature to 1000°C (1832°F)". This observation is interesting in that it is the first example of a metallic alloying component raising the transformation temperature of titanium, and consequently widening the field of the alpha solid solution. Busch and Freyer (2) presented resistivity data which indicated the formation of titanium-rich solid solutions of 1 and 3% aluminum alloys prepared by powder metallurgy methods.

Duwez (3) found only one other intermediate phase besides the known compound $TiAl_3$ (62.7% Al). This phase, designated as gamma, is of variable composition; its crystal structure is of the AuCu type and is therefore based on the composition TiAl (36.02% Al).

Earlier work on the constitution of the aluminum-rich alloys has been reviewed by Hansen (4), and need not be discussed here. The tetragonal crystal lattice of $TiAl_3$, as found by Fink, Van Horn and Budge (5), was confirmed by Brauer (6). Recently, Schubert (7) has reported that $TiAl_3$ is homogeneous within a limited composition range; however, the solubility limits were not given.

The titanium-aluminum phase diagram as presented in this report was determined by micrographic analysis of alloys containing from 1 to 62% aluminum, annealed at and quenched from temperatures between 700° and 1400°C. The phases and phase ranges investigated extend to the compound $TiAl_3$ (62.7% Al) to join the aluminum-rich end of the system determined by other investigators, thus completing the diagram.

1. Experimental procedure

All ingots were carefully weighed after arc melting, to detect possible losses. Comparison of weight before and after melting showed no appreciable weight changes. Also, chemical analyses were in close agreement with nominal compositions (Table I). The diagram as presented is,

therefore, based on nominal compositions. Alloys were prepared having the following nominal aluminum contents: 1 . . . 36 (1% increments), 38, 40, 41, 42.5, 44, 45, 46, 47.5, 49 . . . 64 (1% increments), 67, 70, 80, and 90.

TABLE I

NOMINAL COMPOSITIONS VS CHEMICAL ANALYSIS
FOR TYPICAL TITANIUM-ALUMINUM ALLOYS

Nominal Composition, % Al	Chemical Analysis, % Al
16.0	15.84
27.3	27.08
36.0	35.89
45.0	44.96
53.0	53.16
62.7	62.97

Ingots with up to 14% aluminum were cold pressed various amounts in order to increase the rate of attaining equilibrium structures on heat treatment. The amount of cold deformation that could be applied decreased with increasing aluminum content until alloys containing 12% or more aluminum cracked after only a few per cent deformation.

Samples annealed at temperatures of 700°-1000°C were sealed in evacuated Vycor bulbs. From 1000° to 1200°C, the samples were treated in sealed quartz capsules under a partial pressure of argon. Above 1200°C, an additional precaution was taken to prevent contamination of the samples by wrapping them in molybdenum sheet, to avoid contact between specimens and the quartz capsules in which they were sealed under partial pressure of argon. The annealing times at the various temperatures are presented in Table II.

TABLE II

ANNEALING CONDITIONS FOR TITANIUM-ALUMINUM ALLOYS

Annealing Temperature, °C	Time, Hours	Prior Homogenization Treatment
700	330	
800	180	
800	180	1200°C - 24 hours
850	120	
900	90	
1000	24	
1000	48	1200°C - 24 hours
1050	24	
1100	7	
1150	6	
1200	6	
1250	2	
1300	1/6	
1350	1/6	
1350	1/2	
1400	1/6	

The powders for X-ray diffraction patterns were obtained by filing or crushing annealed specimens. The powders thus obtained were sealed inside a capped titanium container which was, in turn, placed inside an evacuated Vycor capsule and heated to the prior annealing temperature for a short time. The Vycor bulbs were quenched in water, but the bulbs were not broken until the contents were cool.

Solidus data were determined by incipient melting techniques. First, the melting temperature for a specimen of given composition was visually observed. Then a series of specimens of the same composition were quenched at temperature intervals below the observed melting, and subsequently examined metallographically. The accuracy of the solidus data is of the order of ±15°C. Liquidus data were obtained from cooling curves for three titanium-aluminum alloys.

Vickers hardness data obtained using a load of 10 or more kilograms revealed considerable scatter due to irregular or deformed impressions.

Fairly uniform impressions, and consequently more consistent data, were obtained with a 2 1/2 kilogram load.

2. Results and Discussion

The essential features of the phase diagram presented in Figs. 1 and 2 are two peritectic reactions, β + melt $\rightleftharpoons$ γ, and γ + melt $\rightleftharpoons$ TiAl$_3$, at about 1460° and 1340°C, respectively; and one peritectoid reaction, β + γ $\rightleftharpoons$ α, at 1240°C. The temperature of the polymorphic transformation of titanium is raised by addition of 29% aluminum from 885° to 1240°C, giving rise to extended ranges of alpha and beta solid solutions. The solubility of aluminum in alpha titanium is approximately 24.5% at 900°C, and increases to 31% aluminum at 1240°C. The intermediate phase, gamma, is homogeneous over a range of composition from about 37 to 60% aluminum at the solidus temperature, and from 35.5 to 44.5% at 800°C. The phase relationships for the alloys higher in aluminum content than the compound TiAl$_3$ (62.7% Al), which are included in Fig. 2, are based on earlier work (5).

a. Structural characteristics

Microstructures of alloys quenched from the various phase fields are shown in Figs. 3-19.

Specimens quenched from the beta field of the diagram revealed a transformation of beta to serrated alpha (Fig. 3). The duplex structure of specimens quenched from the narrow α + β field is shown in Figs. 4 and 5. Alloys quenched from the alpha phase field were characterized by equiaxed grains of alpha solid solution (Figs. 6 and 7).

The first trace of gamma appears as a precipitate of small particles along parallel striations in the alpha grains (Fig. 8). At slightly higher aluminum contents, in the temperature range 700°-1000°C, gamma precipitates from the alpha solid solution in a lamellar fashion. This precipitate appears to have nucleated at the grain boundaries and subsequently grown into the striated alpha grains (Fig. 9). The amount of the lamellar structure varies from traces up to 100% (Fig. 10), depending on the composition and time at temperature of annealing. The precipitation results from the large decrease in the solid solubility of aluminum in alpha titanium, varying from about 31% at 1240°C to 24.5% at 800°C. Massive gamma appeared in alloys with an aluminum content greater than 31% (Fig. 11).

A typical structure of alloys quenched from the β + γ field is shown in Fig. 12. As in all alloys quenched from the beta field at this temperature level, the white phase appears serrated due to the transformation $\beta \rightarrow \alpha$ during the quench. The gamma phase has precipitated in parallel plates along the boundaries of the original beta grains.

The structure of the gamma phase at 36% aluminum is shown in Fig. 13. As depicted in Fig. 1, this phase is homogeneous over a wide range of composition. Alloys with higher aluminum contents approaching the γ/γ + TiAl$_3$
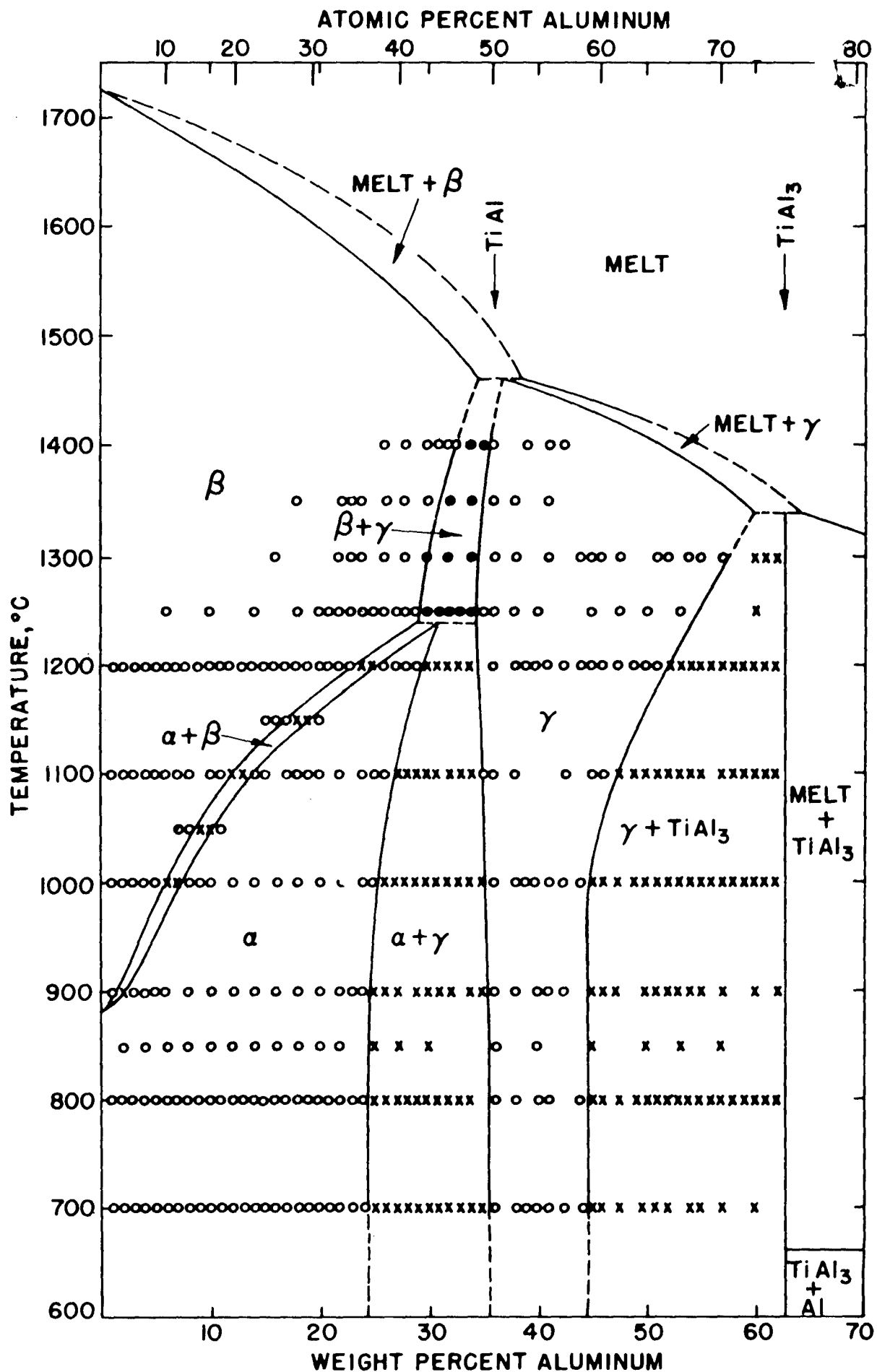
Fig. 1 — Partial Diagram of the Titanium-Aluminum System
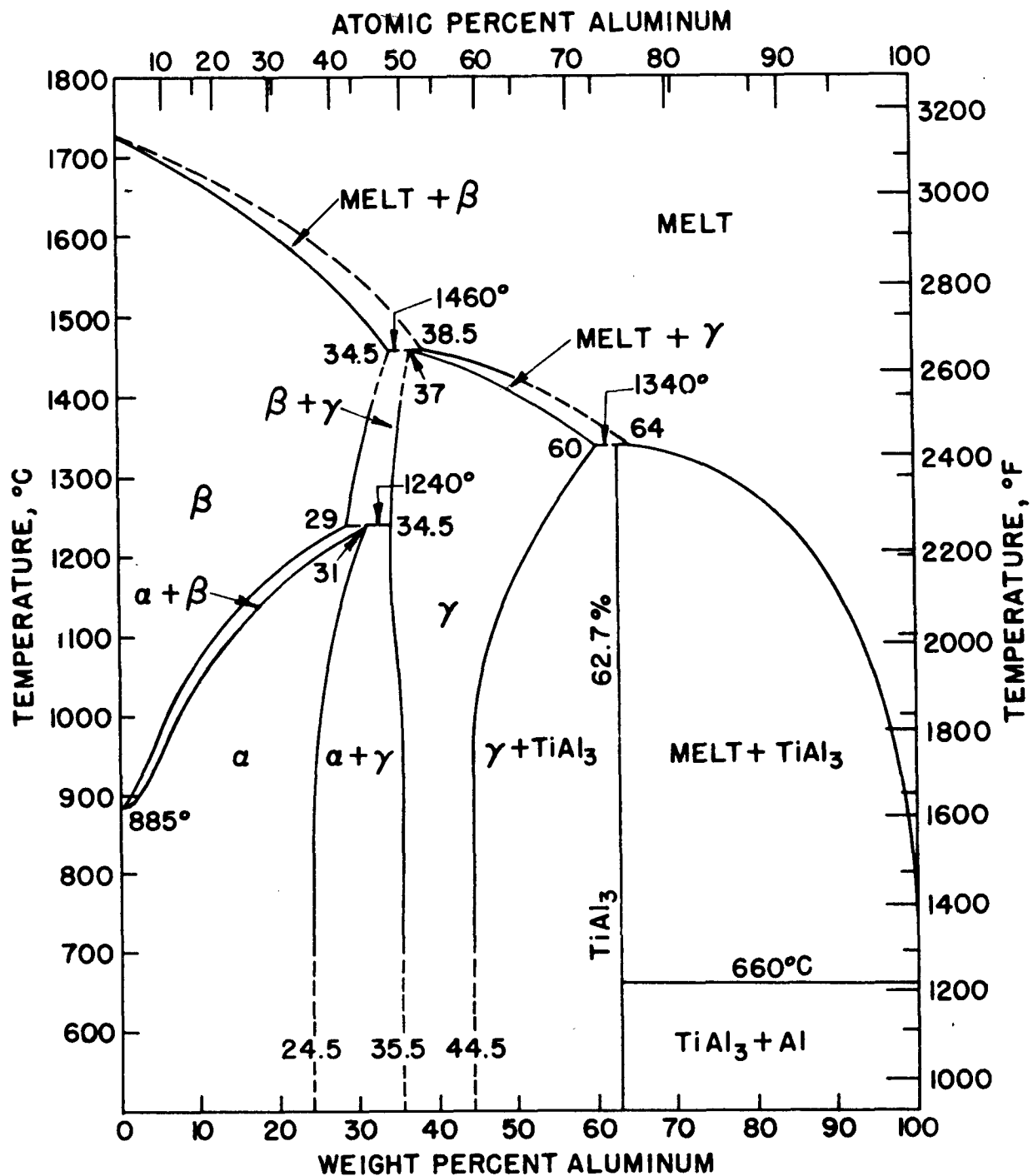
Fig. 2 - The Titanium-Aluminum Phase Diagram
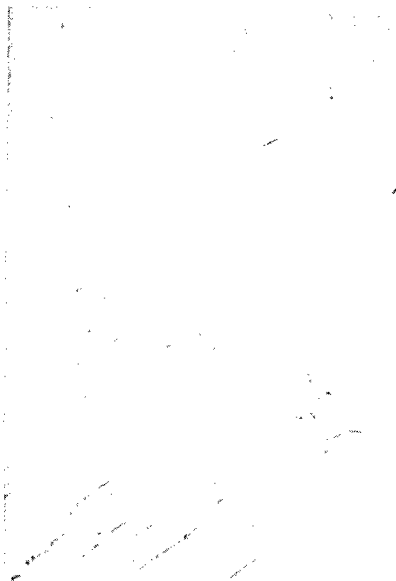
Neg. No. 3725   X250

Fig. 3

23% nominal aluminum alloy water quenched after annealing 2 hours at 1250°C. Typical serrated α transformation structure of alloys quenched from the β phase field.
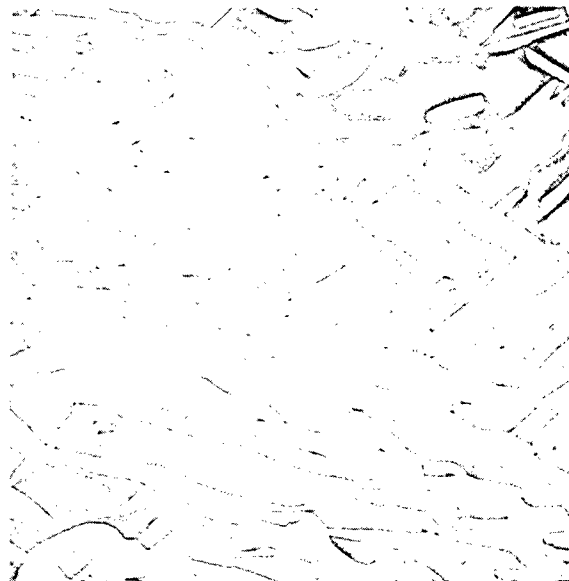
Neg. No. 3410   X250

Fig. 4

7% aluminum alloy pressed 70% and water quenched after 50 hours at 1000°C. The structure shows a mixture of isothermal α plus transformed β (dark).

Neg. No. 3402   X150

Fig. 5

25% aluminum alloy water quenched after 6 hours at 1200°C. Structure shows α plus transformed β.
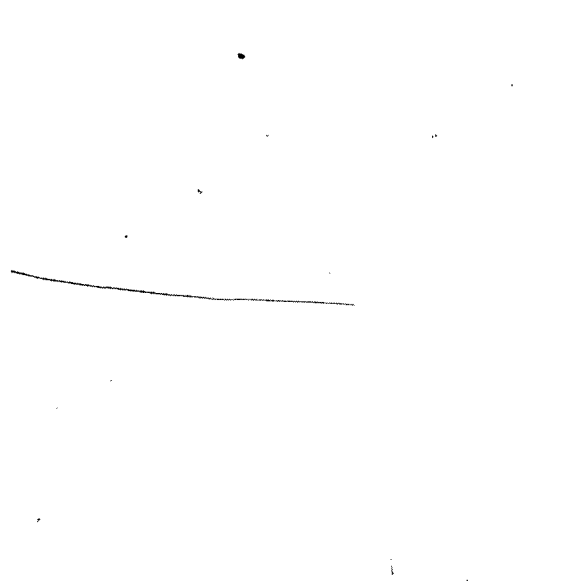
Neg. No. 3340   X250

Fig. 6

8% aluminum alloy pressed 35% and water quenched after 24 hours at 1000°C. Large equiaxed grains of α titanium.

Etchant: 2% HF, 3% HNO_3 in water
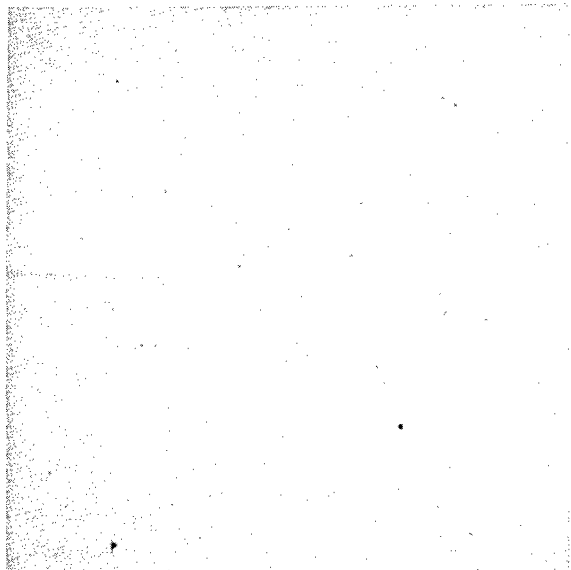
Neg. No. 3341   X250

Fig. 7
25% aluminum alloy water quenched
after 24 hours at 1000°C. Large
equiaxed grains of α titanium.
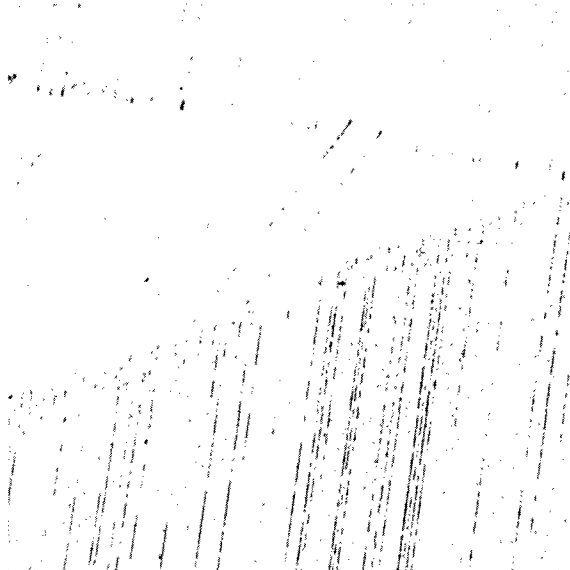
Neg. No. 3349   X250

Fig. 8
25% aluminum alloy water quenched
after 120 hours at 850°C. Structure
shows traces of TiAl precipitated
along parallel planes in α grains.

Neg. No. 3413   X150

Fig. 9
27.3% aluminum alloy water quenched
after 180 hours at 800°C. Structure
shows nucleation and growth of a
lamellar precipitate of TiAl in α.
Note the striations in the α grains.
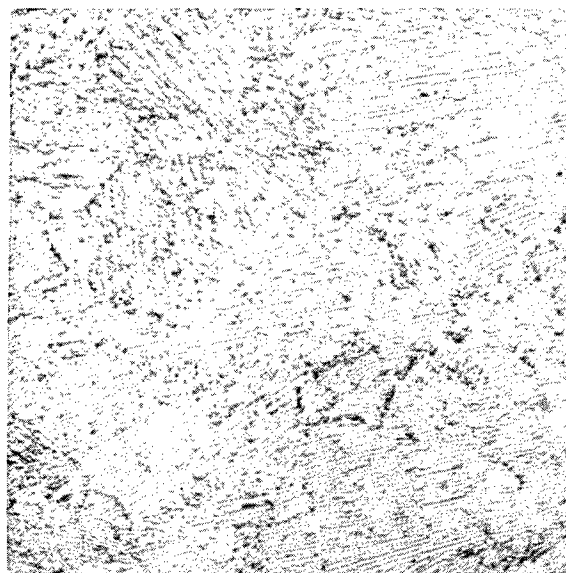
Neg. No. 3415   X800

Fig. 10
30% aluminum alloy water quenched
after 24 hours at 1000°C. Fine
lamellar structure of TiAl and α
titanium.

Etchant: 2% HF, 3% HNO₃ in water

Neg. No. 3404   X250
        2%HF,3%HNO₃ in water

Fig. 11

34% aluminum alloy water quenched
after 6 hours at 1200°C. Structure
shows the last traces of α in TiAl
matrix.

Neg. No. 3641   X200
        60glycerine, 20HNO₃,20HF

Fig. 12

32% aluminum alloy water quenched
after 1/2 hour at 1350°C. Serrated
α grain structure with γ phase char-
acteristic of alloys quenched from
the β + γ phase region of the diagram.

Neg. No. 3409   X150
Polarized light   Unetched

Fig. 13

36% aluminum alloy, pressed 25% and
water quenched after 24 hours at
1000°C. Equiaxed grains of γ phase
as revealed by polarized light.
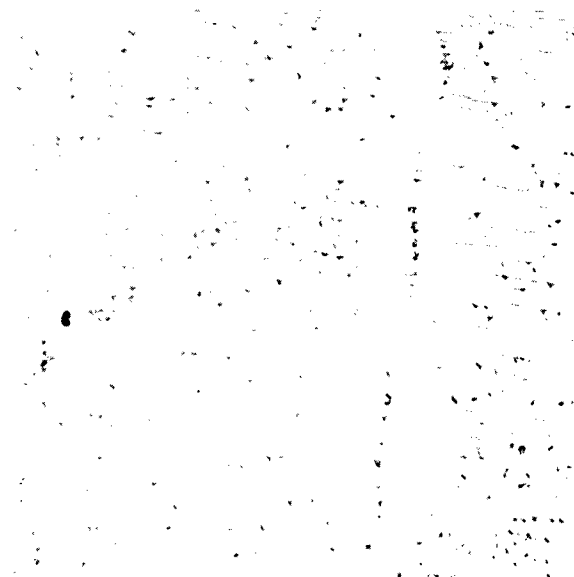
Neg. No. 3642   X800
        60 glycerine,20HNO₃,20HF

Fig. 14

49% aluminum alloy homogenized at
1200°C, furnace cooled and water
quenched after 48 hours at 1000°C.
Structure shows a Widmannstätten
pattern of TiAl₃ platelets pre-
cipitated in a γ matrix.
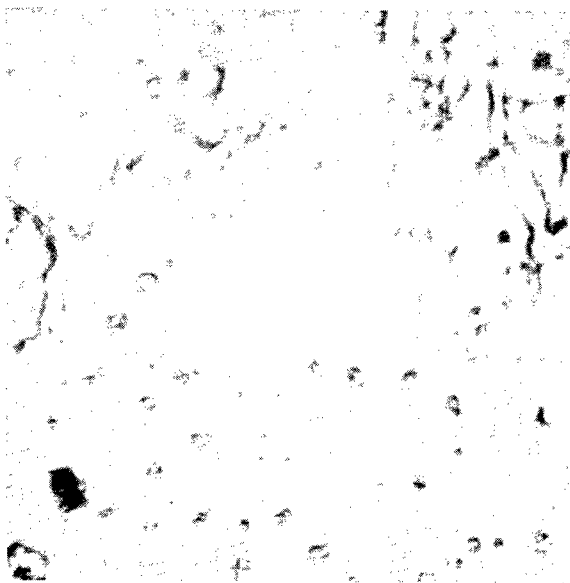
Neg. No. 3643   X800
  60 glycerine, 20HNO$_3$, 20HF

Fig. 15

56% aluminum alloy treated as in Fig.
14. Structure shows Widmannstätten
pattern of TiAl$_3$ precipitate plus
massive globules of TiAl$_3$ in a γ
matrix.
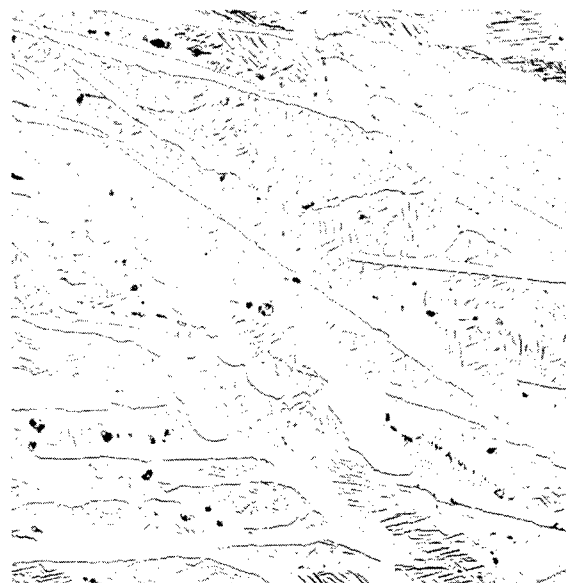
Neg. No. 3346   X250
  60 glycerine, 20HNO$_3$, 20HF

Fig. 16

61% aluminum alloy water quenched
after 24 hours at 1000°C. Structure
shows large primary plates of γ
phase plus Widmannstätten platelets
of precipitated γ in TiAl$_3$ matrix.

Neg. No. 3490   X100
Polarized light   Unetched

Fig. 17

61% aluminum alloy, as cast. Struc-
ture shows primary plates of γ in a
TiAl$_3$ matrix, giving evidence that
TiAl$_3$ was formed by a peritectic
reaction.
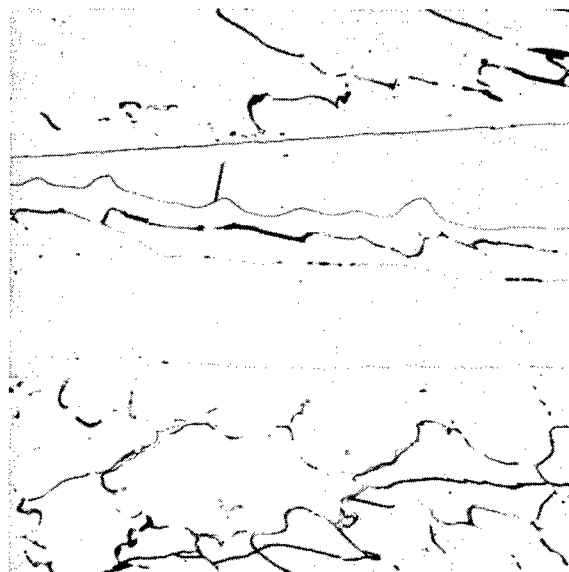
Neg. No. 3491   X250
  60 glycerine, 20HNO$_3$, 20HF

Fig. 18

62% aluminum alloy, as cast. Struc-
ture shows further evidence of a
peritectic reaction. Micrograph
shows two γ plates surrounded by
peritectically formed TiAl$_3$ which,
in turn, is surrounded by low melt-
ing aluminum in the interstices.

Neg. No. 3644   X250
       60 glycerine, 20HNO$_3$, 20HF

Fig. 19

64% aluminum alloy, as cast. Struc-
ture shows primary TiAl$_3$ surrounded
by aluminum in the grain interstices.

boundary become increasingly brittle and contain many cracks, but the structure of these alloys after annealing treatments shows the same response to polarized light as does the 36% aluminum alloy of Fig. 13. In the as-cast condition, these alloys were cored. Although homogenization anneals for as long as 24 hours at 1200°C almost completely eliminated coring, traces of residual inhomogeneity within the grains caused some difficulty in accurately locating the γ/γ + TiAl$_3$ boundary. Longer homogenization times could possibly have eliminated this small amount of residual coring; however, longer exposure times at these high temperatures were considered impractical. The resulting scatter in data limits the accuracy of locating the γ/γ + TiAl$_3$ boundary to about ±1%.

Figure 14 illustrates the structure of a homogenized 49% aluminum alloy quenched after 48 hours at 1000°C, and shows a Widmannstätten pattern of TiAl$_3$ platelets, which precipitated from the saturated gamma phase. Given the same treatment, alloys containing 56-59% aluminum revealed a similar Widmannstätten precipitation of TiAl$_3$ in a gamma matrix with the addition of massive TiAl$_3$ globules (Fig. 15). The latter were apparently formed by the peritectic reaction γ + melt $\longrightarrow$ TiAl$_3$, due to the rapid solidification of the ingot, and were not fully absorbed by the gamma phase during the subsequent homogenization anneal.

Figure 16 illustrates the structure of a 61% aluminum alloy quenched from 1000°C, and shows primary plate-like crystals of the gamma phase in a matrix of TiAl$_3$. The Widmannstätten pattern in the TiAl$_3$ matrix developed during the anneal, and represents gamma platelets precipitated from the saturated TiAl$_3$ phase. This proves that TiAl$_3$ has a certain homogeneity range which becomes narrower with fall in temperature. The extent of this range was not determined, because this subject is beyond the scope of the investigation. Since no detailed information on the homogeneity range of this compound is available, the TiAl$_3$ phase in Fig. 1 was arbitrarily indicated as a vertical line. The fact that TiAl$_3$ is homogeneous within a limited composition range has been reported recently by Schubert (7) without giving the solubility limits.

The TiAl$_3$ phase, previously reported (5) to have a maximum melting point, is formed by the peritectic reaction Melt + $\gamma \longrightarrow$ TiAl$_3$. Evidence of this is given in the as-cast structure of alloys with 61 and 62% aluminum (Figs. 17 and 18). Figure 18 exhibits primary gamma plates surrounded by peritectically formed TiAl$_3$, which in turn is surrounded by the low melting aluminum phase seen in the fine interstices of the TiAl$_3$ crystals. The positive identification of the gamma and TiAl$_3$ phases was aided by their highly different characteristics when examined under polarized light. At aluminum contents higher than that of the TiAl$_3$ phase, the structure, as shown in Fig. 19, reveals primary TiAl$_3$ phase surrounded by low melting aluminum.

b. X-ray diffraction results

X-ray diffraction studies were made on a series of alpha solid solution alloys and also a series of single phase gamma alloys, to determine the lattice parameters and the solubility limits of aluminum in the alpha and gamma phases. It was also desired to determine whether the beta to

alpha transformation on quenching alloys from the beta field could be suppressed.

A summary of the lattice parameter measurements for the alpha phase is given in Table III. A graphic presentation of the effect of aluminum additions on the parameters of the hexagonal close packed lattice, as shown in Fig. 20, reveals the very pronounced effect of initial additions of aluminum on the dimensions of the titanium lattice. Near the solubility limit, the curves appear to flatten off greatly. The markedly reduced slope of the parameter curves makes a parametric determination of the alpha solubility limit impractical. The X-ray results also confirmed the metallographic observation that the beta phase is not retained by rapid quenching.

The crystal structure of the gamma phase between 38 and 55 weight per cent aluminum is ordered face centered tetragonal, with an axial ratio close to unity. A summary of the lattice parameter measurements is presented in Table IV, and a graphic representation appears in Fig. 21. The lattice parameters are linearly dependent upon, and show increasing tetragonality with, increasing percentages of aluminum. These alloys have been quenched from 1200°C, indicating that either the ordered structure is stable to high temperatures, or the disorder → order transformation, if any, cannot be suppressed by quenching.

TABLE III

LATTICE PARAMETERS OF THE ALPHA TITANIUM-ALUMINUM PHASE

Wt.% Al	At.% Al	c (Å)	a (Å)	c/a	Quenched from
0	0	4.679	2.943	1.591	850°C
4	6.88	4.668	2.929	1.594	850°C
7	11.81	4.670	2.923	1.598	1000°C
9	14.95	4.661	2.924	1.594	1000°C
10	16.49	4.661	2.912	1.601	850°C
16	25.27	4.633	2.892	1.602	850°C
22	33.39	4.619	2.882	1.603	850°C
25	37.15	4.614	2.881	1.602	850°C
29	42.04	4.617	2.878	1.604	1200°C

TABLE IV

LATTICE PARAMETERS OF THE GAMMA TITANIUM-ALUMINUM PHASE

Wt.% Al	At.% Al	c (Å)	a (Å)	c/a	Quenched from
38	52.13	4.065	3.984	1.020	1200°C
41	55.23	4.067	3.972	1.024	1200°C
46	60.22	4.085	3.967	1.030	1200°C
55	68.47	4.089	3.949	1.035	1200°C

WEIGHT PER CENT ALUMINUM
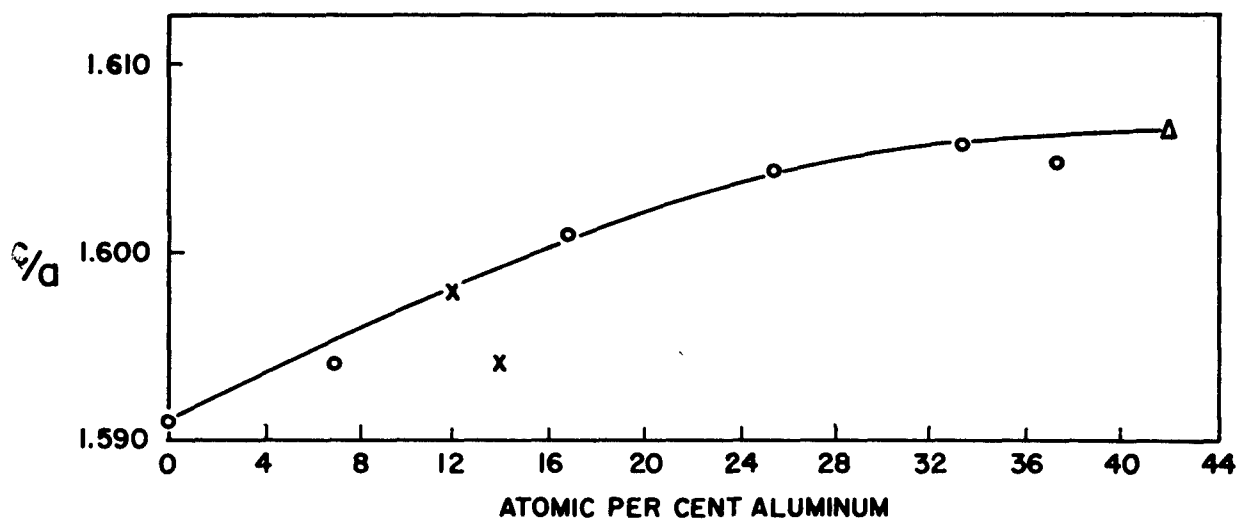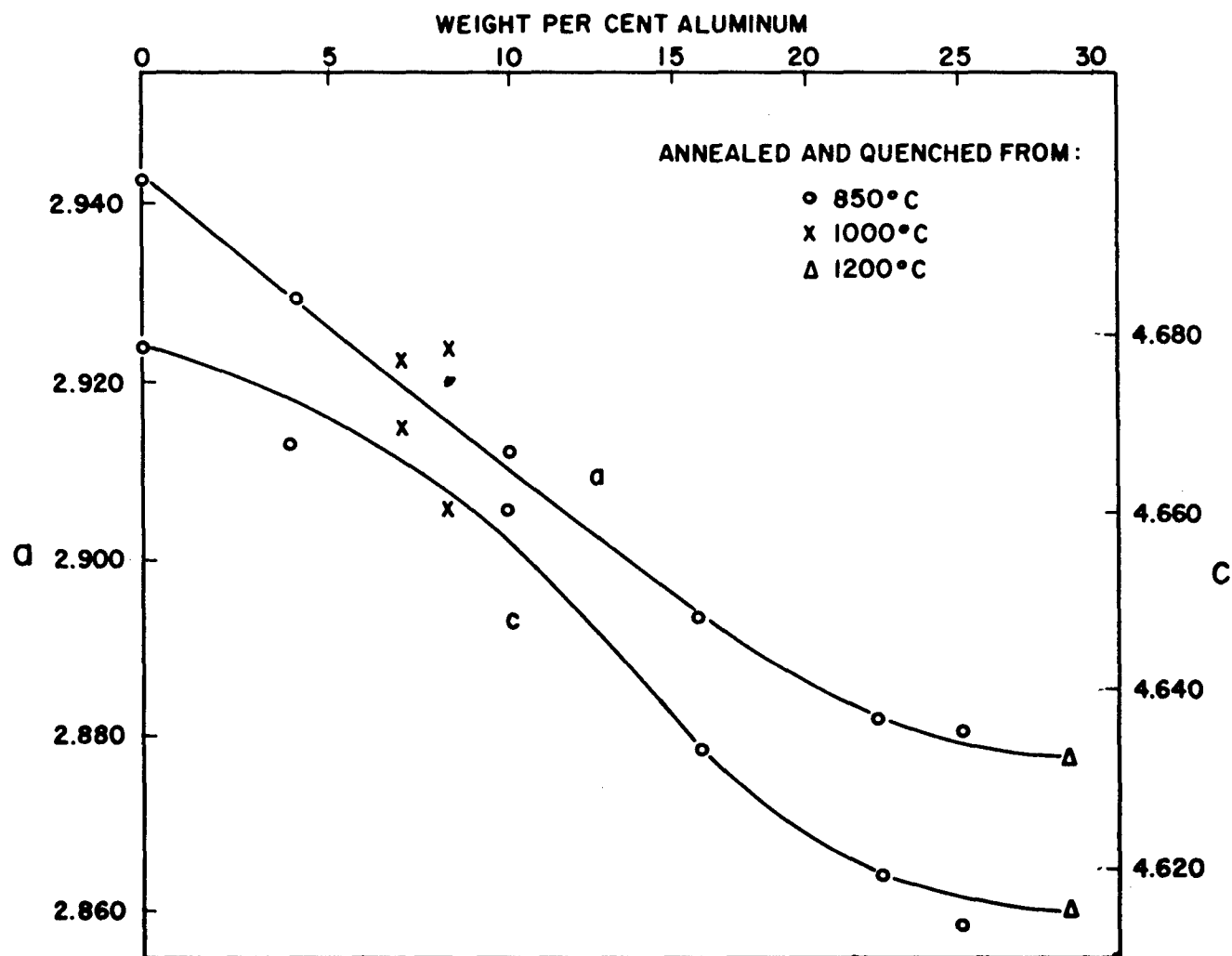
Fig. 20 - Lattice Parameter-Composition Curves for Alpha Solid
Solution Titanium-Aluminum Alloys
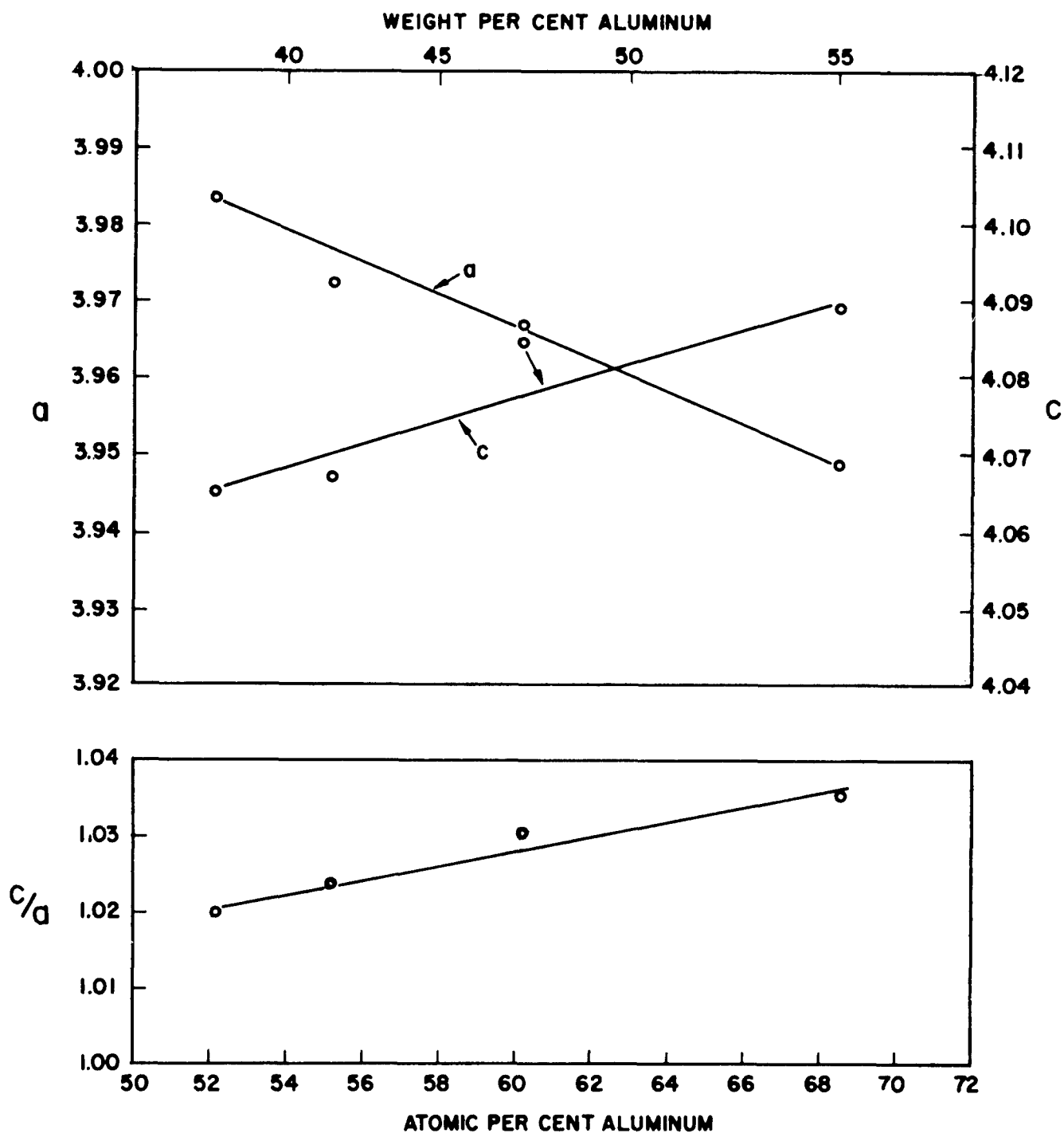
Fig.21 - Lattice Parameter-Composition Curves for Gamma Solid
Solution Titanium-Aluminum Alloys, annealed and quenched
from 1200°C

c. Melting range determinations

The data shown in Fig. 22 were obtained by incipient melting and thermal analysis methods. The solidus curve shows that aluminum additions lower the melting point of titanium to approximately 1460°C at 34.5% aluminum. From 38 to 60% aluminum, a change in slope of the solidus curve occurs, which is in excellent agreement with the liquidus points of alloys with 39, 45, and 50% aluminum, determined by thermal analysis (Fig. 22). All the evidence indicates that there is a peritectic reaction β + melt $\rightarrow$ γ at a temperature close to 1460°C between approximately 34.5 and 38.5% per cent aluminum. This correlates very well with an extrapolation of the boundaries of the β + γ field as shown in Fig. 1.

Thermal analysis did not give a definite indication of the width of the melting range for the three alloys tested (39, 45, and 50% Al); but together with incipient melting data, the range appears to be fairly narrow for the compositions investigated.

Some scatter of the melting temperature was encountered in determining the melting points of the 60-64% aluminum alloys, because of the presence of low melting aluminum phase formed by the incomplete peritectic reaction. The peritectic temperature of 1340°C shown in the diagram (Fig. 1) is lower than the 1355°C melting point of $TiAl_3$ reported by Manchot and Leber (8). These authors did not investigate alloys with lower aluminum contents than $TiAl_3$, and consequently failed to observe a peritectic reaction. On the other hand, the present data are based on the extrapolation of the γ/γ + $TiAl_3$ boundary, together with microscopically observed evidence of a peritectic structure.

d. Hardness test results

Vickers hardness data for as-cast alloys and those heat treated at 800° and 1200°C are presented graphically in Fig. 23. The data include alloys from 0 to 90% aluminum.

Aluminum is a very effective hardener of alpha titanium. The hardness curves show an increase in hardness in the 1-25% aluminum alpha solid solution range. A maximum hardness peak is reached at 25 or 30% aluminum, depending on the treatment. This composition range exhibited the most scatter in hardness data. It appeared that most of the scatter was due to the brittle characteristics of the alloys in this range of composition.

Alloys containing 25-35% aluminum, which structurally revealed an increased amount of gamma phase, showed decreasing hardness, reaching a minimum value for the 36% aluminum alloy. This alloy has been identified metallographically as a single phase, gamma.

Hardness in the 40-60% aluminum composition range increases to a second maximum in the hardness curve, which occurs at $TiAl_3$ (62.7% Al).
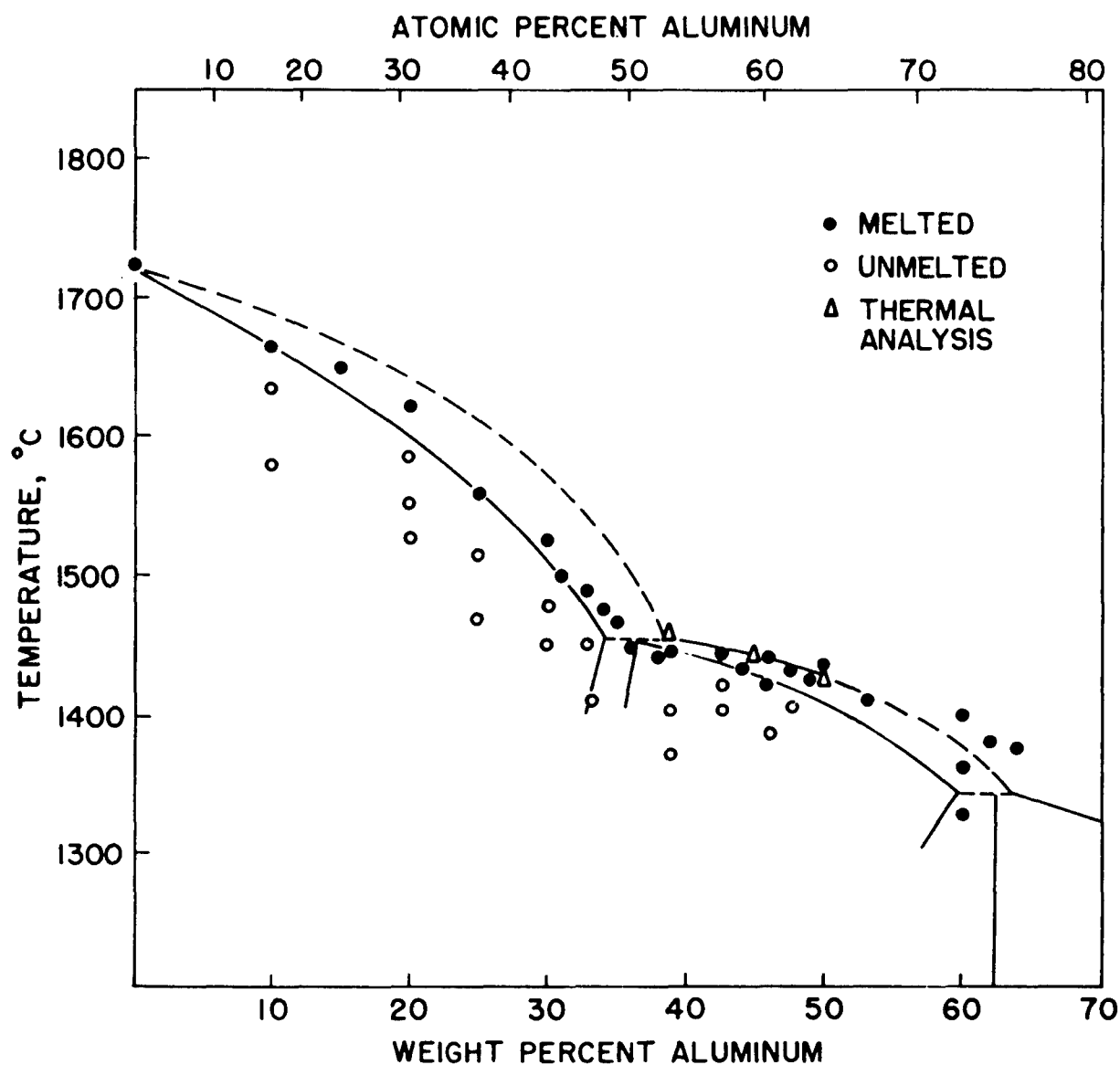
Fig. 22 - Melting Ranges for the Titanium-Aluminum System
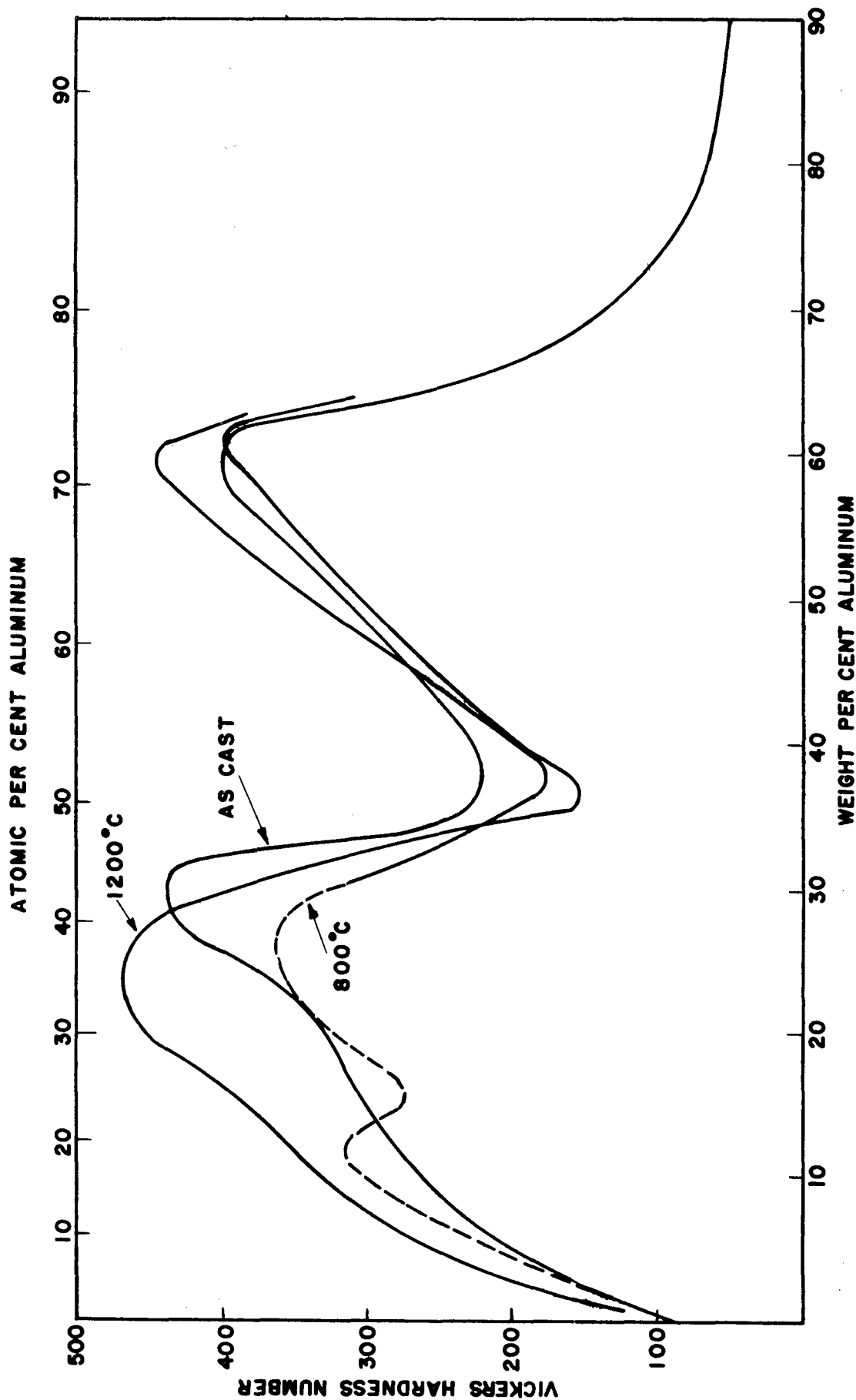
Fig. 23 - Comparative Vickers Hardness-Composition Curves for Titanium-Aluminum Alloys Treated as Indicated

Hardness data for alloys higher than 60% aluminum were restricted to as-cast alloys. The hardness drops sharply from 62 to 90% aluminum, and levels off to approximately the hardness of pure aluminum.

B.   The Titanium-Chromium-Iron System

When the study of the titanium-chromium-iron system was first initiated, no determination of the two binary systems titanium-chromium and titanium-iron had been made using high-purity titanium. Therefore, the first objective was to accurately locate the phase boundaries using high purity alloys. The earlier and contemporary studies of the binaries are reviewed in detail in the sections of this report relating to the respective systems.

1.   The Titanium-Chromium and
      Titanium-Iron Systems

a.   Experimental procedure

Special high purity sponge titanium, manufactured by the Bureau of Mines, was used in the preparation of many of the alloys. The analysis of this material appears in a previous section of this report. With an as-cast hardness of 105 DPN, it compares favorably with iodide titanium (70-90 DPN). As a further check on the high purity of the Bureau of Mines titanium, samples of cold worked sheet were annealed at 10°C intervals for 1/2 hour. The results place the transformation temperature between 880° and 890°C, in good agreement with that of iodide titanium (885°C). Microstructures obtained are identical to those of iodide titanium, thus verifying the excellent purity of the metal.

The charges for the arc melting furnace were weighed to a thousandth of a gram and the ingots were weighed equally accurately after melting. With the exception of a few ingots in the high chromium region, only small weight losses were obtained. This indicates that the actual compositions must follow the nominal compositions very closely. The average weight loss for iodide titanium melts was about 0.02 gram, and that for the Bureau of Mines melts of the order of 0.2 gram. The higher weight losses of the Bureau of Mines titanium-base alloys were due to the fact that it was charged as sponge. The results of typical check analyses are shown in Table V.

TABLE V

TYPICAL CORRELATION BETWEEN NOMINAL COMPOSITION AND CHEMICAL ANALYSIS
FOR TITANIUM-CHROMIUM AND TITANIUM-IRON ALLOYS

Alloy Designation*	Nominal Composition,%	Chemical Analysis Iron,%	Chromium,%
BF14-918	14	14.26	
BF32-930	32	32.17	
BF36-934	36	35.61	
BC14-957	14		14.35
BC50-971	50		49.87

*B = Bureau of Mines titanium; F = iron; C = chromium. For
example, BF14-918 indicates a 14% iron alloy made with
Bureau of Mines titanium, heat number 918.

Most alloys capable of being deformed were cold pressed in order to
increase the rates of attaining equilibrium on heat treatment. Titanium-
iron alloys under 3% iron were cold pressed 25-50%, but the 4% alloy
cracked with slight deformation. The 2% chromium alloy cracked with
cold pressing.

Coring was observed above 14% iron and 6% chromium; therefore these
alloys were homogenized at 1050°C for 24-48 hours. The annealing times
varied from one or two days at 1050°C to a month at and below 550°C.
At more elevated temperatures, the times were shorter, in order to keep
surface contamination at a minimum. At 1260°C, samples were annealed
for two hours, and at 1385°C, 20 minutes was the time used.

Thermal analysis, metallographic analysis after isothermal annealing,
and incipient melting techniques were used to determine the melting range
of the alloys. The samples for metallographic analysis were separated
with molybdenum sheet to prevent contact in case of melting. Solidus
data were determined by incipient melting techniques, for which the first
visual sign of melting on heating was used. The accuracy of the incipient
melting data is estimated to be ±25°C; and that of other melting range
determinations is ±10°C.

b. Results and discussion

(1) The system titanium-chromium

In the first reported work on this system, Vogel and Wenderott (9)
roughly outlined the phase diagram within the range of composition 42-100%
chromium. They reported the existence of the compound Ti_3Cr_2 (42.0% Cr),
was said to form a eutectic at 48% chromium and 1400°C with a chromium-
rich solid solution containing 26% titanium. A tentative phase diagram
of the titanium-rich alloys, based on magnesium-reduced titanium, was
given by Craighead, Simmons and Eastwood (10). According to their data,

the transformation temperature of titanium is lowered by the addition of chromium, giving rise to an extended beta field and a restricted alpha field. McPherson and Fontana (11) have published photomicrographs of alloys with up to 18% chromium, prepared with magnesium-reduced titanium, after various heat treatments. They concluded that about 10% or more chromium apparently stabilizes the beta solid solution down to low temperatures, as no phase changes occurred in these alloys on air cooling from the beta field.

Micrographic analysis of the whole system by M. K. McQuillan (12), using magnesium-reduced titanium, resulted in the diagram presented in Fig. 24; the data points are indicated. Metallographic evidence was given of the decomposition of the continuous series of solid solutions between beta titanium and chromium by precipitation of the intermediate phase, Ti_2Cr_3 (62.0% Cr), within a wide range of composition. The titanium-rich beta phase is shown to decompose eutectoidally at a temperature somewhat above 650°C, the composition of the eutectoid being about 16% chromium. McQuillan established the fact that the only intermediate phase in this system is not Ti_3Cr_2, but one having a composition close to 62 weight per cent chromium; she therefore assigned the formula Ti_2Cr_3.

The partial diagram given by Duwez and Taylor (13), determined with iodide titanium-base alloys, shows that the beta solid solution with about 14.5% chromium decomposes at approximately 660°C into a eutectoid of alpha and the compound $TiCr_2$ (68.5% Cr). The existence of the latter was established by study of the crystal structure, which is face-centered cubic with 24 atoms per unit cell ($MgCu_2$ type). The solubility of chromium in alpha titanium at the eutectoid temperature was estimated to be 1% or less chromium. The solubility of chromium in beta titanium at 1100°C was found to be 26.5%.

(a) Metallographic studies

The partial phase diagram shown in Fig. 25 has been determined mainly by micrographic analysis of alloys with 0.5-75% chromium, annealed at and quenched from temperatures between 650°C and 1420°C. Results are, in general, in accordance with the phase diagram given by M. K. McQuillan (12)(see Fig. 24).

High-purity Bureau of Mines sponge titanium was used in the preparation of alloys. Eight iodide titanium-base alloys of 0.5-13% chromium were made to check any differences between the structures of the two types of titanium-base alloys. Comparing Fig. 25 with the insert of that figure, it can be seen that for the data points obtained, there is no apparent difference between the two for the $\beta/\alpha + \beta$ boundary.

The maximum solubility of chromium in alpha titanium is less than 0.5%. Beta titanium is retained upon water quenching alloys in which the beta phase contains at least 7% chromium.
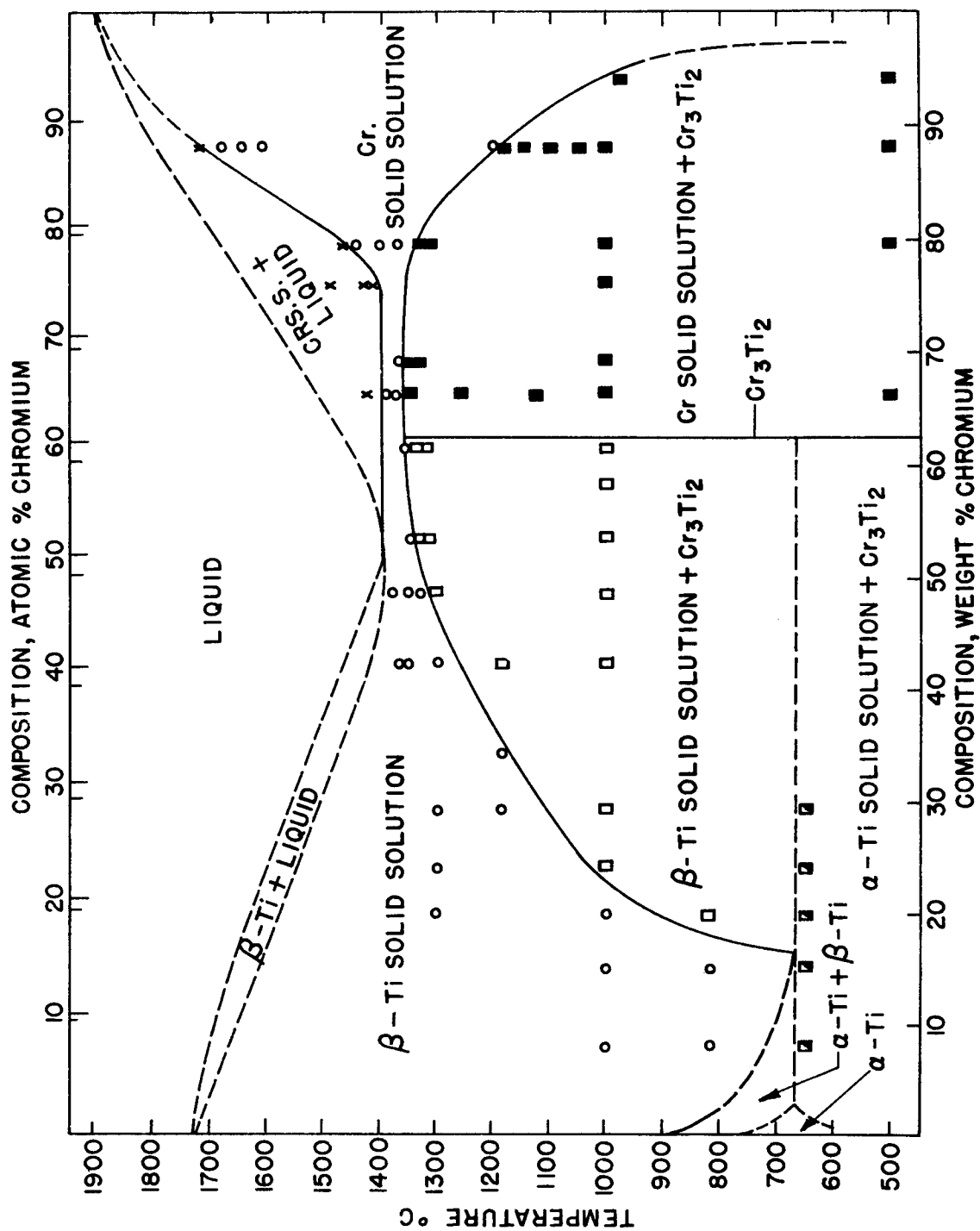
FIG. 24 - THE CONSTITUTIONAL DIAGRAM OF THE TITANIUM—CHROMIUM SYSTEM
AS DETERMINED BY McQUILLAN (6)
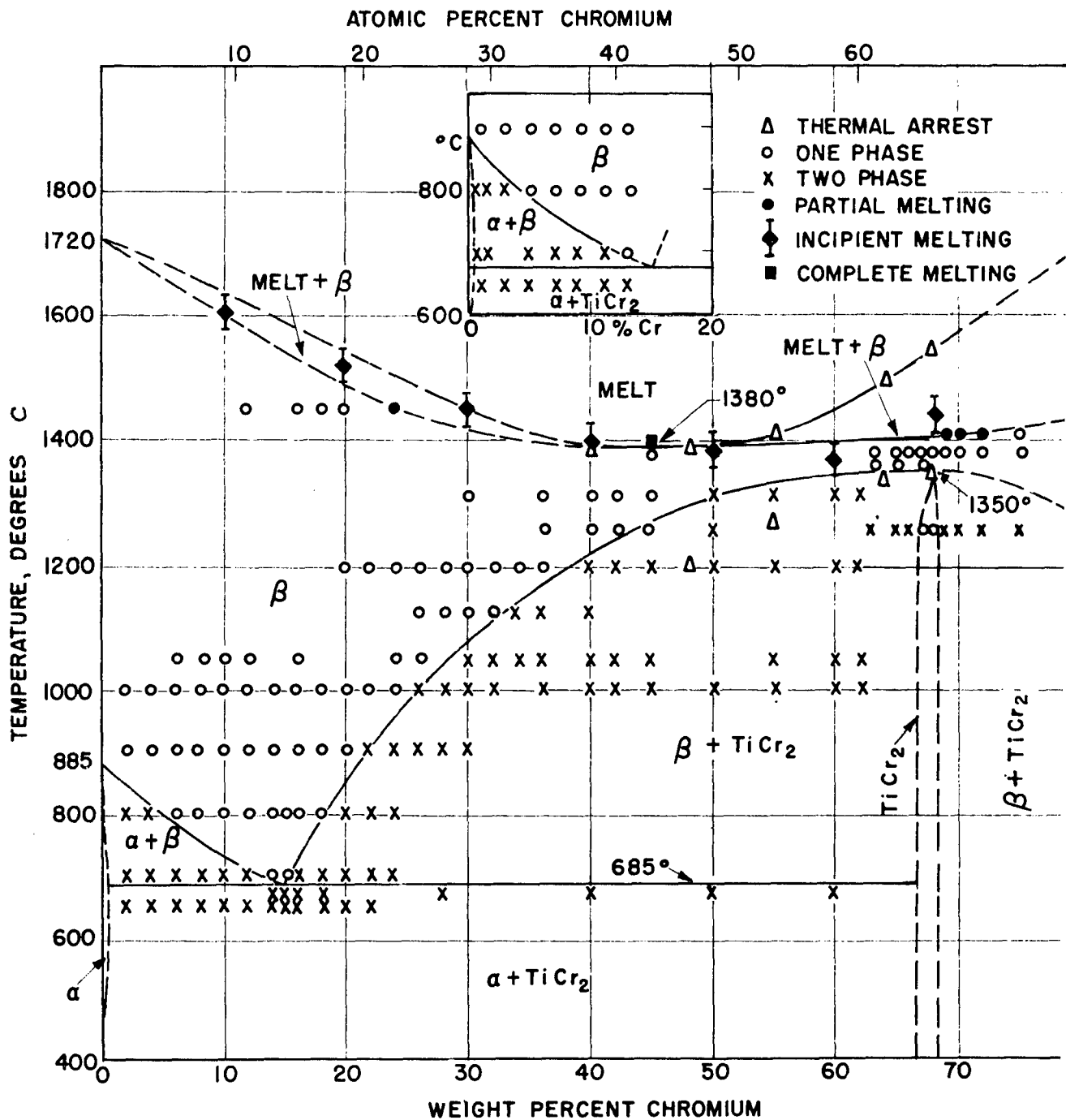
Fig. 25 - Partial Phase Diagram of the Titanium-Chromium System. Insert shows Section of Diagram Duplicated with Iodide Titanium-Base Alloys.

The eutectoid point is located at 15% chromium, between 675°C and 700°C. Figure 26 illustrates the eutectoid decomposition of the beta phase, and shows that it was confined mostly to the grain boundaries, even after 15 days' annealing at 675°C.

After annealing at 650°C for 13 days, typical lamellar eutectoid decomposition was observed only in alloys containing more than 12% chromium. The microstructures of alloys of lower chromium content consisted of fine Widmannstätten alpha in beta, and some alloys showed the start of eutectoid at the grain boundaries. The microstructure of such an alloy is shown in Fig. 27, and is compared to the same alloy annealed above the eutectoid temperature (Fig. 28). The amount of decomposition in alloys annealed at 650°C increased with chromium content up to 22% chromium (the alloy of highest chromium content annealed at this temperature level). Microstructures of alloys annealed at 600°C were extremely fine and unresolvable.

Oxygen contamination greatly increases the rate of eutectoid decomposition. This was proved by simultaneously annealing an 18% Bureau of Mines titanium-base alloy and a 17% Process A titanium-base alloy (containing approximately 0.15% oxygen) for one day at 635°C. In the high purity 18% chromium alloy, the beta solid solution was eutectoidally decomposed about 15%, as compared to the lower purity 17% chromium alloy, in which beta was decomposed approximately 95%.

The absence of a eutectic was established by means of both thermal and micrographic analysis. Above approximately 1350°C, beta titanium and chromium are completely mutually soluble. Upon cooling alloys between 15 and 75% chromium from the beta region, $TiCr_2$ is rejected.

Two thermal arrests were obtained in cooling curves for alloys containing 48, 55, 63, and 68% chromium, as shown in Fig. 25. The first indicates the start of solidification, and the second break gives the first thermal evidence of the breakdown of the beta solid solution. It will be noted that the second arrest shows increasing deviation from the indicated $\beta/\beta + TiCr_2$ boundary, as the chromium content decreases. This can be explained by the fact that appreciable heat evolution for this precipitation is detected only when relatively large quantities of compound are rejected.

Micrographic evidence of the precipitation of $TiCr_2$ from the beta phase is given by the microstructure of a chill-cast 50% chromium alloy (Fig. 29) and that of an alloy with 48% chromium slowly cooled from the molten state (Fig. 30). These structures definitely show a Widmannstätten type precipitate formed by cooling from a single phase field into a two-phase field, and are not of eutectic origin.

Figures 31 and 32 illustrate the microstructures of a 66% chromium alloy quenched from the beta and the $\beta + TiCr_2$ fields, respectively. Upon quenching from 1385°C in the beta field, the solid solution broke down into the serrated structure shown (Fig. 31). An X-ray diffraction pattern of this alloy showed it to be almost entirely $TiCr_2$. Annealing

Neg. No. 3734   X500

Fig. 26
An 18% chromium alloy, homogenized,
annealed at 675°C for 360 hours.
Eutectoid decomposition occurs mostly
along the grain boundary. Matrix is
retained β with a few compound crys-
tals.

Neg. No. 3750   X750

Fig. 27
An 8% chromium alloy, homogenized,
annealed at 650°C for 305 hours. α
plus metastable β showing the start
of eutectoid decomposition in the
grain boundary.
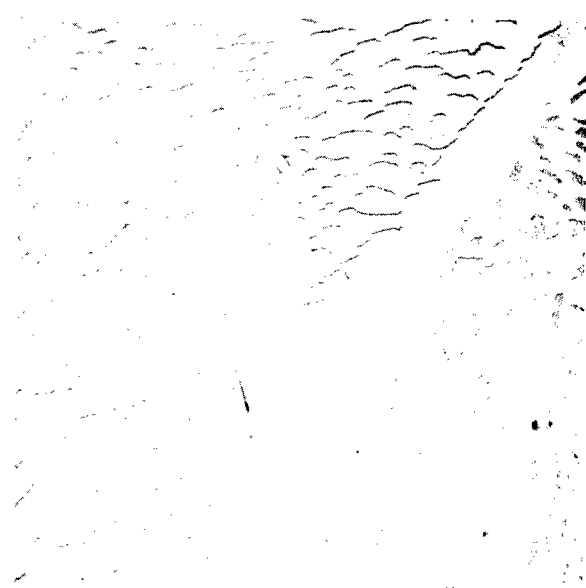
Neg. No. 3751   X750

Fig. 28
Same alloy as Fig. 27, homogenized,
annealed at 700°C for 190 hours.
α + β.

Etchant: 60 glycerine, 20 HNO$_3$, 20 HF
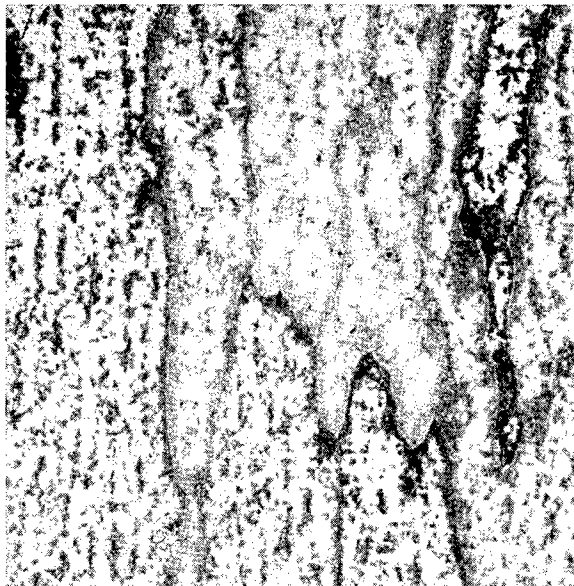
Neg. No. 3514   X250

Fig. 29
A 50% chromium alloy, arc melted and
chill cast. β with precipitate of
compound rejected from the cored
solid solution during fast cooling.
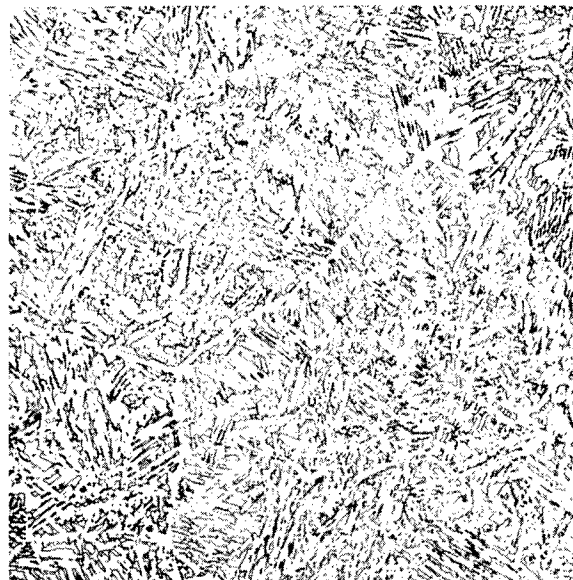
Neg. No. 3519   X250

Fig. 30
A 48% chromium alloy, slowly cooled
in a graphite crucible. No eutectic
is indicated. Structure is of Wid-
mannstätten type typical of an alloy
cooled from a one phase field into
a two phase field.
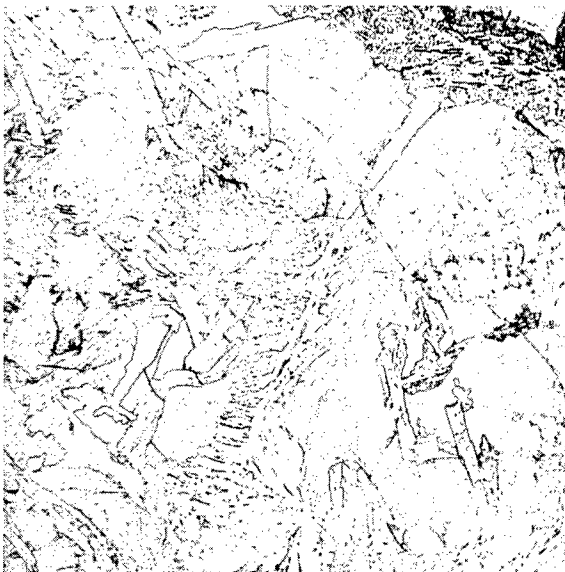
Neg. No. 3747   X250

Fig. 31
A 66% chromium alloy, annealed at
1385°C for 20 minutes and water
quenched. Serrated compound showing
that the alloy was in the β field
prior to quenching.
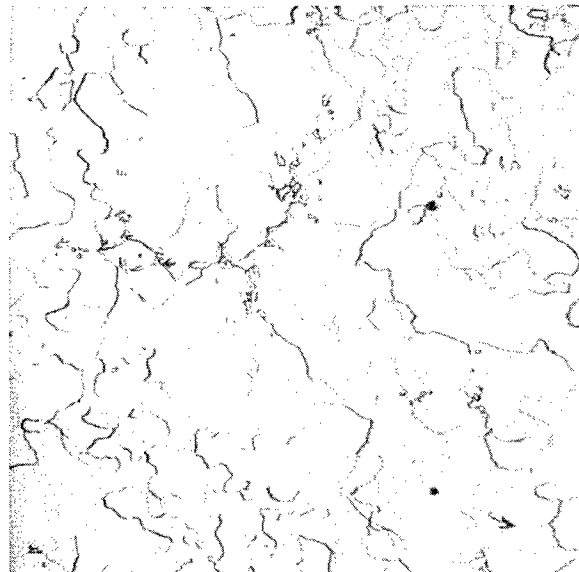
Neg. No. 3746   X250

Fig. 32
Same alloy as Fig. 31, but annealed
at 1260°C for 2 hours and water
quenched. Almost entirely equiaxed
grains of $TiCr_2$ with a trace of β.

Etchant: 60 glycerine, 20 HNO_3, 20 HF

at 1260°C resulted in the microstructure shown in Fig. 32. The equiaxed grains illustrate that the compound was formed isothermally, and that the alloy contains only traces of beta. From the microstructure of the series of alloys annealed at 1260°C, the compound has been shown to exist over a small composition range (67-68% Cr).

It may be noted that $TiCr_2$ showed twinning in the microstructures of samples that had been deformed and subsequently annealed at 675°C. This phenomenon was not further investigated.

(b) Melting range determinations

Incipient melting data were used to outline the melting range of alloys with up to 68% chromium. As these determinations were of a comparatively low order of accuracy, they are used only to locate the dotted melting range up to 40% chromium.

Detection of melting in isothermally annealed samples checked incipient melting data at 24% chromium, and was used to locate the minimum melting temperatures at 45% chromium. Partial melting in annealed samples was also detected at higher chromium contents, thus establishing the flat solidus curve between 45 and 75% chromium.

Thermal analysis located the liquidus curve at higher chromium contents and verified the minimum melting point at 45% chromium. That carbon contamination did not lead to large errors in thermal analysis data was proved in the following manner: Cooling curves were determined for two 48% chromium-titanium alloys and the liquidus points agreed within less than 5°C. However, the microstructure of one showed no visible carbides (Fig. 30), while the other showed appreciable amounts of carbide in the microstructure. Thus, even though the carbon contamination was apparently quite different, the thermal analysis data agreed closely. The results of high temperature annealing treatments are shown in Table VI, and substantiate the thermal analysis data.

TABLE VI

MELTING RANGE DETERMINATIONS FOR TITANIUM-CHROMIUM ALLOYS

A. Thermal Analysis

| | Inflection Temperatures, °C | |
Nominal % Cr	Liquidus	Compound Rejection
68	1544	1344
64	1494	1342
55	1407	1271
48 (Alloy 1)	1384	1201
48 (Alloy 2)	1382	1202
40	1383	

B. Annealing Treatments

Nominal % Cr	Temperature, °C	Outward Appearance	Microstructure
45	1380	No melting	No melting
45	1390	Complete melting	--
69	1420	No melting	Partial melting
70	1420	"	"
72	1420	"	"
75	1420	"	No melting

(2) The System Titanium-Iron

In the following discussion, only the constitution of the titanium-rich alloys with compositions up to and including the phase TiFe (53.8% Fe) will be considered. Laves and Wallbaum (14) briefly reported that the two compounds Ti_2Fe (36.8% Fe; face centered cubic with 96 atoms per unit cell) and TiFe (B_2 type) exist. Wallbaum (15) also published a phase diagram showing these intermediate phases; however, apparently no detailed work was done on the titanium-rich alloys, as no phase relationships based on experimental evidence were given. Craighead, Simmons and Eastwood (10) found that additions of iron lower the temperature of the polymorphic transformation of titanium, giving rise to a very restricted range of alpha solid solution and stabilization of the beta solid solution toward lower temperatures. Their work was confined to magnesium-reduced titanium-base alloys containing up to 2.2% iron. By measuring the hydrogen pressures in equilibrium with very dilute solutions of

hydrogen in iodide titanium-base alloys, A. D. McQuillan (16) determined the $\beta/\alpha + \beta$ boundary above 800°C and between 0 and 5.8% iron.

By means of micrographic and X-ray diffraction methods, using magnesium-reduced titanium of low purity (with a transformation range of 860°-970°C), a general outline of the phase diagram for the titanium-rich portion of the system was established by Worner (17). He found that the beta phase decomposed eutectoidally at 17.5% iron and approximately 600°C into alpha (with 0.9% iron) and the compound TiFe (with a body centered cubic lattice and a melting point of approximately 1250°C). A eutectic of beta, containing 25% iron, and TiFe was established at 32% iron and 1060°C. Although Duwez and Taylor (18), in agreement with Laves and Wallbaum (14), reported the existence of the compound Ti_2Fe, Worner found no evidence of this phase, either metallographically or by X-ray diffraction studies.

In the course of his work on the copper-titanium system, Karlsson (19) found some evidence to support Worner's conclusion that Ti_2Fe does not exist. Karlsson was able to show that the previously reported Ti_2Cu was really an oxide phase having an ideal composition Cu_3Ti_3O, with a titanium-rich solubility limit close to Cu_2Ti_4O. The high oxygen content probably resulted from contamination during heat treatment. He proposed that a similar phase might exist in the titanium-iron-oxygen system.

(a) Metallographic studies

Micrographic analysis of heat treated specimens and a limited amount of thermal analysis and X-ray work have been used in the determination of the partial phase diagram up to the composition of the first compound, TiFe (53.8% Fe). Results are in general accordance with the phase diagram given by Worner (17). Specimens were annealed at and quenched from temperatures between 500° and 1200°C. Iodide titanium was used for the preparation of alloys containing up to 30% iron. High-purity Bureau of Mines sponge titanium was used for alloys of higher iron content.

The partial phase diagram is presented in Fig. 33. The eutectoid point lies between 575° and 600°C, between 15 and 16% iron. No eutectoid was observed in samples annealed at 600°C for as long as 745 hours. Evidence of the eutectoid is shown in the microstructure of an 18% alloy annealed at 550°C for 740 hours (Figs. 34 and 35). These photomicrographs illustrate the fact that the decomposition has started at the grain boundaries, and is extremely sluggish. As for the titanium-chromium system, eutectoid decomposition was found only in hypereutectoid alloys and hypoeutectoid alloys near the eutectoid point. Figure 36 illustrates the microstructure of a 13% iron alloy annealed at 550°C for 740 hours and shows no eutectoid decomposition of the beta phase. Decomposition was observed in alloys as low as 11% iron for samples annealed at 500°C. Similar to the results of the titanium-chromium system, it was found that oxygen accelerates the eutectoid decomposition.
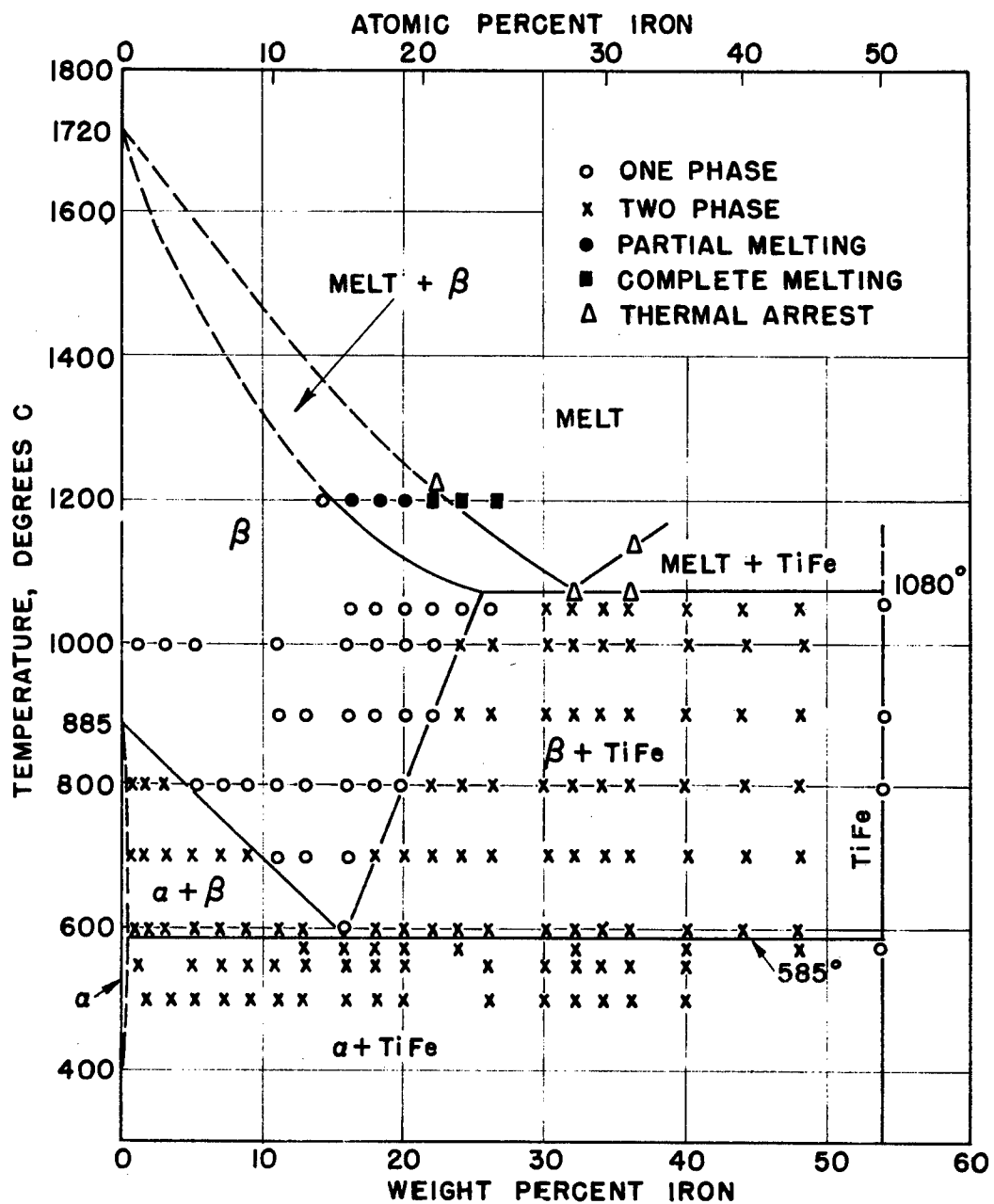
Fig. 33 - Partial Phase Diagram of the Titanium-Iron
System.

Neg. No. 3488   X100   Neg. No. 3489   X750
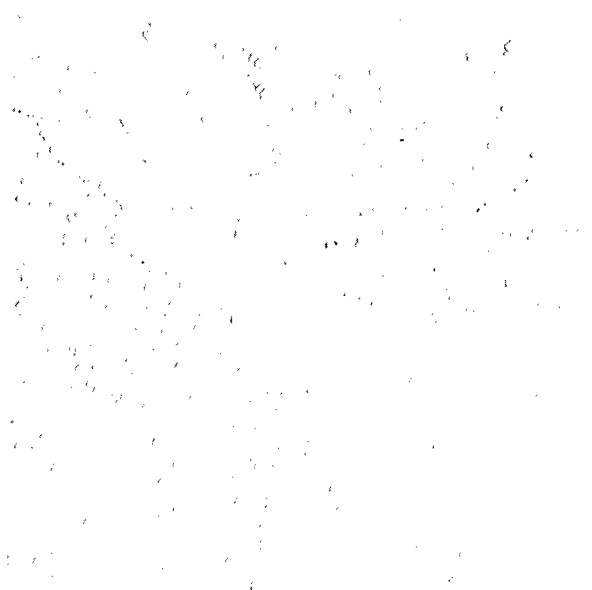
Fig. 34   Fig. 35
An 18% iron alloy, homogenized and   Same alloy as Fig. 34, but at higher
water quenched after annealing at   magnification. This clearly shows
550°C for 740 hours. Eutectoid de-   the eutectoid structure and primary
composition along grain boundaries.   compound in a matrix of retained β.

Neg. No. 3731   X250

Fig. 36
A 13% iron alloy treated the same as
the 18% alloy (Fig. 34). α in a
matrix of retained β. No eutectoid
is evident.

Etchant: 60 glycerine, 20 HNO₃, 20 HF

The solubility of iron in alpha titanium is less than 0.5%. Beta titanium is retained upon water quenching alloys in which the beta phase contains at least 4% iron.
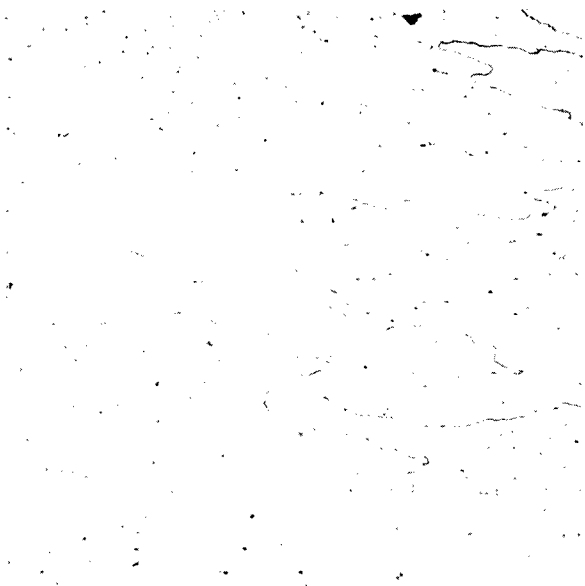
The maximum solubility of iron in beta titanium at the eutectic temperature, 1080°C, is 25% iron. The eutectic point lies at 32% iron. The intermediate phase coexisting with the beta solid solution corresponds to the stoichiometric composition of TiFe (53.8% Fe), and is shown in the single phase microstructure of a 54% iron alloy annealed at 900°C for 72 hours (Fig. 37).

No evidence was found of the compound Ti_2Fe (36.8% Fe), reported by other investigators (14, 18). The microstructures of the alloys in the β + TiFe field show a consistent increase in the amount of TiFe as the iron content increases, and no other phase was indicated. It was thought that Ti_2Fe might be formed by a sluggish peritectic reaction (TiFe + melt $\longrightarrow Ti_2Fe$), and thus would not be seen in the fast-cooled arc melted alloys. Therefore, a 36% iron alloy was held in a graphite crucible at 1105°C, just above the eutectic temperature, for 20 minutes and slowly cooled. If Ti_2Fe exists, and is formed peritectically, it would appear in the microstructure of this sample as a peritectic wall around the primary TiFe phase. However, Fig. 38, a photomicrograph of the above alloy, does not show any indication of Ti_2Fe. The structure consists of about 20% primary compound (TiFe) and a coarse eutectic of beta and TiFe.

(b) X-ray studies

X-ray diffraction was used in an attempt to isolate the Ti_2Fe phase. Diffraction patterns of a 48% iron alloy annealed in the β + TiFe field gave lines which could be accounted for only by the phase mixture of beta titanium and TiFe. The latter phase was identified as having a body centered cubic structure with a lattice parameter of 2.982 Å, in good agreement with the results of Duwez and Taylor (18). There was no indication of Ti_2Fe.

With Karlsson's work (19) as the impetus, alloys corresponding to the stoichiometric composition of Ti_2Fe, Ti_3Fe_3O, and Ti_4Fe_2O were prepared. Iodide titanium and very pure TiO_2 were used. Powder patterns were taken of the homogenized alloys. The Ti_2Fe alloy gave predominantly the structure of the TiFe phase, and extra lines belonging to either alpha or beta titanium, depending upon heat treatment. Both the Ti_3Fe_3O and the Ti_4Fe_2O alloys yielded single phase patterns which were almost identical to those reported by Duwez and Taylor. A comparison of the diffraction lines is shown in Table VII. It appears, therefore, that a ternary phase exists in the titanium-iron-oxygen system which permits a broad replacement of iron atoms by titanium atoms.

Neg. No. 3732   X150

Fig. 37
A 54% iron alloy, homogenized, an-
nealed at 900°C for 72 hours and
water quenched. The intermediate
phase TiFe.
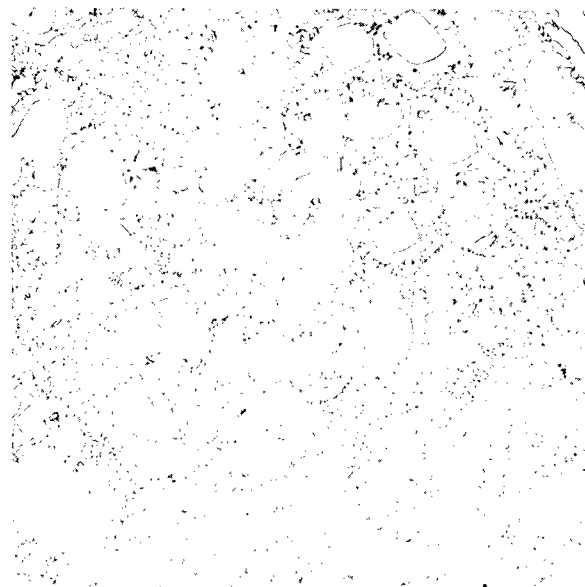
Neg. No. 3645   X150

Fig. 38
A 36% iron alloy, held at 1105°C, 20
minutes, and slowly cooled in a graphite
crucible. Primary TiFe plus coarse
eutectic of β and TiFe.

Etchant: 60 glycerine, 20 HNO$_3$, 20 HF

TABLE VII

COMPARISON OF INTERPLANAR SPACINGS FOR Ti_4Fe_2O AND Ti_2Fe REPORTED ELSEWHERE (18)

hkl	$d_{hkl}(\text{Å})$ Ti_4Fe_2O	$d_{hkl}(\text{Å})$ Ti_2Fe (18)	hkl	$d_{hkl}(\text{Å})$ Ti_4Fe_2O	$d_{hkl}(\text{Å})$ Ti_2Fe (18)
332	2.386		842	1.230	1.234
422	2.293	2.31	933,771,755	1.132	1.136
500,430	2.250		862	1.106	1.109
431	2.203		666	1.084	1.087
333,511	2.163	2.17	775	1.016	1.019
440	1.986	2.00	955,971	0.9997	0.9886
442,600	1.872	1.88	882	0.9838	0.9847
622	1.745	1.72	866	0.9682	0.9697
444	1.619	1.63	10,62	0.9523	0.9563
551,711	1.572	1.59	12,00-884	0.9397	0.9423
553,731	1.478	1.472	11,51-777	0.9300	0.9330
650,643	1.463	1.41	10,64-12,22	0.9146	0.9172
733	1.375	1.382	10,82	0.8711	0.8726
821,742	1.353		13,11-11,55	0.8633	0.8648
660,822	1.328	1.334	11,73-13,31	0.8440	0.8456
555,751	1.301	1.305	13,33-955	0.8294	0.8277
840	1.259		14,20-10,86	0.7984	0.7997
911,753	1.238	1.242			

(c) Melting range determinations

The results of the melting range determinations are given in Table VIII and are plotted in Fig. 33. The 22, 32, and 36% alloys were studied by thermal analysis, which definitely established the eutectic point at 32% iron and 1080°C. The low carbon pickup of about 0.1% for the 32 and 36% iron alloys indicates that the breaks in the cooling curves could not be greatly displaced by contamination.

To further substantiate the results of thermal analysis, and to determine the slope of the solidus curve at low iron contents, a series of alloys was annealed at 1200°C for 15 minutes, followed by water quenching. Figures 39 to 42 illustrate a series of structures used to determine the melting range.
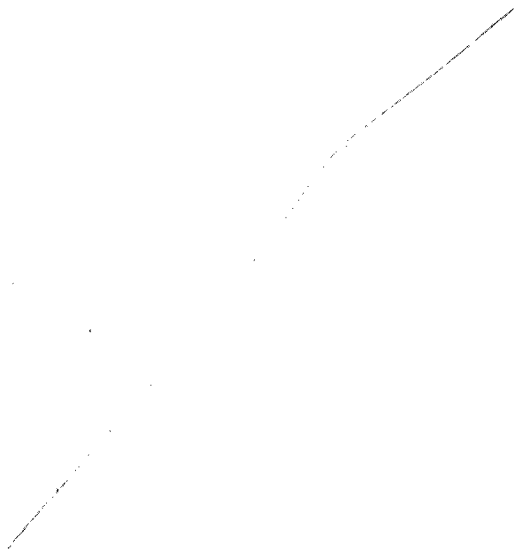
Neg. No. 3728   X250

Fig. 39

A 14% iron alloy, homogenized and
water quenched after annealing at
1200°C for 15 minutes. Retained β.

Neg. No. 3733   X250

Fig. 40

A 16% iron alloy treated the same as
the 14% alloy (Fig. 39). Partial
melting in retained β.
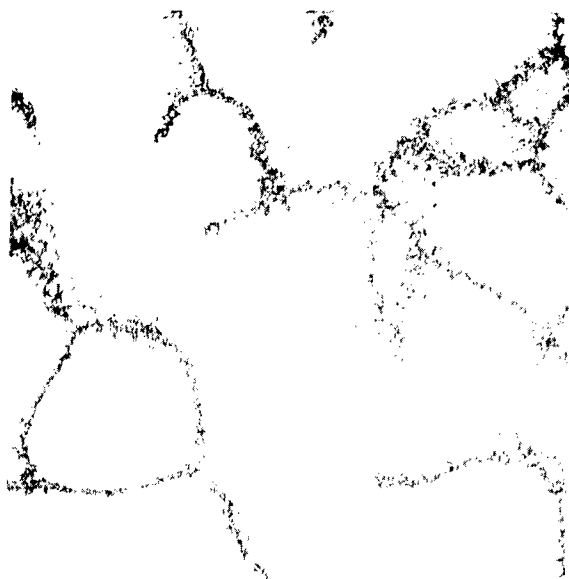
Neg. No. 3729   X250

Fig. 41

A 20% iron alloy treated the same as
the 14% alloy (Fig. 39). Greater
amount of melting in retained β.
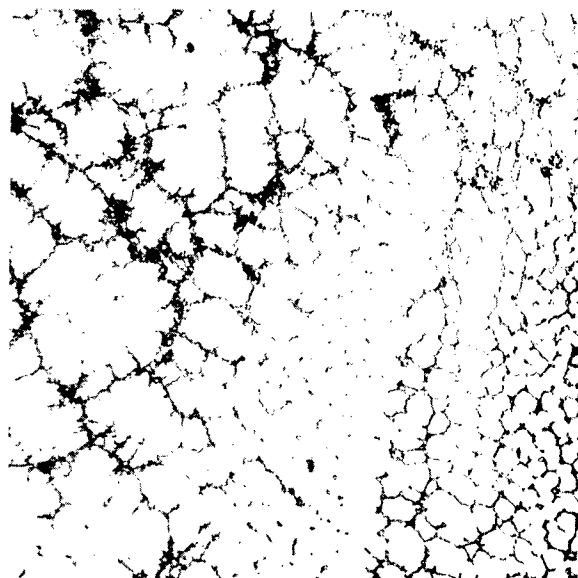
Neg. No. 3730   X250

Fig. 42

A 22% iron alloy treated the same as
the previous alloys. As-cast struc-
ture showing the sample was completely
molten at temperature.

Etchant: 60 glycerine, 20 HF, 20 HNO_3

TABLE VIII

MELTING RANGE DETERMINATIONS

A. Thermal Analysis

Nominal % Fe	Liquidus	Eutectic
22	1224	
32		1082
36	1146	1080

B. 1200°C Annealing Treatments

Nominal % Fe	Outward Appearance	Microstructure
14	No melting	No melting
16	"	Partial melting
18	"	Greater partial melting
20	"	Greater partial melting
22	Complete melting	Complete melting
24	"	--
26.3	"	--

(3) Hardness of Titanium-Chromium
     and Titanium-Iron Alloys

Vickers diamond pyramid hardness tests (10 kg load) were made on several groups of annealed and water quenched alloys. The results of some of these measurements are shown in Fig. 43. The curves for the alloys quenched from 1000°C are typical of hardness trends in both systems for samples quenched from 800°C and above. The hardness peaks in each case correspond to the compositions at which beta is retained on quenching; i.e., 4% iron and 7-8% chromium. Beyond the peak, the hardness of chromium alloys drops to a minimum at about 13% chromium, and increases to about 800 DPN in the region of $TiCr_2$ (67-68% Cr). The titanium-iron curve reaches a minimum at approximately 11% iron, increases to 30% iron, and then shows a gradual drop to the compound TiFe (54% Fe).

Hypoeutectoid alloys of either system, annealed at 700°C for 360 hours, have $\alpha + \beta$ structures and the beta is of sufficiently high alloy content to be retained on water quenching. These mixed structures are much softer than the acicular products obtained by quenching from above the transformation temperature (see Fig. 43). By annealing at 700°C, the hardness of the 4% iron alloy was reduced to 255, and that of the 7% chromium alloy, to 275 DPN.
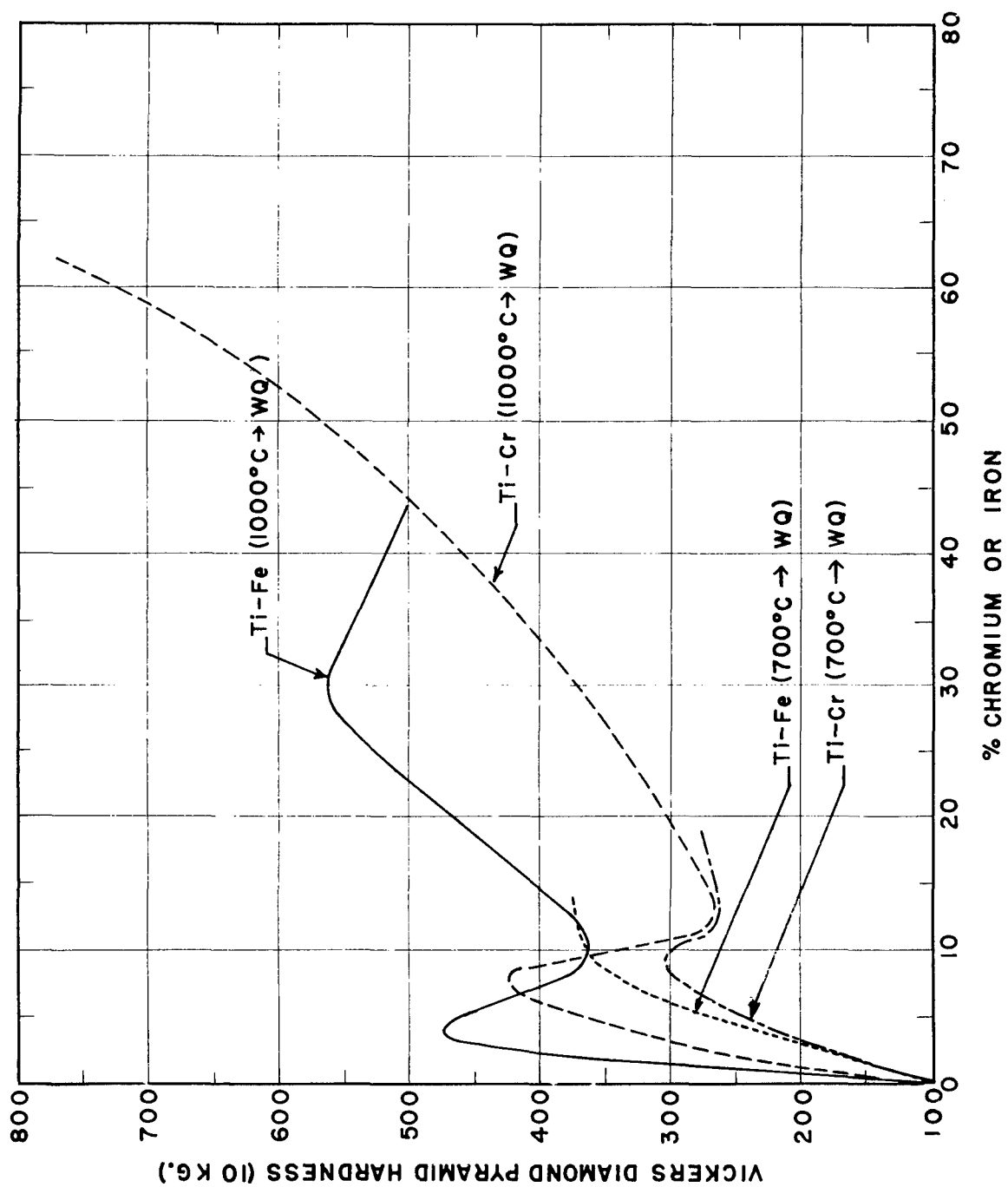
Fig. 43 -Vickers Hardness vs Composition for Chromium and
Iron Titanium-Base Alloys

2.   The Titanium-Chromium-Iron System

The literature yields no information concerning the constitution of the titanium-rich corner of the titanium-chromium-iron system. The determination of phase relationships in isothermal sections was the experimental approach used to obtain the ternary phase diagram. Therefore, isotherms have been used to describe the diagram. Although applied in the coordination of experimental data, vertical sections are not presented at this time.

From the data obtained, which are neither complete nor final, the ternary eutectoid point has been placed at approximately 8% chromium and 13% iron, and slightly below 550°C. The solubility of iron and chromium in alpha titanium is less than 1% total alloy content. Additional work is now in progress to more accurately establish the phase boundaries in the high alloy region and in space about the ternary eutectoid. The melting range of the ternary alloys also remains to be determined.

a.   Experimental procedure

As for the binary systems, the charges and the melted alloys were accurately weighed and weight losses were very low; therefore, nominal compositions have been used in plotting the data.

Coring was observed in some titanium-base alloys containing over 5% total alloy content of chromium and iron. Thus all alloys containing over 5% total alloy were homogenized at 1050°C for 24 hours.

Information on the annealing times used for various temperatures is given in Table IX. All samples treated below 800°C were first heated at 900°C for 2-8 hours and then slowly cooled to the temperature of final annealing. Long holding times have been used and, with the exception of the lower temperature treatments, probably greatly exceeded the time required to reach equilibrium. Despite this careful sample preparation, some segregation was observed in a number of the microstructures.

TABLE IX

ANNEALING CONDITIONS FOR TITANIUM-CHROMIUM-IRON ALLOYS

Temperature, °C	Time, Hours	Temperature, °C	Time, Hours
1050	24	700	192-288
900	72	650	432
800	144	600	576-600
750	192-288	550	744

In general, microscopic interpretation for the placement of phase boundaries was consistent with the lever rule, and only in a few instances, where data were omitted, were major dislocations due to segregation noted.

In such cases, the phase boundaries of the isothermal sections were drawn with emphasis on the binary intercepts, and the majority of the data which were in consistent agreement.

b.   The space model

Figure 44 is a schematic space model of the titanium-rich corner of the ternary system, illustrating only the solid state reactions. Points Y and Z are in a vertical plane arbitrarily cut through the system, and do not represent compounds.

The alpha space is bounded in the ternary system by the following surfaces:

$$X \; A_1 \; A \; A_2 \; X$$
$$A_1 \; a_1 \; a \; A \; A_1$$
$$A_2 \; a_2 \; a \; A \; A_2$$
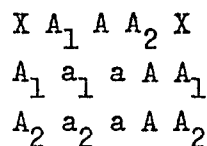
The maximum solubility of chromium and iron in alpha titanium, point A, is at the temperature of the ternary eutectoid.

The space of the ternary beta solid solution is bounded by the following surfaces:

$X \; E_1 \; T \; E_2 \; X$	at the X corner
$Y \; E_1 \; T \; E_3 \; Y$	at the Y corner
$Z \; E_2 \; T \; E_3 \; Z$	at the Z corner
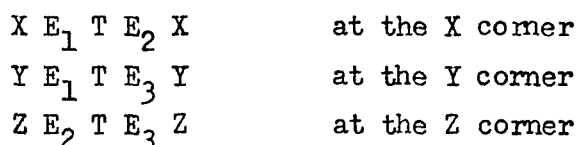
Intersections of these planes produce space curves of double saturation of the ternary beta phase (E_1T; E_2T; E_3T). They fall, with decreasing temperature, intersecting at T, the ternary eutectoid point. At this point the following eutectoid decomposition takes place:

$$\beta(T) \longrightarrow \alpha(A) + TiCr_2 + TiFe$$
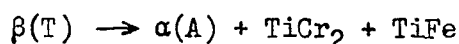
Point T lies in the plane AHI. If extended, the lines AI, TD, TC, and AH would meet at the respective compounds. Tie lines TA, TC, and TD extend from T to each of the phases in equilibrium with beta at the temperature of the ternary eutectoid.

It will be seen, that the eutectoid transformations:

$$\text{ternary } \beta \longrightarrow \text{ternary } \alpha + TiCr_2 \quad \text{and}$$
$$\text{ternary } \beta \longrightarrow \text{ternary } \alpha + TiFe$$
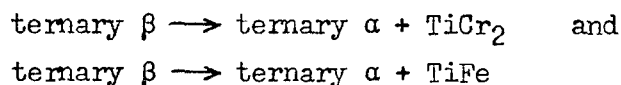
take place within a temperature range (rather than at a constant temperature, as in the binary systems titanium-chromium and titanium-iron), resulting in the formation of the spaces: $\alpha + \beta + TiCr_2$ and $\alpha + \beta + TiFe$. The upper surfaces of these spaces are identical with the lower surfaces of the beta space, and their lower surface is the horizontal plane representing the temperature of the ternary eutectoid.

Fig. 44 – Space Model of the Solid State Reactions in the System
Titanium-Chromium-Iron

c. Isothermal sections

Isothermal sections at temperatures between 900° and 550°C are presented in Figs. 45-51, respectively. Figure 52 shows the isotherms of the lower surfaces of the beta phase space; thus, it compares all the isothermal sections. At 900°C, Fig. 45, the beta field extends over almost the entire composition area investigated. The transition from transformed to retained beta after water quenching these specimens is shown as a shaded line. This appears to be a straight line joining the similar transition points in the binary systems; that is, between 3 and 4% iron, and 6 and 7% chromium. The samples of lower alloy content transformed partially or completely during water quenching, and those of higher alloy content consisted entirely of retained beta. Sections through the space model at 800°, 750°, and 700°C (Figs. 46-48) show the enlargement of the $\beta + \alpha$ and $\beta +$ compound fields.

The exact location of the ternary phase boundaries at 650°C and below is greatly impeded by the fact that the rate of diffusion at these temperatures is extremely low. Even annealing times up to a month's duration are not sufficient to start and/or complete the eutectoid decompositions: $\beta \rightarrow \alpha + TiCr_2$ and $\beta \rightarrow \alpha + TiFe$, in the chromium-rich and iron-rich binary alloys, respectively. As a consequence, the ternary beta phase remains in a metastable state and only in the hypereutectoid alloys rich in chromium was microscopic evidence found of the eutectoid transformation $\beta \rightarrow \alpha + TiCr_2$.

In the iron-rich ternary alloys, the eutectoid decomposition $\beta \rightarrow \alpha + TiFe$ will start below the eutectoid temperature of the titanium-iron system (585°C). Therefore, it is not surprising that at these low temperature levels equilibrium is approached only at a very low rate.

The solubility of iron and chromium in alpha titanium is less than 1% total alloy content. The curve of maximum solubility has been arbitrarily drawn at equal iron and chromium contents.

The eutectoid point in the titanium-chromium system (E_1 in the space model, Fig. 44) occurs at 15% chromium and 685°C. Eutectoid decomposition was observed in ternary alloys on the chromium side, annealed at 650°C. As shown in Fig. 49, many of the hypoeutectoid alloys in the $\alpha + \beta + TiCr_2$ field were actually found to be only two phase. The beta phase is apparently very metastable, for no eutectoid is evident even after annealing at 650°C for 432 hours. The fact that eutectoid decomposition did not occur in the hypoeutectoid alloys of low alloy content was also observed in the binary systems (Figs. 25 and 33).

Alloys of low iron and chromium content could not be used for the determination of the $\alpha + \beta + TiCr_2$ space, because of the reluctance of the eutectoid to develop. However, alloys of composition near the space curve of double saturation (E_{1T}) showed eutectoid decomposition, and could be used to position the space boundary at this temperature level.

Fig. 45 - Partial Isothermal Section at 900°C of the
System Titanium-Chromium-Iron

Fig. 46 - Partial Isothermal Section at 800°C of the
System Titanium-Chromium-Iron

Fig. 47 - Partial Isothermal Section at 750°C of the
System Titanium-Chromium-Iron

Fig. 48 - Partial Isothermal Section at 700°C of the System Titanium-Chromium-Iron
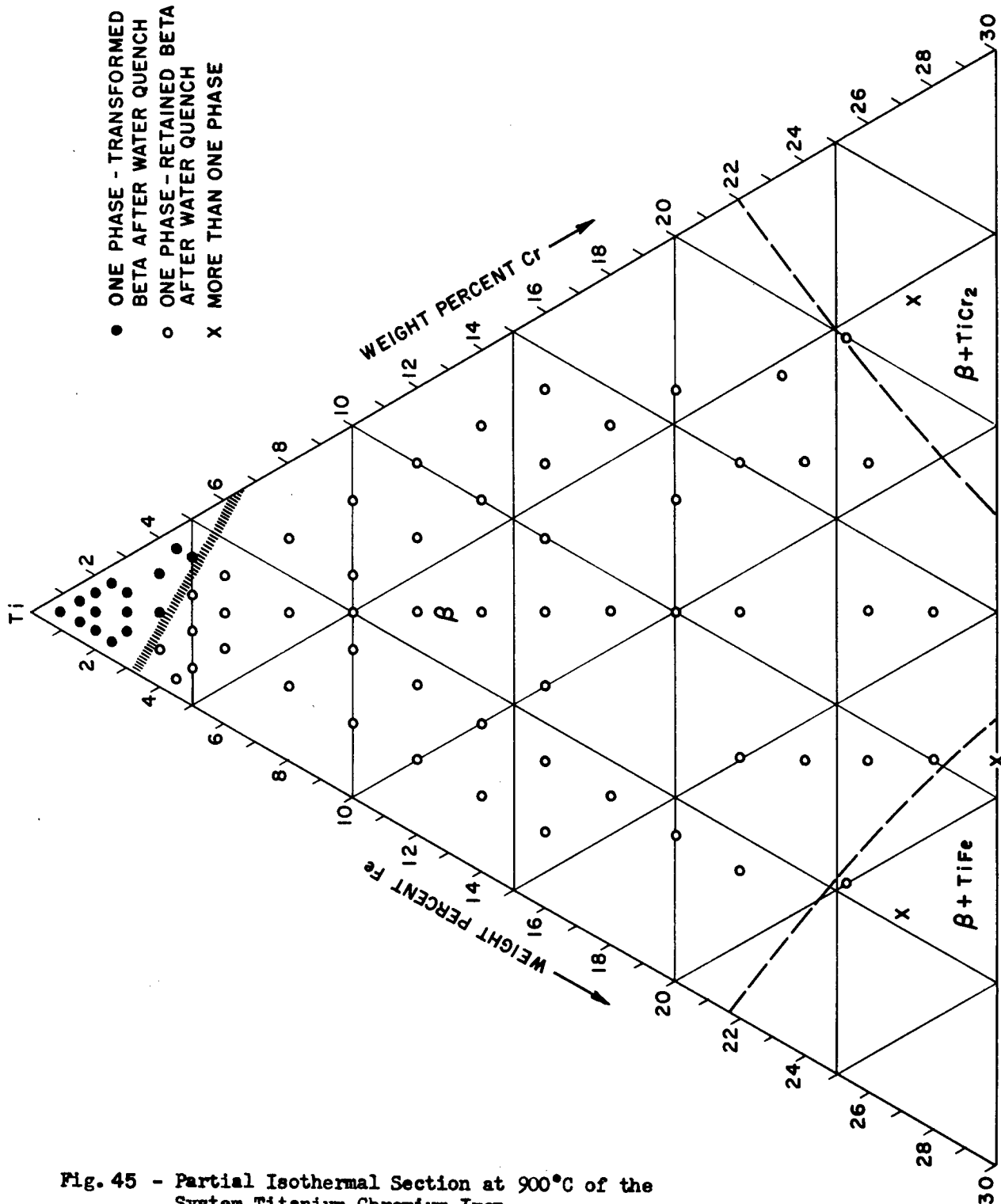
Fig. 49 — Partial Isothermal Section at 650°C
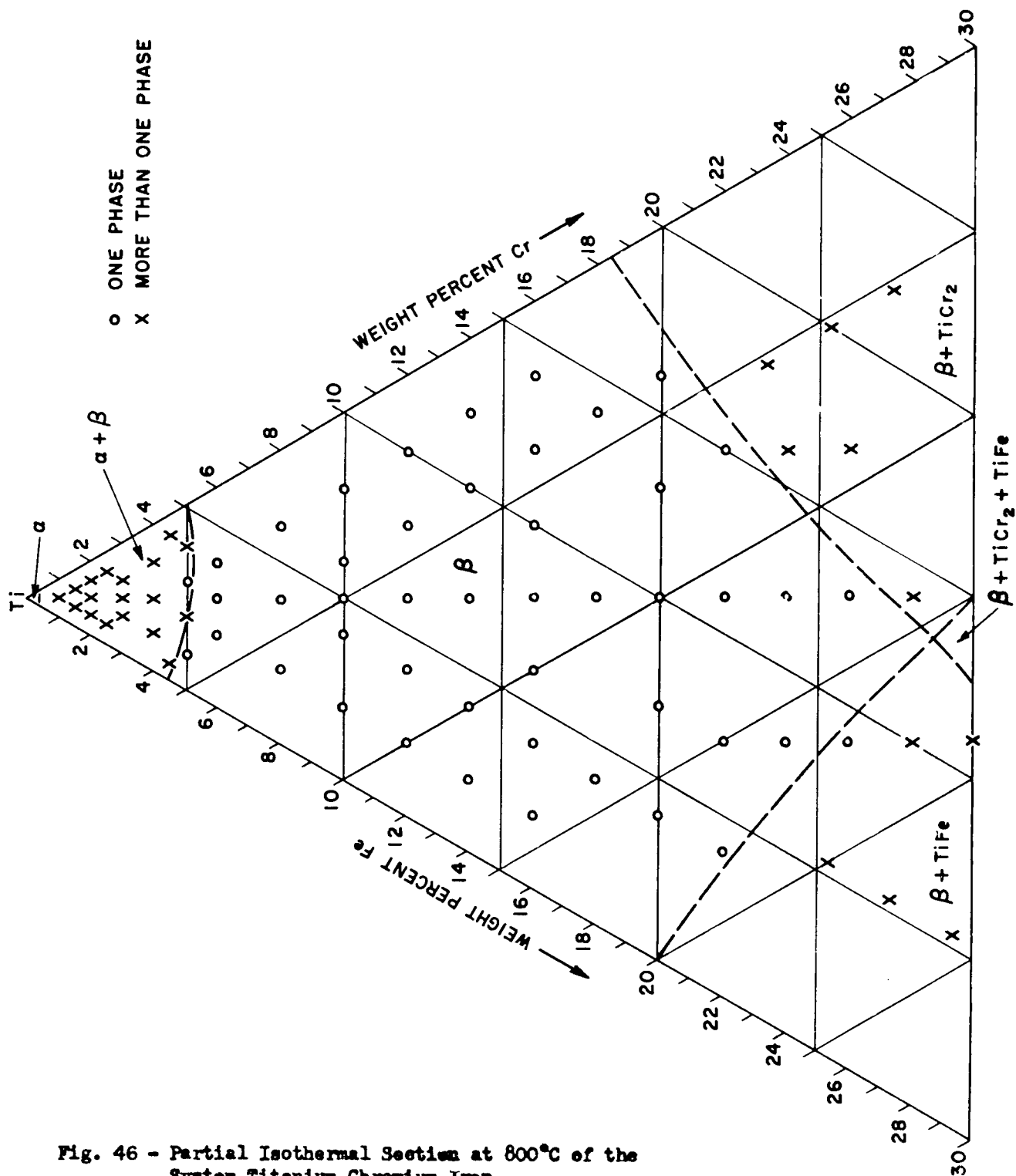of the System Titanium-Chromium-Iron

Fig. 50 - Partial Isothermal Section at 600°C of the
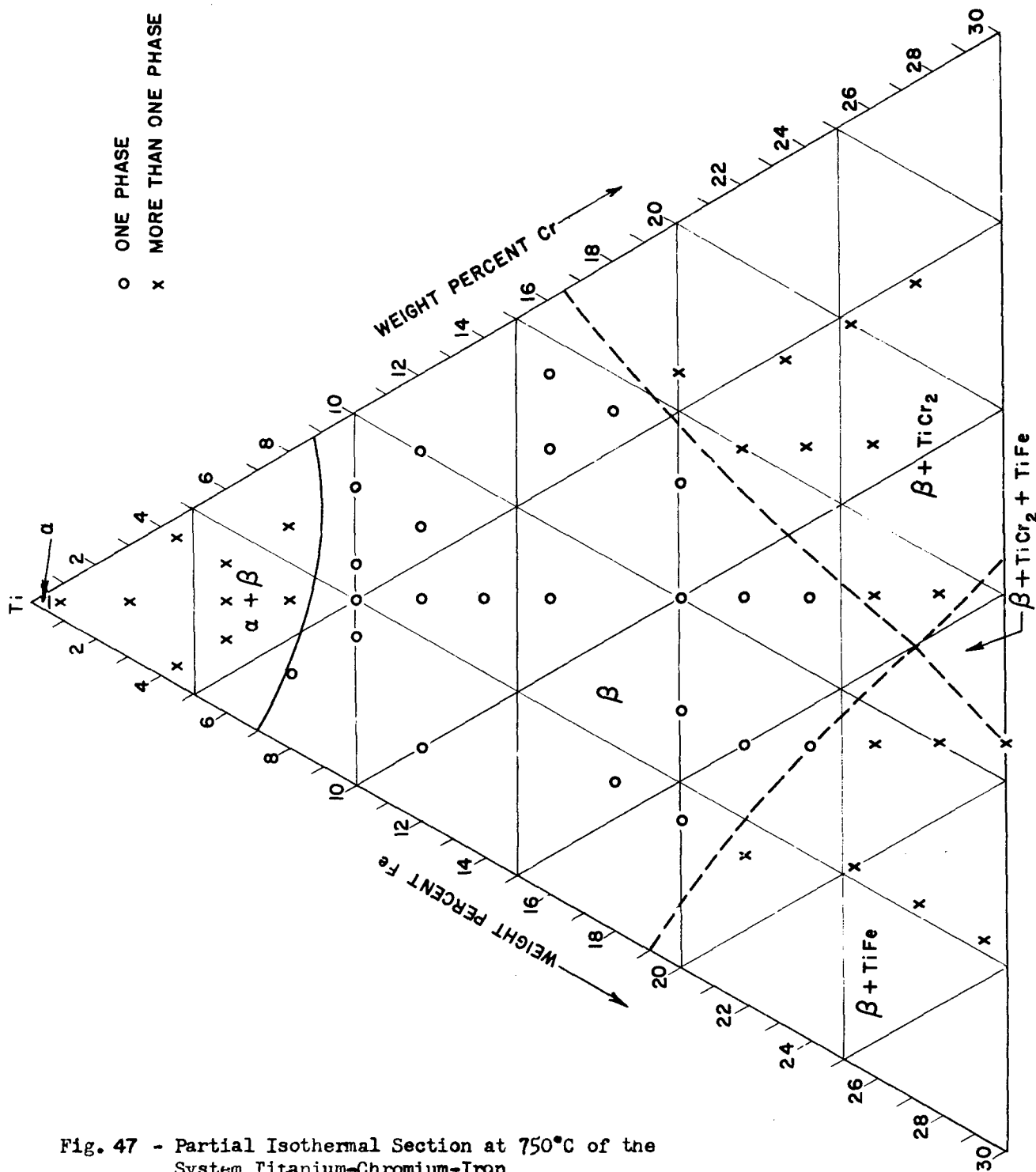System Titanium-Chromium-Iron

Fig. 51 – Partial Isothermal Section at 550°C of the
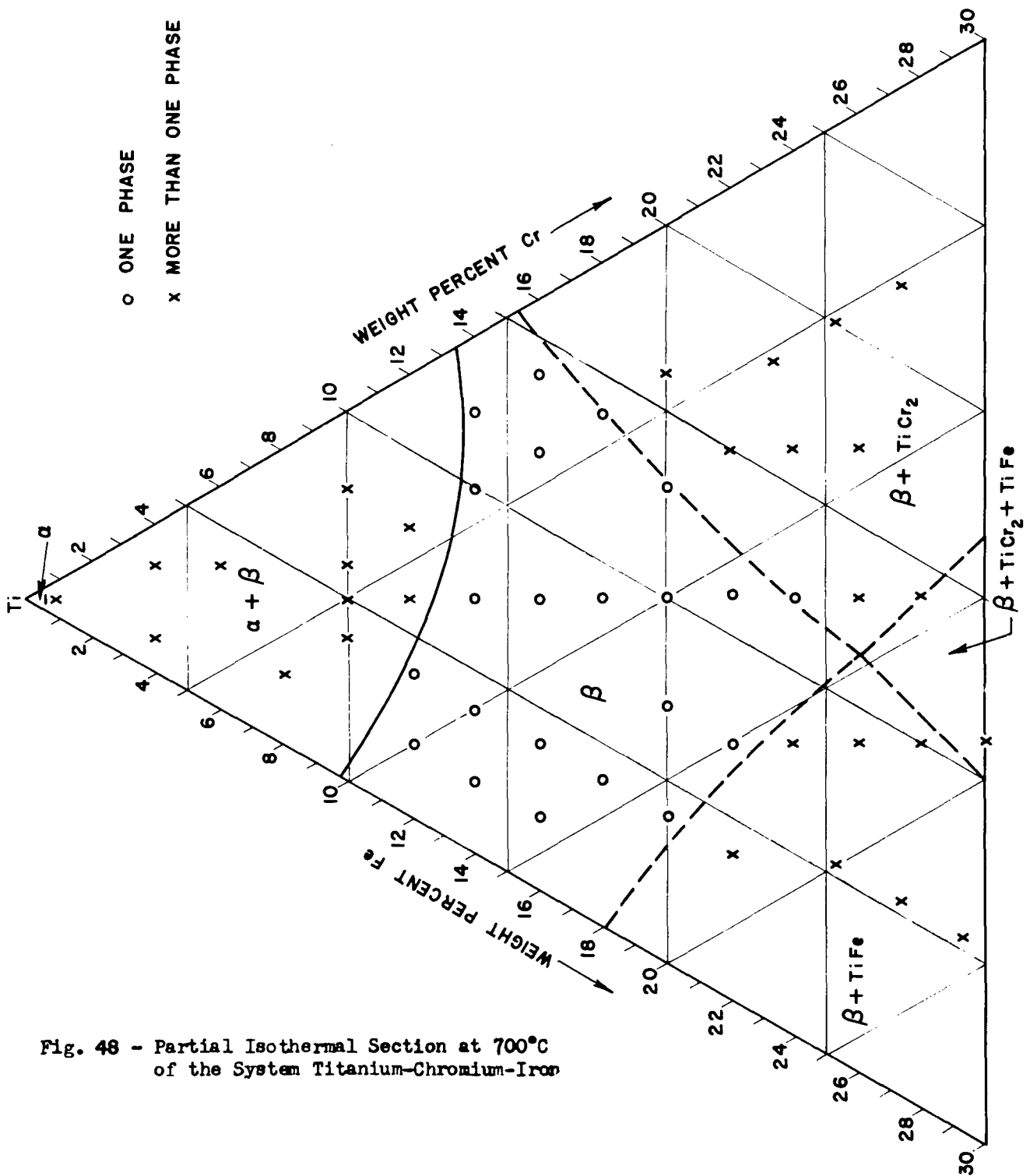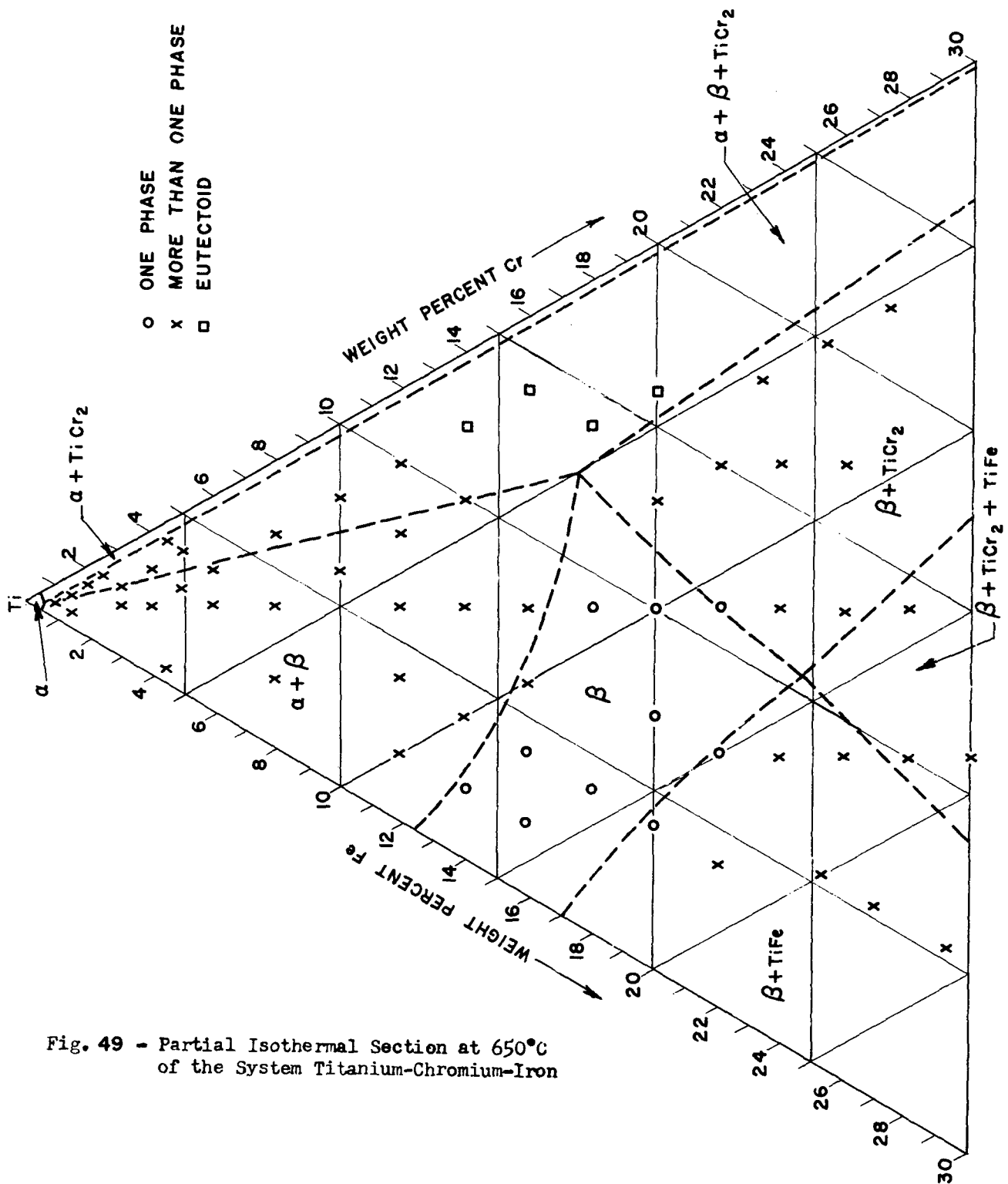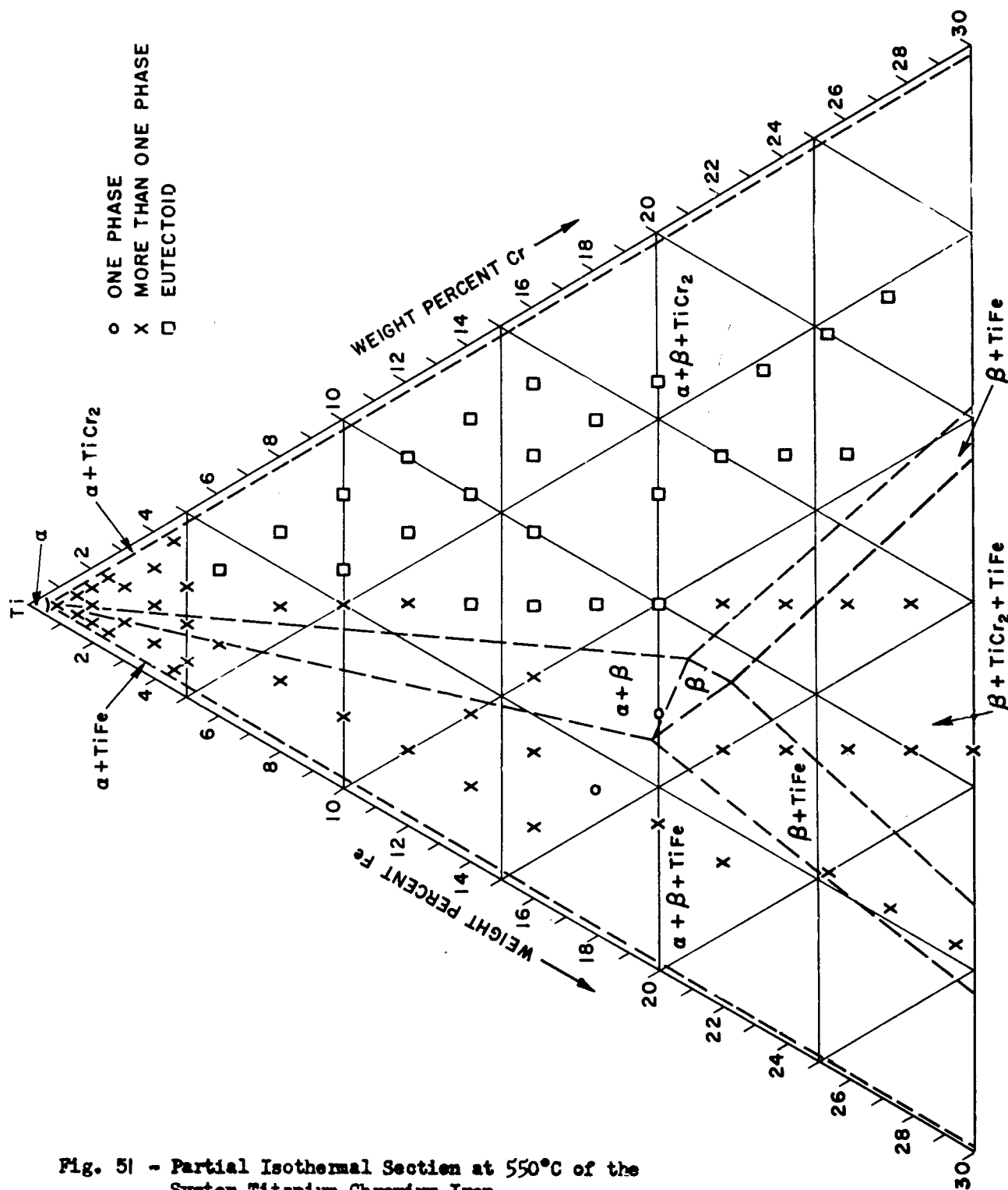System Titanium-Chromium-Iron
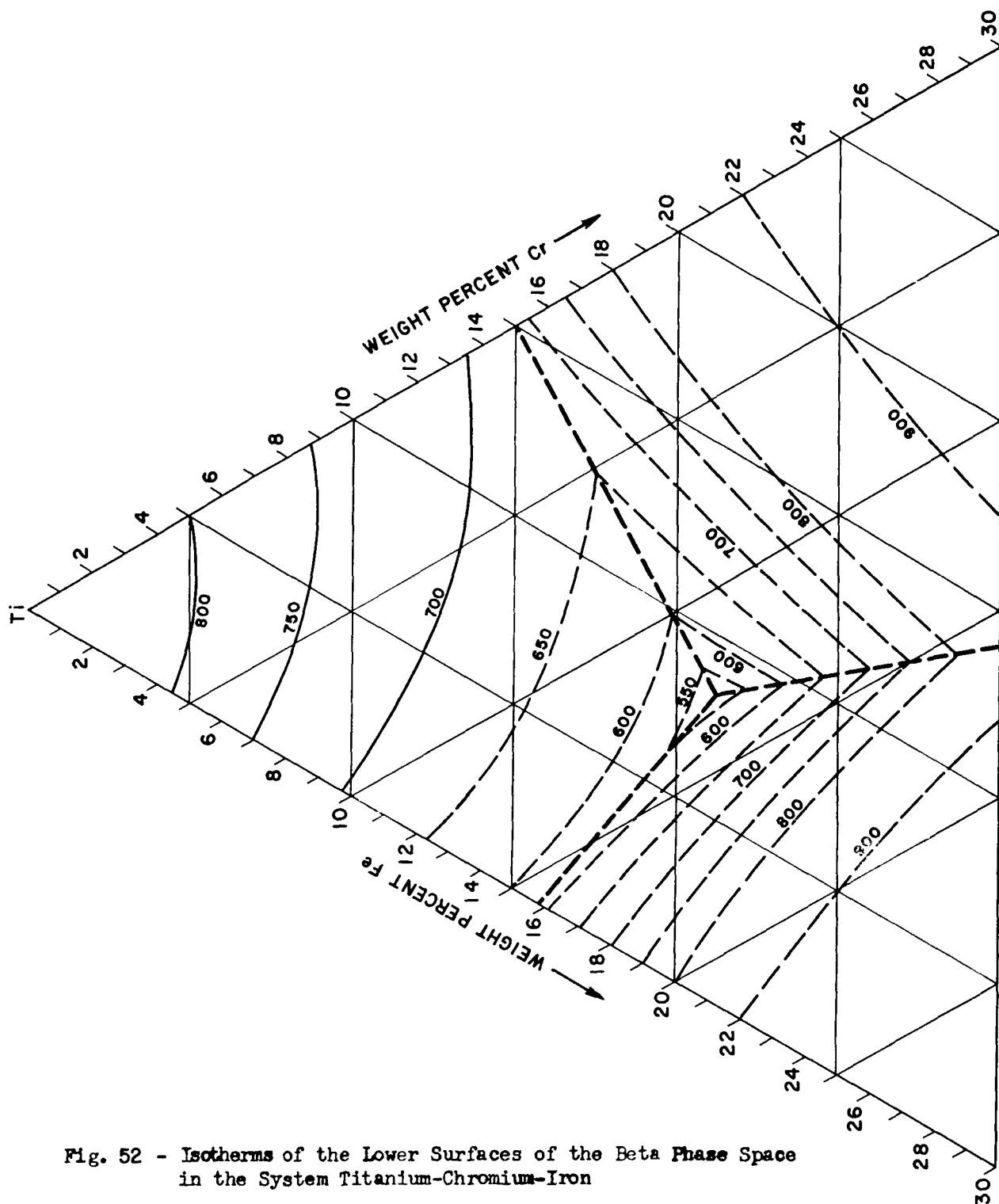
Fig. 52 - Isotherms of the Lower Surfaces of the Beta Phase Space
in the System Titanium-Chromium-Iron

WADC TR 52-16

A three phase space (β + α + TiCr$_2$) of triangular cross section and consistently increasing size with falling temperature exists between the binary and ternary eutectoid temperature levels. The vertex point of this triangular field is on the space curve E_1T, which was positioned by the identification of either alpha or TiCr$_2$ constituents in the microstructures of alloys lying on either side of the curve. The other corners of the three phase field are anchored at alpha and TiCr$_2$.

Only a very narrow duplex phase space exists between alpha and TiCr$_2$, because of the restricted solubility of iron and chromium in alpha titanium. At equilibrium, the eutectoid reaction would be complete in this region, and beta is consumed. No attempt was made to locate the extent of the α + TiFe or α + TiCr$_2$ fields at high alloy contents.

The isothermal section at 600°C (Fig. 50) is similar to that at 650°C, with changes only in the extent of the phase fields. Eutectoid decomposition was observed in a greater number of alloys with falling temperature, although the beta phase in samples of low alloy content continued to be metastable. The section at 550°C (Fig. 51) is below the binary titanium-iron eutectoid level, 585°C; therefore, the β + TiFe and α + β + TiFe fields should be evident. It can be seen from the data points that no eutectoid structures were observed in alloys on the iron side annealed at 550°C.

Although not shown, a number of vertical sections were drawn. It was seen from the extrapolation of data above 650°C to lower temperatures that many of the observed two phase samples would consist of three phases under equilibrium conditions. Therefore, graphical interpolation, using all of the data known to approach equilibrium, has been used for the accurate placement of the space curves, particularly on the iron side of the ternary diagram.

At first appearance, the phase boundaries of the isothermal sections below 650°C may not appear to be entirely consistent with the data points. For example, at 550°C (Fig. 51), the microstructure of the 14% iron, 4% chromium alloy is one phase (β), but the alloy is located in the α + β + TiFe phase field. The apparent anomaly can be readily explained on the basis that the composition lies very close to the space curve of double saturation, E_2T (see Fig. 44). Thus, no proeutectoid constituents would be expected in the microstructure, and the indicated beta must be metastable. At equilibrium, the microstructure would show, in addition to the beta, a eutectoid of alpha and TiFe. Other alloys in the α + β + TiFe space, of lower or higher alloy content, had proeutectoid alpha or TiFe plus beta structures. At equilibrium, these samples would also be three phase, due to the eutectoid decomposition of beta.

Figure 52, which is a composite of isotherms of the lower surfaces of the beta phase space, illustrates the good correlation obtained on combining all the results. The ternary eutectoid point has been placed at the intersection of the three curves of double saturation, and is located at approximately 8% chromium, 13% iron, and at a temperature slightly below 550°C.

d. Microstructures

Only a limited number of ternary alloy photomicrographs are presented, as in general microstructures observed were similar to those for the alloys of the binary systems. Typical microstructures representative of the various phase fields are presented in Figs. 53-59. Evidence of the transition from transformed to retained beta is shown in Figs. 53 and 54. Alpha plus beta microstructures are illustrated in Figs. 55 and 56. The first is predominantly alpha, and the second contains mostly retained beta.

Figure 57 illustrates the α + TiCr$_2$ eutectoid structure of the α + β + TiCr$_2$ space. As previously discussed in other sections, no microstructural evidence of eutectoid decomposition in the α + β + TiFe space was observed. Also, no ternary eutectoid decomposition was noted at 500°C, although this temperature is below the ternary eutectoid plane.

Figures 58 and 59 illustrate the β + compound structures; the first contains TiFe and the latter, TiCr$_2$. A marked difference can be seen in the appearance of the two intermediate phases. As shown in the diagram presented, a three phase space containing both compounds exists between the two duplex spaces. The precipitation of the two compounds is a reaction of double saturation: β → TiCr$_2$ + TiFe. Thus, such microstructures would contain the two compounds either in massive form or in a eutectoid type structure. It was anticipated, therefore, that alloys containing β + TiCr$_2$ + TiFe could be properly identified using micrographic analysis.

However, upon careful metallographic examination, only a few alloys appeared to consist of three phases, and for these positive identification was difficult. As it is only at lower temperatures that even a few of the compositions used in this study are in the β + TiCr$_2$ + TiFe field, more alloys of higher alloy content will be prepared and annealed. X-ray diffraction techniques will be employed to determine the extent of this three phase field.

e. Hardness

Vickers hardness data of titanium-chromium-iron alloys annealed at and quenched from temperatures between 900° and 650°C are presented graphically in Fig. 60. The alloys used are on the vertical section through the ternary system such that the iron:chromium ratio is 1:1. These alloys exhibit the same trends observed in the binary systems titanium-iron and titanium-chromium (see Fig. 43). The hardness curves for samples quenched above 800°C reach a peak at about 5% total alloy content, which corresponds to the composition at which beta is retained upon water quenching. At the same temperature level, hardness peaks were obtained at 4% iron and 7-8% chromium in the respective binary systems.

Annealing the ternary alloys at 650° or 700°C resulted in a linear increase in hardness with alloy composition up to 10%. Such alloys have α + β structures, and are much softer than the products obtained by quenching from above the transformation temperature.
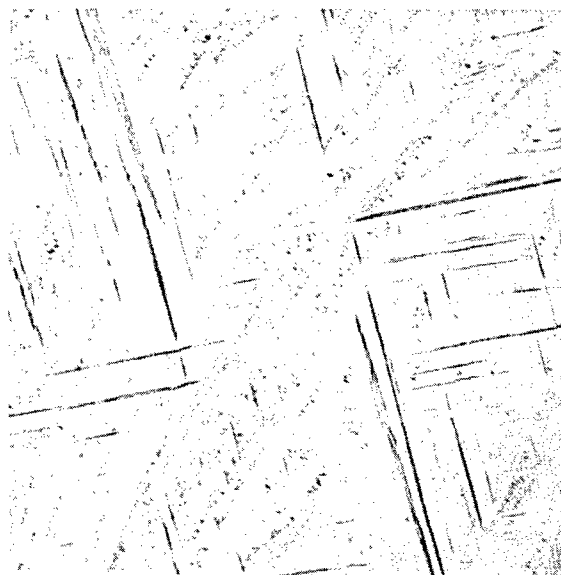
Neg. No. 3879   X250

Fig. 53
A 2% iron, 2% chromium alloy annealed
at 900°C for 72 hours and water
quenched. Shows some transformed β.
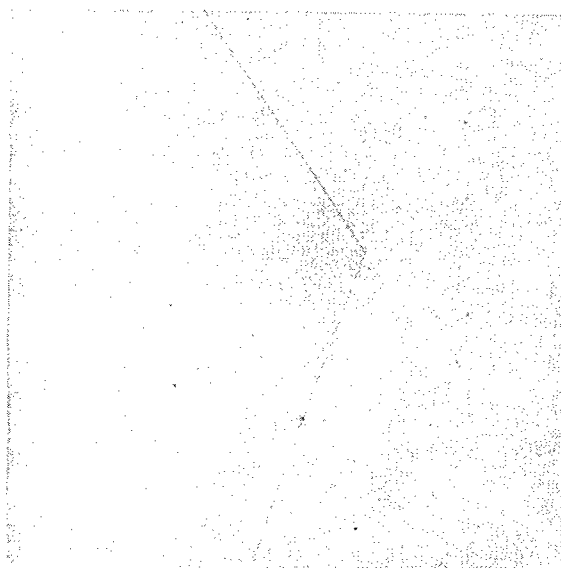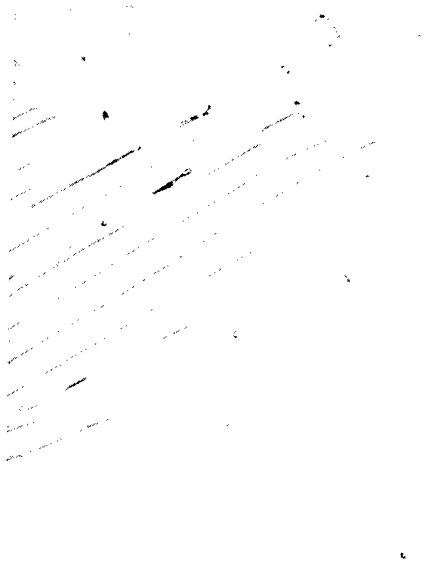
Neg. No. 3880   X250

Fig. 54
A 2% iron, 3% chromium alloy, homo-
genized, annealed at 900°C for 72
hours and water quenched. Retained
β.

Etchant: 60 glycerine, 20 HNO₃, 20 HF

Neg. No. 3881   X500   Neg. No. 3882   X500

Fig. 55   Fig. 56
A 0.5% iron, 0.5% chromium alloy,   A 10% iron, 4% chromium alloy, homo-
water quenched after annealing at   genized, annealed at 650°C for 432
650°C for 432 hours. α + retained   hours. α plates in retained β matrix.
β (approx. 15%).

Neg. No. 3885   X500

Fig. 57
A 2% iron, 12% chromium alloy homo-
genized, annealed at 650°C for 432
hours. Eutectoid (α + TiCr$_2$) and
α in a matrix of retained β.

Etchant: 60 glycerine, 20 HNO$_3$, 20 HF
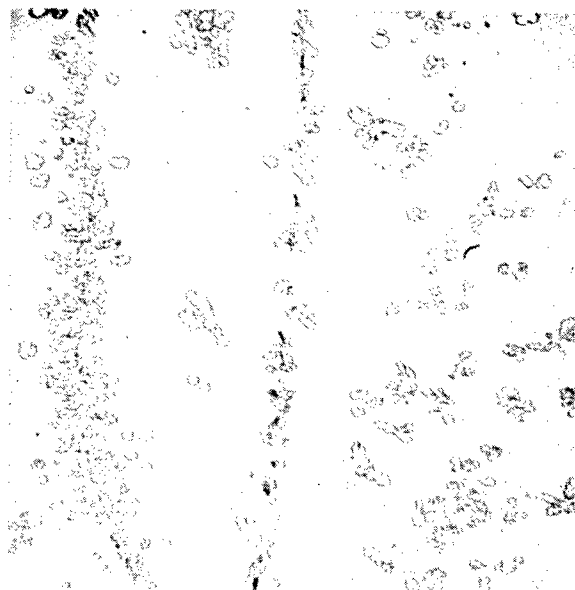
Neg. No. 3883   X500

Fig. 58

An 18% iron, 4% chromium alloy, homo-
genized, annealed at 650°C for 432
hours, and water quenched. β + TiFe.
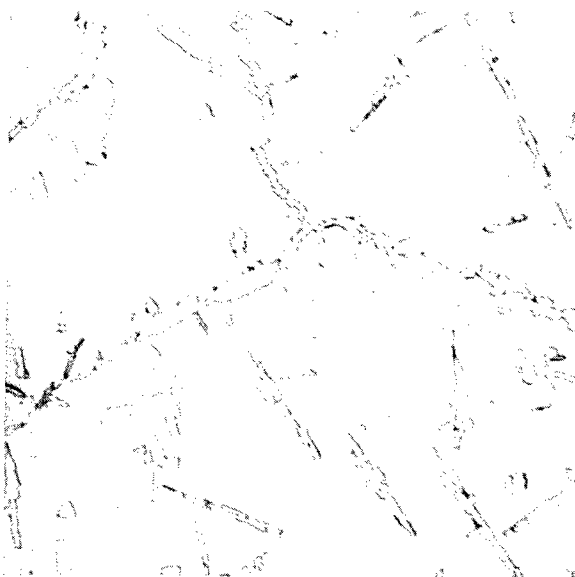
Neg. No. 3884   X500

Fig. 59

An 8% iron, 16% chromium alloy, homo-
genized, annealed at 650°C for 432
hours, and water quenched. β + TiCr$_2$.

Etchant: 60 glycerine, 20 HNO$_3$, 20 HF
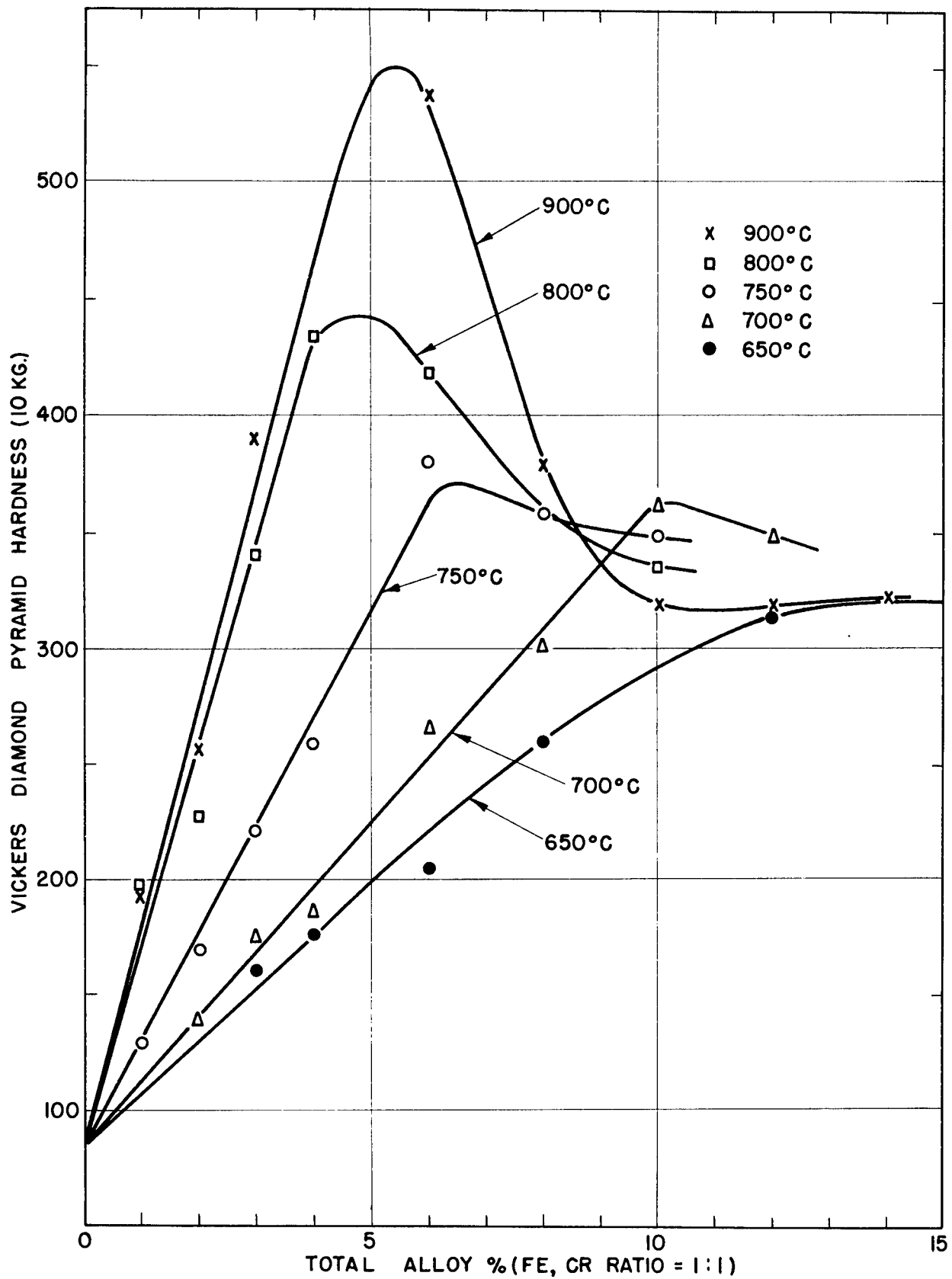
Fig. 60 - Vickers Hardness of Titanium-Chromium-Iron Alloys
(Iron-Chromium Ratio = 1:1)

WADC TR 52-16

It can be seen from Fig. 60 that the hardness of alloys in the lower composition range, i.e. those in the commercial alloy region, may be very greatly changed by heat treatment. The hardness of the 5% alloy annealed at 650°C is 200 DPN, but quenching the same alloy from 900°C resulted in a hardness of over 500 DPN.

C.   The Titanium-Oxygen System

The literature contains several papers concerning the compounds existing in the titanium-oxygen system (20-23). The bulk of this information is concerned with chemical and structural identification of the following phases:

1.   TiO, having a crystal lattice of the NaCl type with a melting point of 1750°C.

2. Ti_2O_3, having a corundum type crystal lattice.

3. TiO_2, which is stable in the following modifications: rutile and anatase I, II which are tetragonal; brookite, which has an orthorhombic structure.

Anatase II changes at 642°C into anatase I, which is stable up to 915°C, where rutile becomes the stable modification. Rutile is the most stable form of TiO_2, and will usually exist below 915°C with the transformation to anatase I being suppressed. At 1300°C, rutile transforms to brookite, which melts at 1900°C.

The phases present in the system up to the composition of the dioxide TiO_2, and their approximate ranges of homogeneity as determined by Ehrlich (21, 22, 23), are shown in Fig. 61. These data were obtained by X-ray analysis of samples prepared by sintering mixtures of titanium with TiO and/or TiO_2 at 1500°-1600°C in vacuum, followed by furnace cooling and a two-day anneal at 750°C. Ehrlich showed that approximately 29.5 atomic per cent oxygen are soluble in alpha titanium.

The first intermediate phase, TiO, was shown to have a homogeneity range from 38 to 55.5 atomic per cent (17-29.3 wt.%) oxygen. The next intermediate phase, based on the composition Ti_2O_3 (60 at.% oxygen), was stable between 59.3 and 61.3 atomic per cent (32.5 and 34.5 wt.%) oxygen.

Ehrlich placed a new phase, having a heavily distorted rutile lattice, between 63 and 64.2 atomic per cent oxygen. The lower limit of TiO_2 was located at 65.5 atomic per cent oxygen.

The phase relationships in titanium-rich alloys containing up to 1 weight per cent (3 at.%) oxygen have been studied by Jaffee, Ogden and Maykuth (24) by micrographic analysis of annealed and quenched alloys. They found that the α/β transformation temperature is raised with increasing oxygen content.

In reporting the effects of small oxygen additions on the mechanical properties of iodide titanium, Jaffee and Campbell (25) observed that
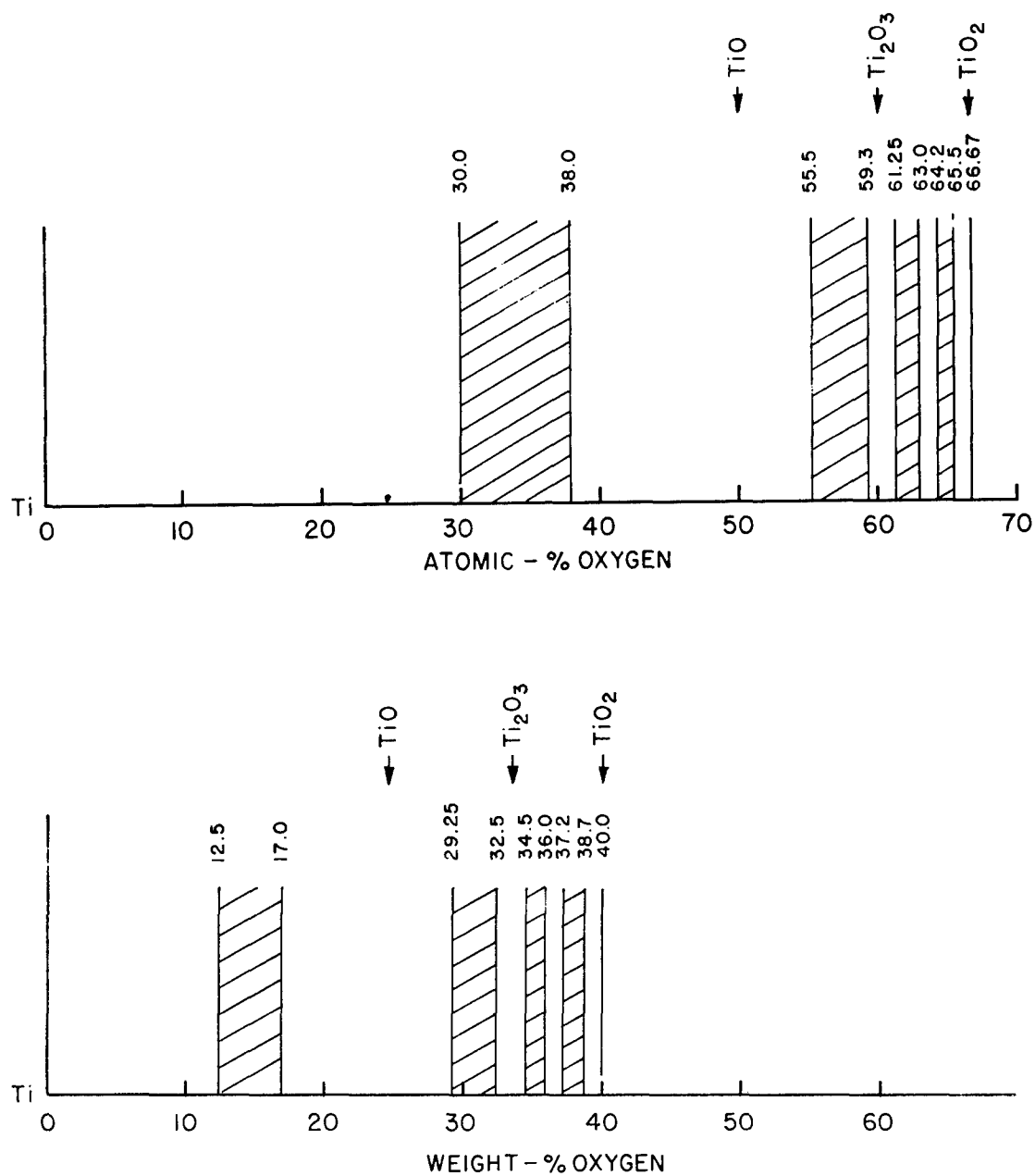
Fig. 61 - Phases and Phase Ranges in the System Titanium-Oxygen (Ehrlich)

oxygen refines the structure, making the plates of alpha titanium smaller and the Widmannstätten pattern more regular. This was also confirmed by Sutcliffe (26).

Using X-ray diffraction and micrographic methods, Womer (27) confirmed Ehrlich's value of approximately 12.5 weight per cent (30 at.%) oxygen being soluble in alpha titanium. He also observed that oxygen addition increased the transformation temperature. More recently, Jenkins and Womer (28) established the limits of the α + β region up to 5 atomic per cent oxygen by means of measurements of thermoelectric power at various temperatures, and verified their results by micrographic analysis.

The titanium-oxygen phase diagram as presented here was determined by micrographic analysis of alloys containing 0.2-30.0 weight per cent oxygen, annealed at and quenched from temperatures between 700° and 1850°C. Solidus and X-ray diffraction data are also presented.

1.   Experimental procedure

a.   Preparation of alloys

The alloys were prepared by the copper block melting method. The charges consisted of 1/4 inch sections of iodide titanium previously rolled to 1/16 inch sheet, and 1/4 inch lumps of fractured compacts of high purity TiO$_2$. It was found that by proper placing of the charge in the copper block, the arc (previously started against the tungsten insert) could be easily transferred to the charge. Even pure TiO$_2$ was easily melted by this method. Weight losses could not be used as a basis for judging the   ssible variance in composition on melting, because ingots of the brittle high-oxygen alloys spalled badly when the arc was struck during the remelting operations. However, analytical results for a number of alloys (see Table X) showed very good agreement with nominal compositions. As the nominal values are well within the accuracy of the analytical results, the phase diagram as presented is based on nominal compositions. Alloys were prepared having the following nominal oxygen contents: 0.2, 0.4, 0.6, 0.8, 1 . . . 40 (1% increments).

TABLE X

CHEMICAL ANALYSIS OF AS-CAST TITANIUM-OXYGEN ALLOYS

Heat No.	Nominal % Oxygen	Analyzed % Oxygen
1198	3.0	3.3
1	4.0	4.2
	10	9.9
	14	14.0
1213	15	15.5
1215	17	16.4
1217	19	18.5
1218	20	20.1
1219	21	21.6
1222	24	23.7

The following color variations were recorded by visual observation of the as-cast surface of the ingots:

TABLE XI

APPEARANCE OF TITANIUM-OXYGEN ALLOY INGOTS

Composition Range, % 0	Color
1-11	Shiny metallic luster (silvery)
12-19	Dull metallic luster (silvery)
20-21	Dull metallic luster (possible tinge of yellow)
22-30	Shiny metallic luster changing from tinge of yellow at 22% to deep gold at 30% oxygen
31-33	Shiny metallic luster changing from gold to purple (mixture) with increasing oxygen contents
34-36	Frangible shiny shell rubbed off easily, leaving dull nonmetallic purple substance
37-38	Nonmetallic blue
39-40	Bluish rutile luster (almost metallic)

b.   Annealing treatments

Annealing treatments consisted of sealing samples in Vycor or quartz capsules, heating to temperatures ranging from 700° to 1500°C, followed by water quenching (see Table XII). Short time annealing treatments at 1600°C and above were accomplished by heating a series of samples in a molybdenum sheet container in a high frequency induction furnace under vacuum conditions and quenching onto a water cooled brass plate at the bottom of the furnace. The temperature control at these high temperatures was of the order of ±25°C. The rate of heating varied considerably with the age of the tantalum heater of the furnace, with an approximate average rate of 20°C per minute in the temperature range 1500°-1900°C. At these high temperatures, the holding times were quite short and were limited by the accuracy of control of the induction unit. Therefore, the metallographic results obtained on samples treated above 1500°C may not be as accurate as those at lower temperatures. The accuracy is limited by the short heating times (questionable equilibrium conditions) and limited temperature control.

TABLE XII

ANNEALING CONDITIONS FOR TITANIUM-OXYGEN ALLOYS

Annealing Temperature, °C	Time, Hours	Container	Atmosphere
700	300	Vycor	Vacuum
800	120	Vycor	Vacuum
800	500	Vycor	Vacuum
900	70	Vycor	Vacuum
900	24	Vycor	Vacuum
950	72	Vycor	Vacuum
1000	24	Vycor	Vacuum
1100	24	Quartz	Argon
1200	4	Quartz	Argon
1300	1	Quartz	Argon
1400	2	Quartz	Argon
1500	1/2	Quartz	Argon

It had been reported that titanium-oxygen alloys lose oxygen at elevated temperatures. A check was made to verify this by weighing samples before and after annealing. This was done for a complete series of alloys from 1 to 40% oxygen annealed at 1200°C and 1400°C for four hours and one hour, respectively. Weight losses after annealing at these temperatures varied from 0 to 3% of the total weight of the specimen, with no apparent correlation with the composition of the alloy. This same amount of weight loss was obtained for unalloyed titanium control samples included with the series. It was concluded from these data that little, if any, oxygen was lost during annealing treatments up to 1400°C, under the conditions of testing used.

A further and more conclusive check of possible oxygen losses at elevated temperatures was made by X-ray diffraction methods. Diffraction patterns for 5, 7, and 11% oxygen alloys quenched from 1850°C showed identical lattice parameter measurements, for the same series of alloys quenched from 900°C.

2. Discussion of Results

a. The phase diagram

The essential features of the phase diagram presented in Fig. 62 are two peritectic reactions: Melt + $\alpha \rightleftarrows \beta$, and Melt + $\alpha \rightleftarrows$ TiO, at 1740° and 1770°C, respectively; and a peritectoid reaction: α + TiO $\rightleftarrows \delta$ at approximately 925°C. Alpha titanium has a maximum melting temperature of about 1900°C at 10% oxygen (approx. 25 at.% O). The maximum solubility of oxygen in alpha titanium is approximately 14.5% oxygen between 700° and 1600°C. The $\alpha + \beta$ field extends from 0% oxygen at 885°C to the peritectic temperature, 1740°C. At this temperature, the two-phase field
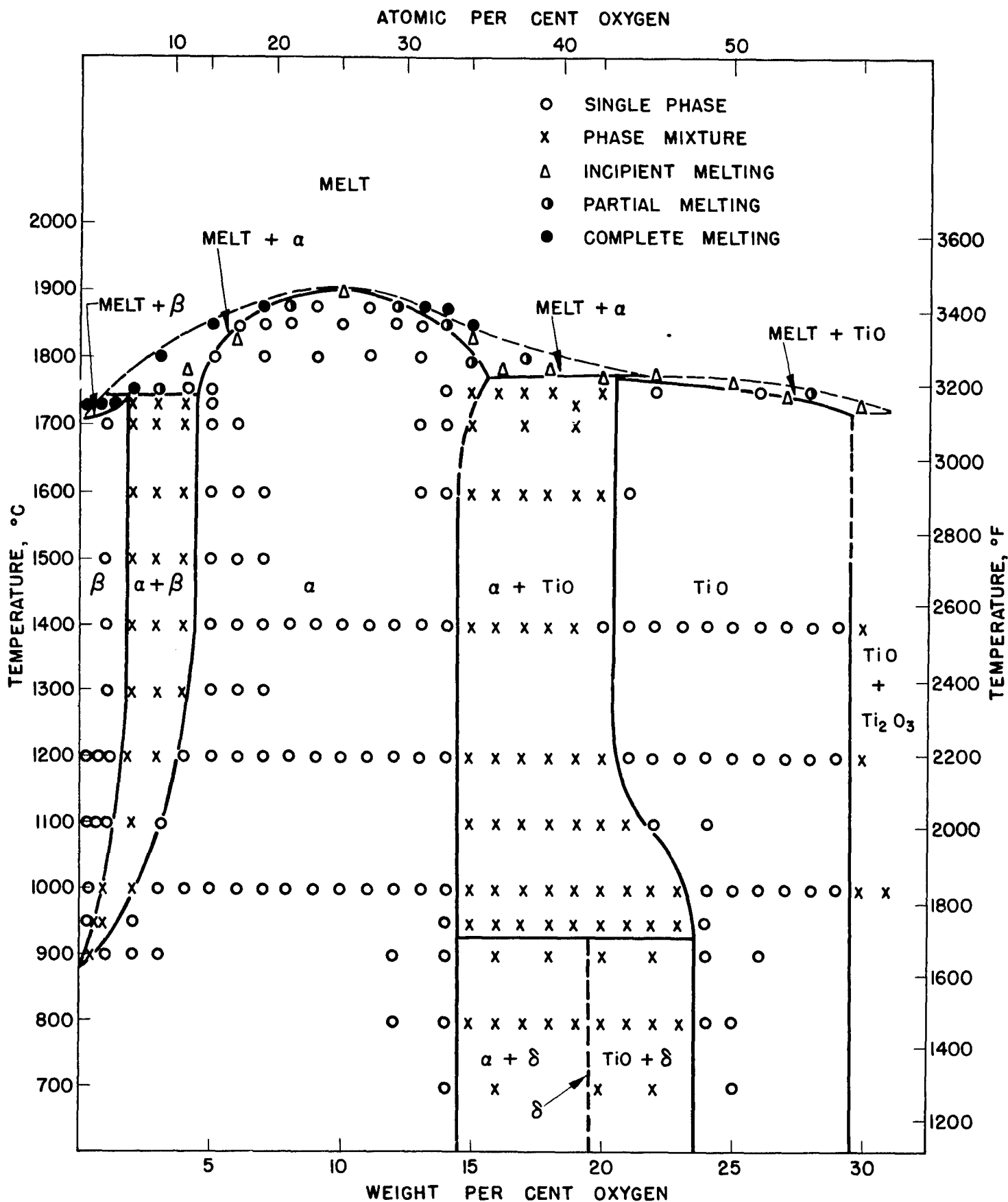
Fig. 62 – Partial Phase Diagram of the Titanium-Oxygen
System

extends between approximately 1.8 and 4.3% oxygen. The titanium-rich section of the equilibrium diagram, shown in Fig. 63, depicts the effect of dilute solutions of oxygen on the transformation temperature from 885° to 1500°C.

The intermediate phase, TiO, is homogeneous over a broad range of composition from about 20.5 to 29.5% oxygen at 1400°C, and from about 23.5 to 29.5% oxygen at 800°C. At about 925°C, an intermediate phase, delta, forms from the peritectoid reaction α + TiO $\rightleftarrows$ δ, between 18 and 20% oxygen. This composition range includes the stoichiometric ratios corresponding to the formulas Ti_3O_2 (18.2%) and Ti_4O_3 (20.0%).

b. Structural characteristics

Microscopic studies involved the evaluation of both etched and unetched structures as revealed by means of ordinary reflected light and polarized light, respectively. Typical microstructures illustrating various phase fields depicted in the diagram are shown in Figs. 64-80.

Illustrations of structures characteristic of alloys quenched from the beta field are shown in Figs. 64 and 65. A 0.2% oxygen alloy quenched after 48 hours at 950°C revealed a serrated alpha type of transformation structure, as shown in Fig. 64. Specimens quenched from the beta field but with compositions nearer the β/α + β boundary showed a basket weave type of transformation structure (Fig. 65). This transformed beta structure was coarser, the higher the temperature of treatment, as shown in Fig. 66.

Microstructures of alloys quenched from the α + β field are shown in Figs. 67-69. At 1000°C, the amount of alpha phase in a 1.0% alloy was estimated as approximately 30%. The α + β structure, as shown in Fig. 67, indicates that the white alpha phase was present at the temperature of treatment and the dark structure in the interstices was formed by the transformation of the beta phase during the quench. Figure 68 shows that the last traces of beta occur essentially at the alpha grain boundaries. Aside from extensive growth of constituents, the high temperature α + β structures are similar to those of alloys quenched from the lower temperature (Fig. 69).

The structure of the alpha phase of a 12% oxygen alloy quenched from 1200° and 1850°C, respectively, is shown in Figs. 70 and 71.

The α + TiO mixture is characterized by banded twin-like structures. Near the α/α + TiO phase boundary small patches of a banded structure were observed in the alpha titanium matrix (Fig. 72). The structures of alloys containing 16-18% oxygen consisted almost entirely of plate-like bands, as shown in Figs. 73 and 75. On the basis of Ehrlich's (22) investigations and X-ray diffraction studies carried out in connection with this work, this banded structure was interpreted to be a mixture of the alpha phase and TiO. It was impossible to delineate between the two phases. Annealing at 1700°C coarsened the structure considerably (Fig. 74), but there was no tendency for the phases to coagulate. Figure 75
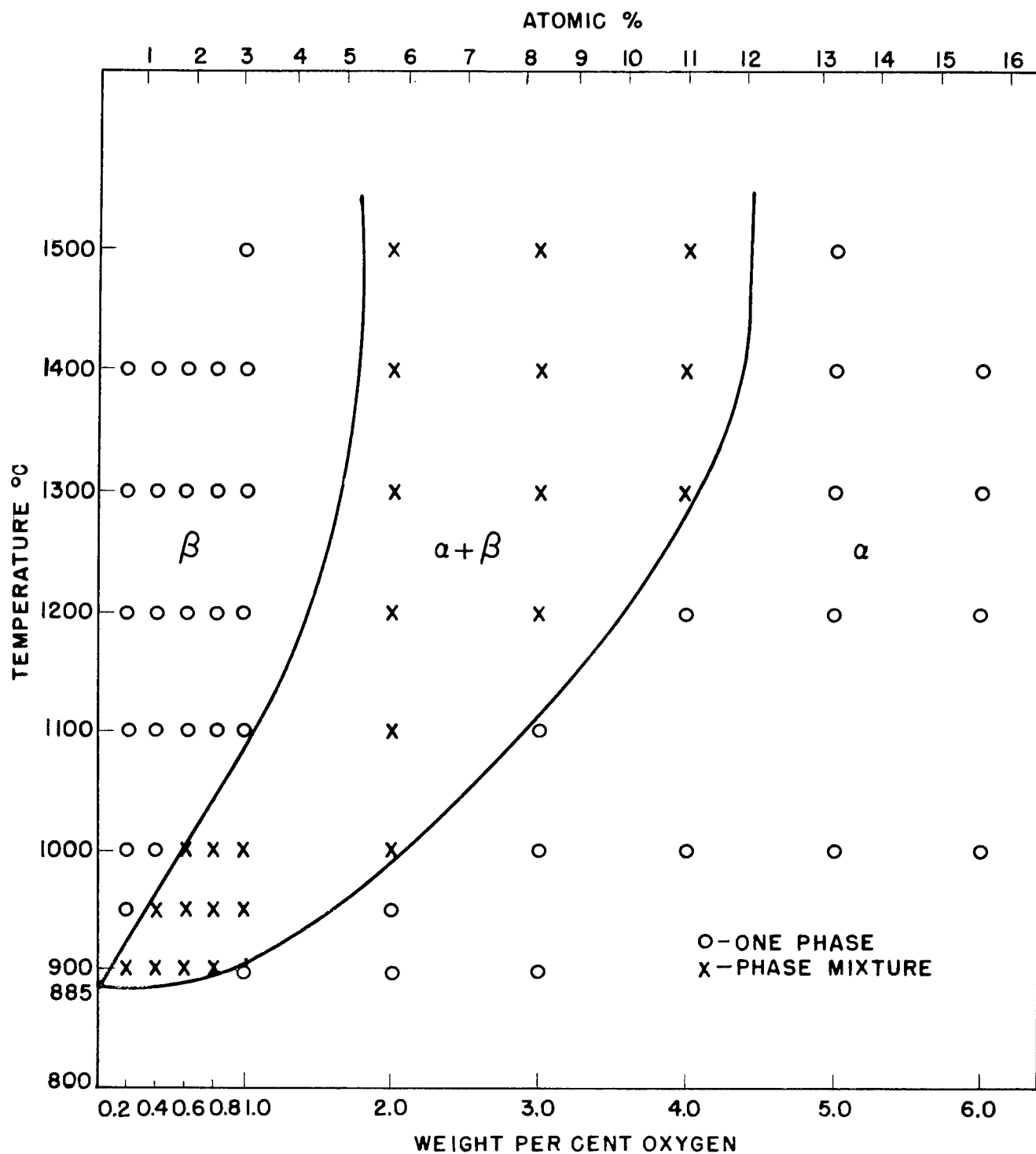
Fig.63 - Titanium Rich Portion of the Titanium-Oxygen System
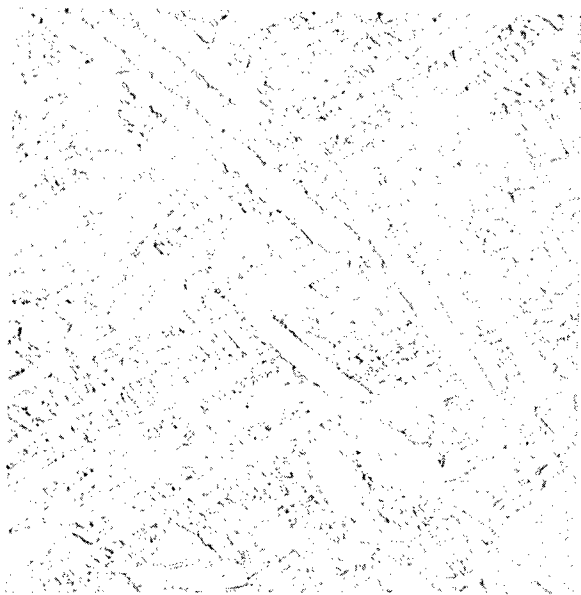
Neg. No. 3903   X150
              Fig. 64
A 0.2% oxygen alloy quenched after
48 hours at 950°C, showing a serrated
α type of transformation structure.
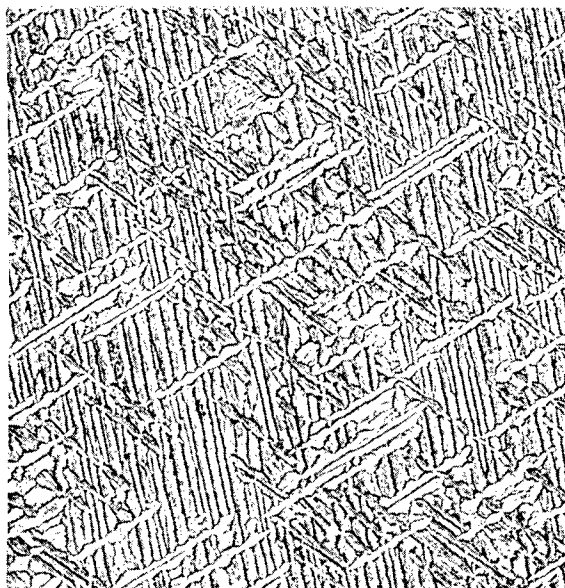
Neg. No. 3611   X150
              Fig. 65
A 1.0% oxygen alloy quenched after
4 hours at 1200°C. Structure re-
veals a typical basket weave type
of transformation structure.
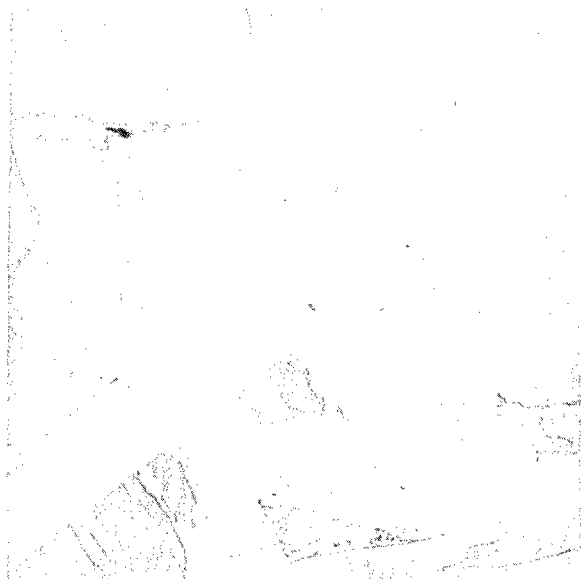
Neg. No. 3752   X 75
              Fig. 66
A 0.8% oxygen alloy quenched from
1700°C. Structure shows an extremely
coarse transformation structure.

Neg. No. 3656   X150
              Fig. 67
A 1.0% oxygen alloy quenched after
24 hours at 1000°C. Structure shows
approximately 35% α in a transformed
β matrix.

Etchant: 60 glycerine, 20 HF, 20 HNO$_3$

Neg. No. 3657   X150

Fig. 68

A 2.0% oxygen alloy quenched after
24 hours at 1000°C. Structure shows
approximately 95% α, with transformed
β in the grain boundaries.
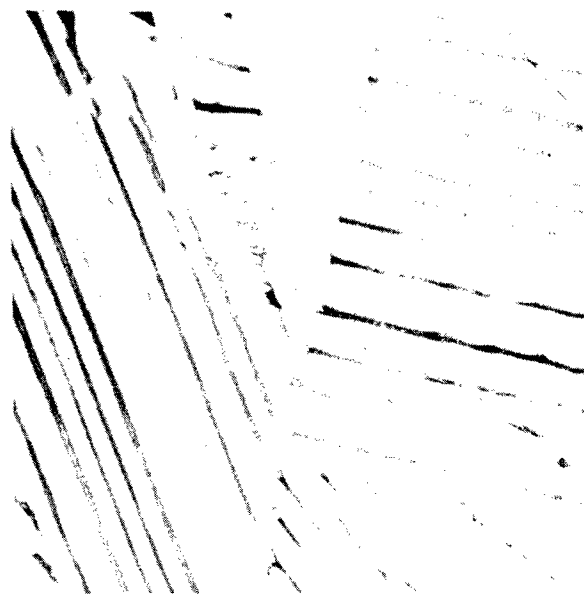
Neg. No. 3753   X 75
                          Unetched
Fig. 69

A 3.0% oxygen alloy quenched from
1700°C. Structure shows duplex α
(white) plus transformed β (dark).
Note the large grain growth.

Neg. No. 3612   PL, X 75

Fig. 70

A 12% oxygen alloy quenched after 4
hours at 1200°C. Structure shows
polyhedral grains of α titanium solid
solution.

Neg. No. 3754   PL, X 75

Fig. 71

A 12% oxygen alloy quenched from
1850°C. Large equiaxed grains of
α titanium existing at a tempera-
ture higher than the melting point
of pure titanium.

Etchant: 60 glycerine, 20 HF, 20 HNO$_3$

Neg. No. 3646   PL, X 75
                                Unetched
            Fig. 72
A 15% oxygen alloy quenched after 4
hours at 1200°C. Structure shows
patches of banded α + TiO phase
mixture in α titanium matrix.

Neg. No. 3614   PL, X 75
                                Unetched
            Fig. 73
A 17% oxygen alloy quenched after 4
hours at 1200°C. Nearly 100% twinned
structure of a two phase mixture of
α + TiO.

Neg. No. 3755   PL, X 75
                                Unetched
            Fig. 74
A 17% oxygen alloy quenched from
1700°C. Coarse banded structure
characteristic of the α + TiO field.
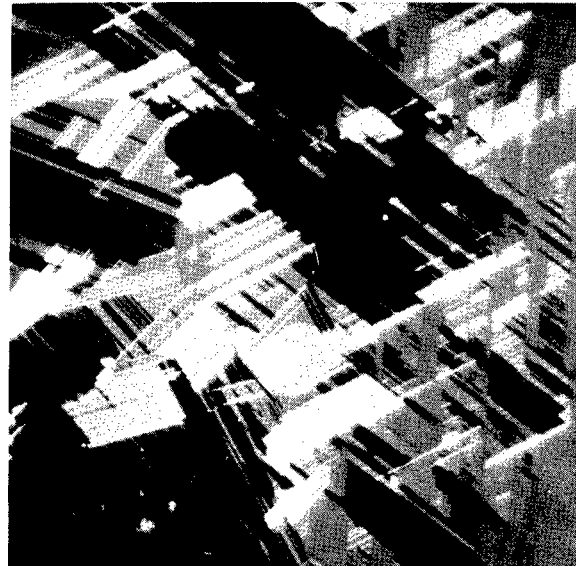
Neg. No. 3748   PL, X500
                                Unetched
            Fig. 75
A 17% oxygen alloy quenched after
2 hours at 1400°C. Banded α + TiO
structure at higher magnification.

Neg. No. 3615   PL, X 75
   Fig. 76   Unetched
A 19% oxygen alloy quenched after 4
hours at 1200°C. α + TiO phase with
traces of massive α at grain bound-
aries. Note decreased amount of twin-
ning.
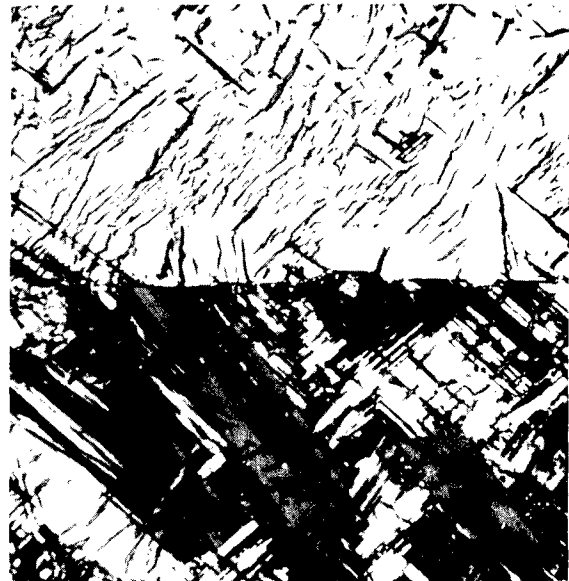
Neg. No. 3768   PL, X150
   Fig. 77   Unetched
An 18% oxygen alloy quenched after
120 hours at 800°C. Structure shows
the precipitated δ phase with the
banded α + TiO structure in the back-
ground.
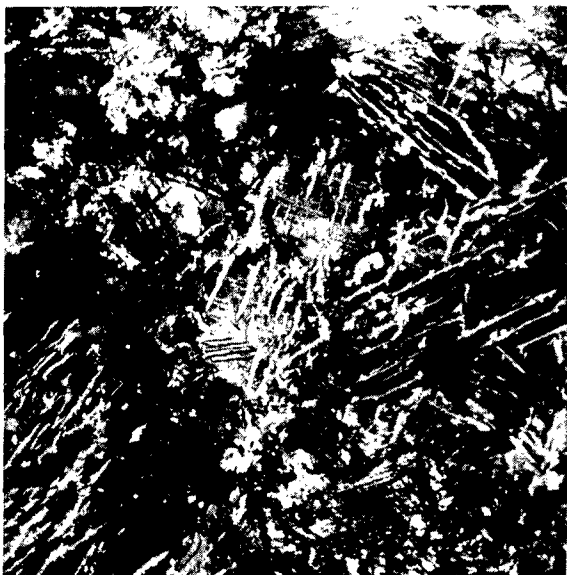
Neg. No. 3904   PL, X150
   Fig. 78   Unetched
A 20% oxygen alloy quenched after
500 hours at 800°C. Approximately
20% δ phase precipitated in a TiO
matrix.
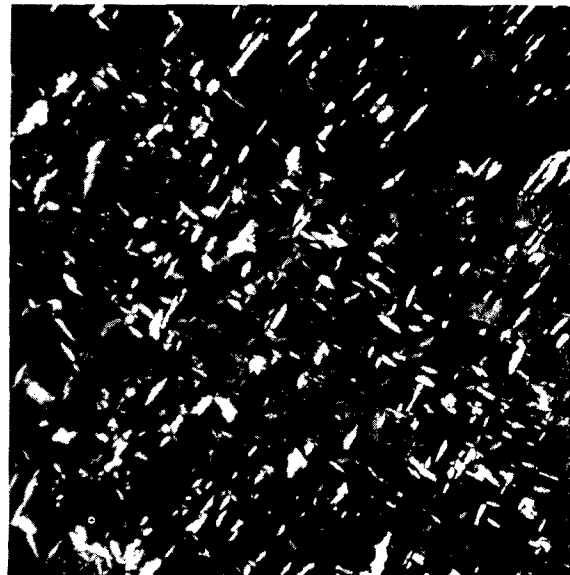
Neg. No. 3769   PL, X150
   Fig. 79   Unetched
A 22% oxygen alloy quenched after
120 hours at 800°C. Small particles
of δ phase in a TiO matrix.
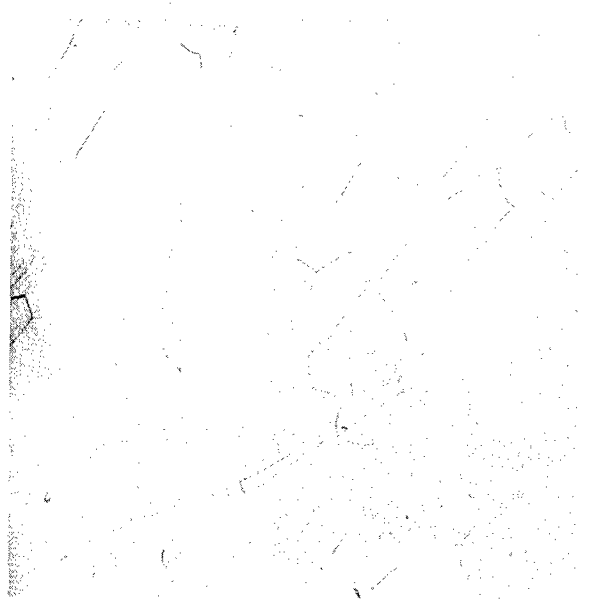
Neg. No. 3616   X75

Fig. 80
A 29% oxygen alloy quenched after 4
hours at 1200°C. Structure shows
polyhedral grains of TiO phase.

Etchant: 60 glycerine, 20 HNO$_3$, 20 HF

is presented to show the fine details of the banded structure at a higher magnification. At higher oxygen contents, the amount of the banded structure decreases, with the last traces of alpha showing up at the grain boundaries. (See Fig. 76.)

The twin-like structure of the α + TiO alloys is very similar to the banded $\alpha + K$ structure in copper-silicon alloys investigated by Smith (29), who advanced a theory of matching crystallographic planes to account for the unusual stability of this structure. Calculations along this line were made from lattice parameter measurements of the titanium-oxygen system.

When a face centered cubic precipitate is rejected from a hexagonal close packed matrix, the information available suggests that the crystallographic relationship is such that the {0001} planes of the matrix, face the {111} planes of the precipitate. Whether this condition actually obtains in the precipitation of TiO from alpha cannot be easily verified, but certainly it is a reasonable assumption. The atomic array in both (0001) and (111) planes follows hexagonal close packing. The interatomic distance in the (0001) plane of the alpha phase at saturation has been measured as 2.955 Å. If one considers the NaCl structure of TiO to be two interlocking face centered cubic structures of titanium atoms and oxygen atoms, the interatomic spacing of the titanium atoms on the (111) planes is 0.707a Å. From the lines of TiO in the phase mixture of α + TiO, the lattice parameter of the TiO was calculated to be 4.176 Å. Accordingly, the interatomic spacing of the titanium atoms on the (111) plane is 2.952 Å. This corresponds very closely to the atomic spacing in the (0001) planes of alpha. The degree of disregistry is about 0.1%. Therefore, it would appear that Smith's explanation for the origin of the stable banded structure is applicable to the case under discussion.

If the above explanation for the formation of the banded structure is accepted (i.e., the precipitation of a face centered cubic phase from a hexagonal close packed solid solution), the phase diagram should show the α/α + TiO boundary curving toward higher oxygen contents and intersecting the peritectic horizontal at a greater oxygen concentration than is obtained at lower temperatures. Actual data points at 1600°, 1700°, and 1750°C do not indicate such curvature of the α/α + TiO boundary; but it is quite possible that the alpha phase could not be retained on quenching from these higher temperatures. Curvature for this boundary has been shown in Fig. 62, because the 15% oxygen alloy had a higher melting point than the 16% alloy.

The phase diagram (Fig. 62) indicates the presence of the hitherto unknown delta phase at approximately 18-20% oxygen below 925°C. Only traces of this precipitate were observed in the 18, 20, and 22% oxygen alloys annealed at 900°C. After annealing at 800°C for 120 hours, the amount of precipitate increased from a trace in the 15% alloy to more than 20% in the 19 and 20% oxygen alloys, and subsequently decreased until no trace was found in the 24% oxygen sample. Treatment for 500 hours at 800°C did not increase the amount of the precipitated phase.

The banded structure appeared to break down with the appearance of the precipitate at 800° and 900°C. Figures 77-79 are presented to show the appearance of the precipitate as revealed in the 18, 20, and 22% oxygen alloys annealed at 800°C.

Figure 80 depicts the single phase TiO structure of a 29% oxygen alloy.

The determination of phase relationships for alloys containing 30-40 weight per cent oxygen was not attempted because most of these alloys were too friable to prepare by metallographic techniques after heat treatment. By extremely careful handling, a series of samples of as-cast alloys from 30 to 40% oxygen were prepared for examination.

A phase mixture of TiO + Ti_2O_3 was observed in the as-cast 31-32% oxygen alloys, while the 33% alloy appeared to be a single phase, corresponding to Ti_2O_3. A mixture of Ti_2O_3 + TiO_2 was revealed in 34-37% oxygen alloys, and the as-cast 38-40% oxygen alloys appeared to be cored single phase structures of TiO_2. These phases and phase ranges confirm, in general, X-ray diffraction studies reported by Ehrlich.

c.   Melting range determinations

Solidus data for this system as determined by incipient melting techniques are shown in Table XIII, and also in Fig. 62, together with melting range data obtained by annealing treatments. These results indicate whether the specimens were completely melted, partially melted, or unmelted. As shown in the diagram, the annealing data are in fairly close agreement with the incipient melting results.

The temperature of the peritectic reaction Melt + $\alpha \rightleftarrows \beta$ was placed between 1730° and 1750°C, because after annealing at 1730°C the 2, 3, and 4% oxygen alloys show an $\alpha + \beta$ structure with no evidence of melting; whereas the treatments at 1750°C gave microstructures showing complete melting, α + partial melting, and unmelted α, respectively, for the same alloys. Similarly, the peritectic temperature of the Melt + $\alpha \rightleftarrows$ TiO reaction was placed at 1770°C as determined by examination of a series of specimens which showed various amounts of melting at 1800°C and did not exhibit melting when treated at 1750°C. Typical peritectic microstructures were not obtained in any of the alloys at either of the indicated peritectics. Between the two peritectics, a maximum melting point of approximately 1900°C at 10% oxygen was obtained for the alpha phase.

The incipient melting temperature for a 25 weight per cent oxygen alloy, corresponding to the theoretical composition TiO, was determined to be 1760°C, which is in very close agreement with a previously reported melting point of 1750°C (30).

TABLE XIII

MELTING TEMPERATURES OF IODIDE TITANIUM-OXYGEN ALLOYS

Weight % Oxygen	Melting Point[*], °C	Weight % Oxygen	Melting Point[*], °C
0	1725	14	1840
2	1750	15	1830
3	1750	16	1780
4	1776	18	1780
6	1822	20	1770
8	1850	22	1765
10	1905	25	1760
11	1875	26	1770
12	1875	27	1740
13	1870	30	1725

[*]Accuracy of determination approximately ±25°C.

d. X-ray diffraction studies

X-ray diffraction studies were undertaken to determine the structure of the intermediate phase TiO and, by means of the parametric method, to check certain points on solubility boundaries as established by metallographic observations.

The patterns were taken in a 14 cm Debye-Scherrer powder camera using filtered CuK_α radiation. The specimens were prepared largely by crushing and screening. Only at low oxygen contents was it necessary to use filing to prepare powdered specimens. Lattice parameters were calculated by solution of simultaneous equations for a number of high angle lines or by the well-known cosine square extrapolation in the case of cubic structures.

(1) Alpha primary solid solution

This phase possesses the hexagonal close packed structure of the low temperature allotropic modification of titanium. The lattice parameters of this structure as a function of oxygen content are presented in Fig. 81. The pronounced increase in the "c" parameter would tend to confirm that this is an interstitial type of solid solution.

In general, there is some deviation from the results of Ehrlich's work, especially at low oxygen contents. The direction of the deviation points to the relative impurity of his titanium metal. From the "c" parameter of the alpha phase in a phase mixture with TiO as quenched below 900°C, the saturation composition of alpha was determined as 34±0.5 atomic per cent (14.5 wt.%) oxygen. This is in exact agreement with that value established by metallographic examination.
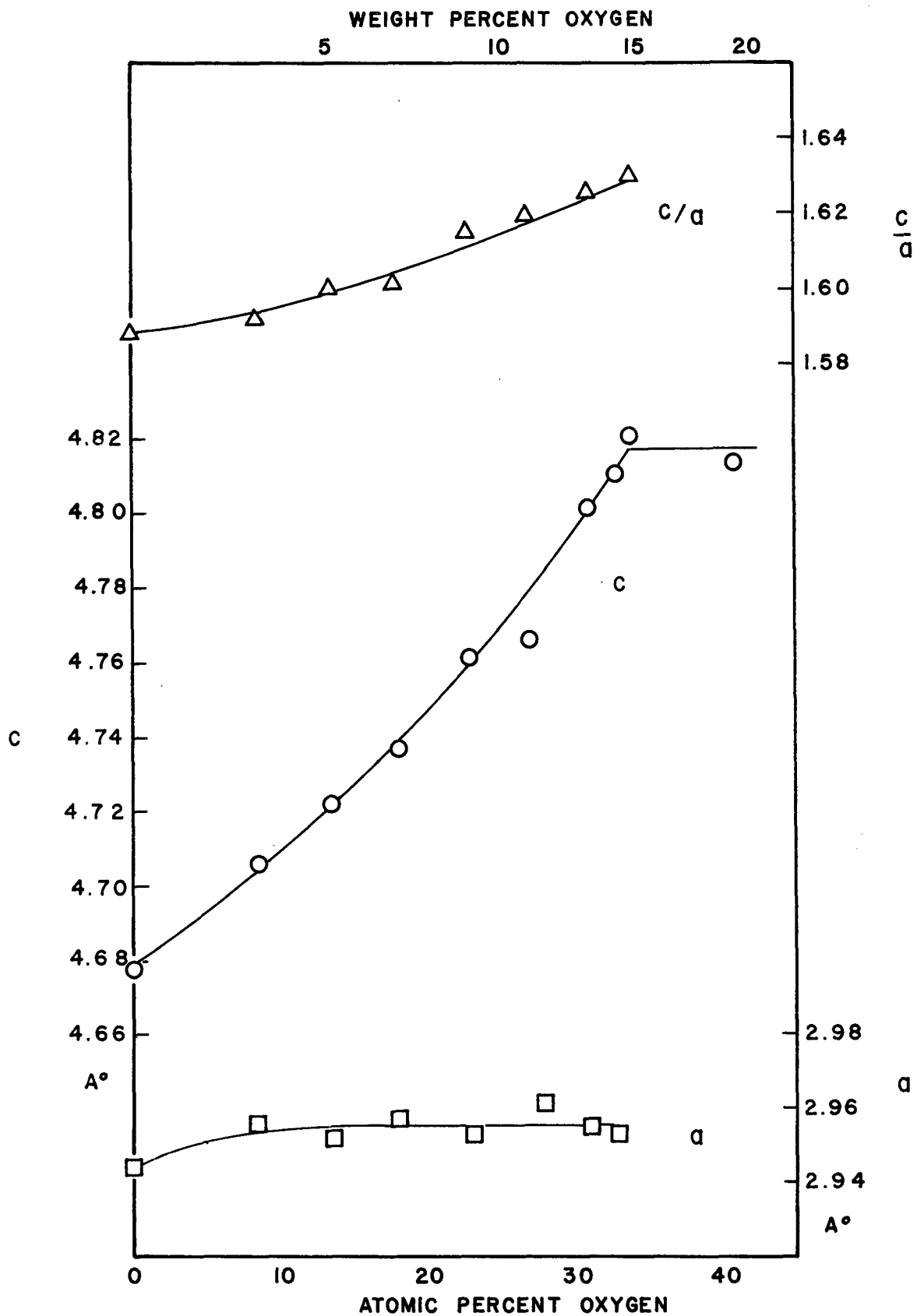
Fig. 81 - Lattice Parameter-Composition Curves for the Alpha
Phase in Titanium-Oxygen Alloys

(2) The intermediate phase TiO

Ehrlich has reported this phase to have a cubic structure of the NaCl type. This was confirmed by the present work. The lattice parameter as a function of oxygen content is shown in Fig. 82. It will be seen that a simple linear relationship occurs. The results are quite close to those reported by Ehrlich. From the pattern of a phase mixture field as quenched from 900°C and containing 40 atomic per cent oxygen, the parameter of the TiO phase was calculated to be 4.180 Å. This sets the saturation composition of TiO on the titanium side for 900°C at 46 ± 0.5 atomic per cent (approximately 23 wt.%). This agrees closely with the metallographic estimate of 23.5 weight per cent.

(3) The intermediate phase between alpha and TiO

On long term annealing of alloys containing between 15 and 23 weight per cent oxygen below 900°C, metallographic examination disclosed the presence of a new phase tentatively named delta. Diffraction patterns of these structures showed a large number of new.faint lines which could not be accounted for by either alpha or TiO. Although the determination of the structure of a new phase is best performed when the phase has been isolated, this was not possible. As an alternative, which can only provide tentative results, the extra lines were examined as a group. It was found possible to index all but one of these lines on a Hull-Davy chart for the tetragonal system. The lattice parameters calculated for this tetragonal lattice are: c = 6.645 Å, a = 5.333 Å, c/a = 1.246. The measure of success in relating calculated to observed spacings is shown in Table XIV. The check is quite close.

e. Hardness determinations

Vickers pyramid hardness data (5 kg load) for alloys with from 0.2 to 30% oxygen are presented graphically in Fig. 83. Two curves are shown, one representing the hardness of as-cast alloys and the other, the hardness of a series of alloys annealed at 1000°C.

The hardness curves show an increase from approximately 170 to 950 and 1200 Vickers in the alpha solid solution range of 0.2-13% oxygen. The impressions in specimens of this range of composition were of uniform shape, despite cracks and chipping due to brittleness, which usually accompanies extremely high hardness. On the other hand, impressions in specimens in the 14-20% oxygen range of composition were surrounded by deformation bands. This evidence of ductility supports the drop in hardness for alloys which microscopically revealed the banded α + TiO phase mixture. From 20 to 30% oxygen, hardness again increases to extremely high values.
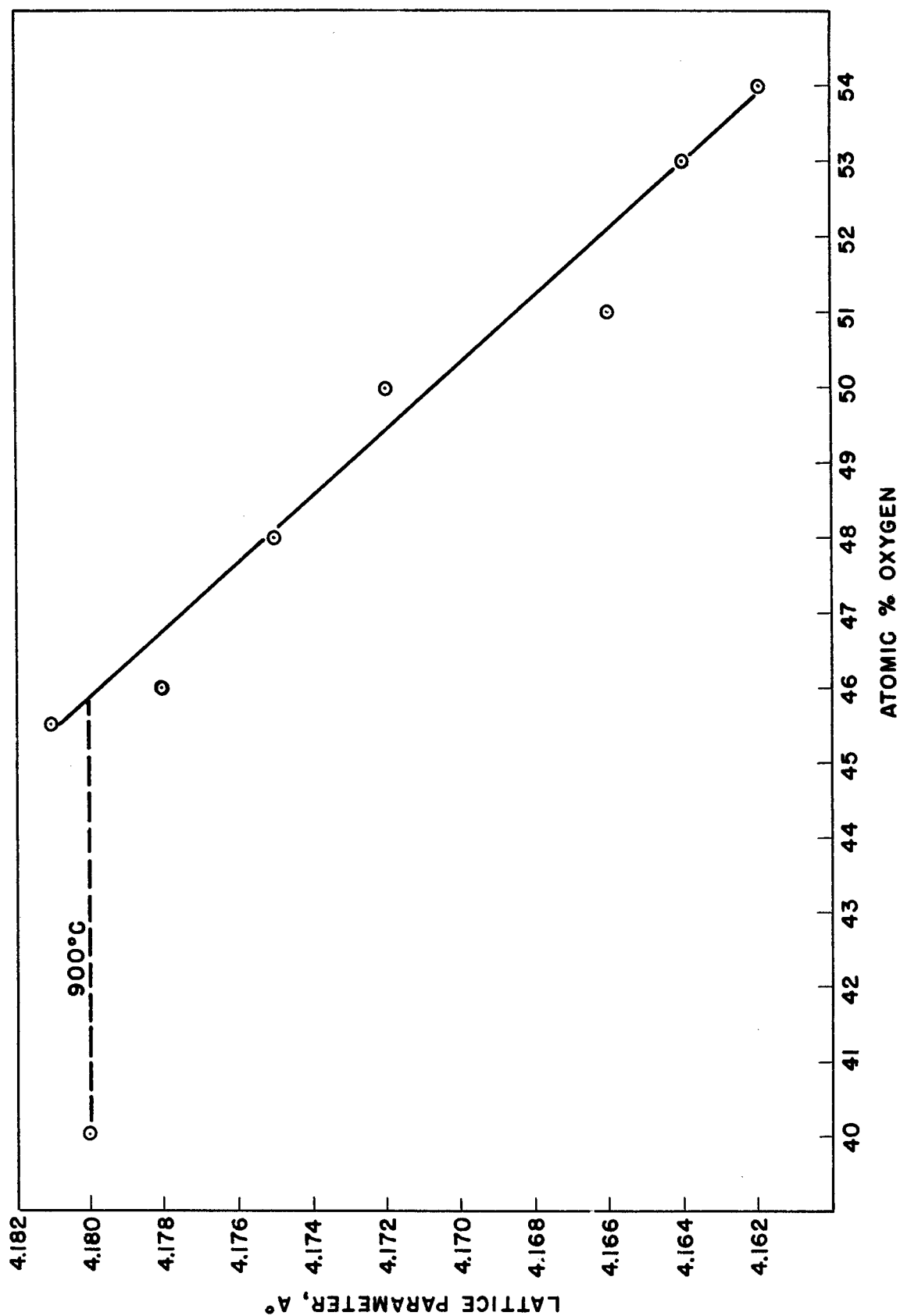
Fig. 82 – Lattice Parameter-Composition Curves for TiO Solid Solution
Titanium-Oxygen Alloys

TABLE XIV

SUMMARY OF OBSERVED AND CALCULATED DATA
ON THE DELTA PHASE

Observed Intensity	hkl	$d_{observed}$	$d_{calculated}$
vw	112	2.474 Å	2.493 Å
vw	120	2.373	2.385
vft	?	2.324	---
vft	202	2.058	2.079
ft	220	1.874	1.885
vvft	221	1.805	1.814
vw	301	1.716	1.717
vvft	004	1.655	1.661
vw	223	1.432	1.435
vw	204	1.414	1.410
vvft	303	1.386	1.386
vvft	105	1.293	1.289
vw	115	1.242	1.253
vvft	304	1.219	1.214
vft	240	1.191	1.193
ft	324	1.102	1.104
ft	502	1.014	1.016
ft	334	0.9999	1.002

vw = very weak
ft = faint
vft = very faint
vvft = very very faint
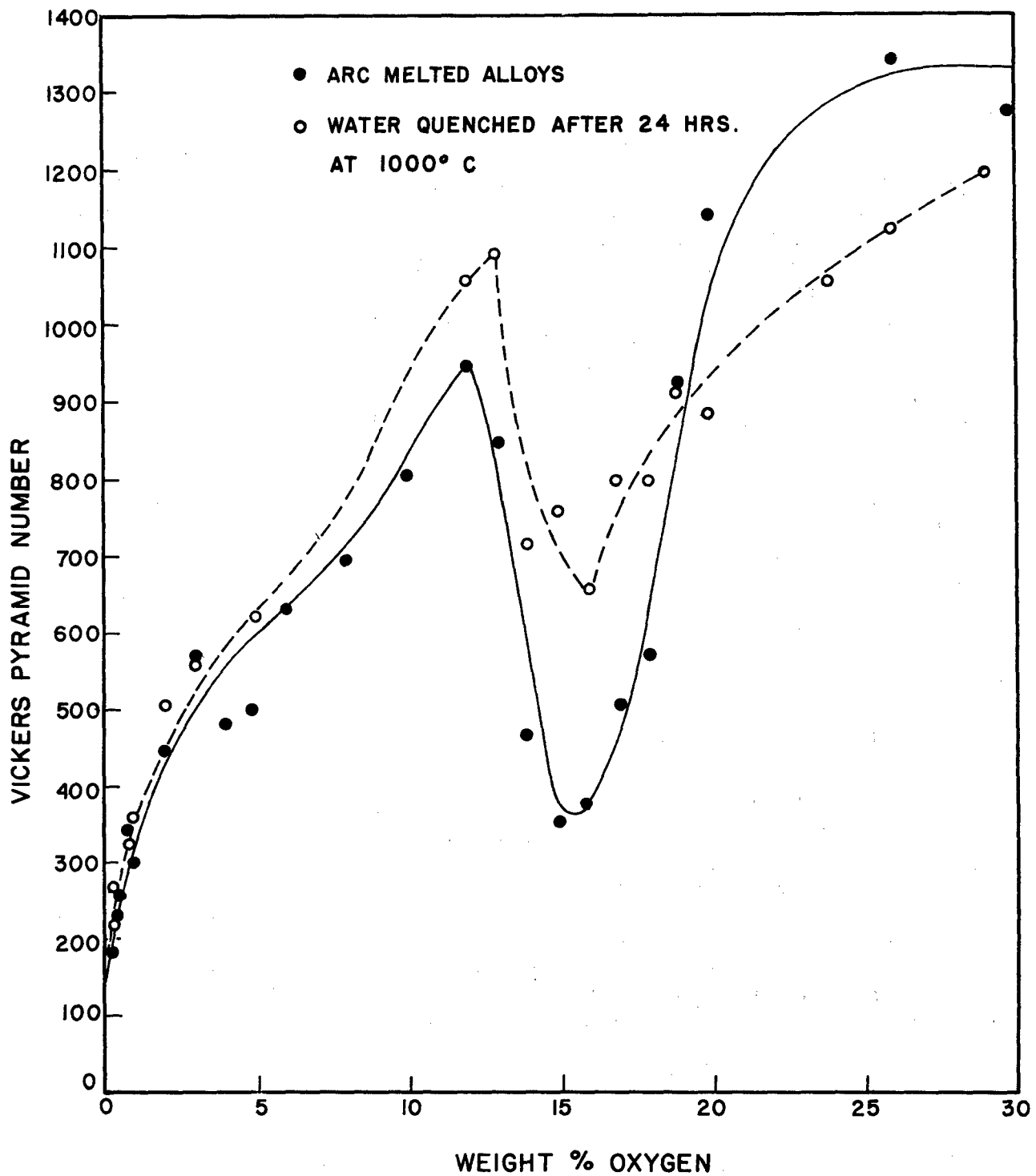
Fig. 83 - Vickers Diamond Pyramid Hardness vs Oxygen Content

IV. SUMMARY OF RESULTS

A. The Titanium-Aluminum System

The principal features of the diagram are as follows: A peritectic reaction, β + melt $\rightleftarrows$ γ, between 34.5 and 38.5% aluminum at approximately 1460°C. A second peritectic reaction, γ + melt $\rightleftarrows$ TiAl$_3$, between 60 and 64% aluminum at 1340°C. A peritectoid reaction, β + γ $\rightleftarrows$ α, between 29 and 34.5% aluminum at approximately 1240°C. The β $\rightleftarrows$ α transformation temperature is raised from 885°C at 0% aluminum to 1240°C at 29% aluminum. A narrow α + β field is indicated. The beta phase transforms to serrated alpha on quenching. The solubility limit of aluminum in alpha titanium is 24.5% at 900°C. The maximum solubility of aluminum in beta titanium is 34.5% at 1460°C. The lattice parameters of the solid solution change considerably with initial additions of aluminum and level off near the solubility limit. X-ray diffraction patterns confirmed the metallographic observation that beta is not retained by rapid quenching. Gamma phase is of variable composition, from 37 to 60% aluminum at the solidus and from 35.5 to about 44.5% aluminum at 800°C. The gamma phase has an ordered face centered tetragonal lattice, with an axial ratio close to unity, and is based on the composition TiAl. Increasing aluminum content increases the axial ratio slightly. The hardness of alpha solid solution alloys increases with the addition of aluminum to titanium. The gamma phase has a minimum hardness at 36% aluminum, which increases with further additions, of aluminum, reaching a maximum at the composition TiAl$_3$.

B. The Titanium-Chromium System

The transformation temperature of titanium (885°C) is lowered with increasing chromium content, resulting in a eutectoid decomposition of beta at 15% chromium and 685°C into alpha, containing less than 0.5% chromium, and the intermediate phase, TiCr$_2$. The beta phase is retained on quenching alloys in which beta contains 7% or more chromium. Beta titanium and chromium are completely mutually soluble at high temperatures, beta decomposing at 1350°C into TiCr$_2$, which exists within a narrow range of composition from about 67 to 68% chromium. The melting temperatures decrease from that of titanium (1720°C) with increasing chromium content, reaching a minimum at 45% chromium and 1380°C.

C. The Titanium-Iron System

The transformation temperature of titanium drops with increasing iron content, resulting in a eutectoid decomposition of beta at 15-16% iron and 585°C into alpha, with less than 0.5% iron, and TiFe. Beta is retained in alloys in which the beta phase contains 4% or more iron. A eutectic exists at 32% iron and 1080°C between beta, having a composition of 25% iron, and TiFe. The intermediate phase, TiFe, occurs at 54% iron and is apparently formed peritectically.

Hardness curves are presented for several groups of annealed and water quenched alloys of both systems, showing the typical results obtained over

the range of compositions investigated.

D.   The Titanium-Chromium-Iron System

The outstanding feature of the titanium-chromium-iron system is the
ternary eutectoid point at approximately 8% chromium and 13% iron at about
540°C. The maximum solubility of iron and chromium in titanium is less
than 1% total alloy content. The change from transformed to retained
beta on water quenching from the beta field occurs along a straight line
joining the similar transition points in the two binary systems. The
ternary system shows the same hardness trends indicated for the two bin-
aries. A peak hardness is obtained at the composition where the transi-
tion occurs from transformed to retained beta. Work on the titanium-
chromium-iron system is not completed, and will be concluded during the
next year's extension of the project.

E.   The Titanium-Oxygen System

The titanium-oxygen phase diagram has the following features: A
peritectic reaction: Melt + $\alpha \rightleftarrows \beta$, between 1 and 5% oxygen, at ap-
proximately 1740°C. A second peritectic reaction: Melt + $\alpha \rightleftarrows$ TiO,
between 14.5 and 20.5% oxygen at approximately 1770°C. A peritectoid
reaction: α + TiO $\rightleftarrows$ δ between 14.5 and 23.5% oxygen at approximately
925°C. The alpha phase exhibits a maximum melting point of approximately
1900°C at about 10% oxygen. The solubility limit of oxygen in alpha
titanium is approximately 14.5% oxygen from 800° to 1700°C. The lattice
parameters of the alpha solid solution increase with increasing oxygen
content. X-ray diffraction patterns for the TiO phase indicate a cubic
structure of the NaCl type, with a linear decrease in parameter constants
with increasing oxygen content. Lattice parameter measurements confirmed
the alpha and TiO solubility limits determined by micrographic methods.
The existence of the newly discovered δ phase was confirmed by X-ray
studies, and the structure was tentatively identified as tetragonal.
The composition range in which the new phase occurs corresponds to the
stoichiometric ratios for either Ti_3O_2 or Ti_4O_3.

A marked increase in hardness was obtained with the addition of
oxygen to titanium. The hardness curve dipped to a minimum for α + TiO
phase mixture alloys and then showed a rapid increase for the TiO solid
solution alloys.

V.   FUTURE WORK

The titanium-chromium-iron partial phase diagram remains to be com-
pleted. The melting range will be determined. A more intensive study
will be made with new alloys and annealing treatments to pin-point the
ternary eutectoid. The phase limits of the β + TiFe + $TiCr_2$ space will
be located using additional alloys and X-ray diffraction techniques.

A study will be made to determine the phase relationships brought about by oxygen additions to the ternary systems. This work was suggested by the discovery of the Ti_3Fe_3O phase, which may in some ways influence the properties of commercial titanium-chromium-iron alloys.

VI. CONTRIBUTING PERSONNEL

The following personnel were the major contributors to the work reported herein:

E. S. Bumps	Titanium-aluminum and titanium-oxygen systems
M. Hansen	Supervisor
C. A. Johnson	Metallography
H. D. Kessler	Project engineer
W. Rostoker	X-ray diffraction analysis
R. J. Van Thyne	Titanium-chromium, titanium-iron, and titanium-chromium-iron systems

VII. LOGBOOKS

Data related to the work are recorded in the following Foundation logbooks: B-2019, B-2020, C-1283, -1284, -1285, -1293, -1294, -1559, -1886.

BIBLIOGRAPHY

1. D. I. Brown, Iron Age 1950, Sept. 14, 85-88.

2. Navy Contract No. NOa(S)8698, 1948; see also E. I. Larsen, E. F. Swazy, L. S. Busch, and R. H. Freyer, Metal Progress 55, 1949, 359.

3. Private communication by P. Duwez (April 23, 1951).

4. M. Hansen, Der Aufbau der Zweistofflegierungen, J. Springer, Berlin, 1936, 158-160.

5. W. L. Fink, K. R. Van Horn and P. M. Budge, Trans. AIME, Inst.Met. Div. 93, 1931, 421-436. Disc. 436-439.

6. G. Brauer, Z.anorg.allg.Chem. 242, 1939, 1-22.

7. K. Schubert, Z.Metallkunde 41, 1950, 420-421.

8. W. Manchot and E. Leber, Z.anorg.allg.Chem. 150, 1926, 26-34.

9. R. Vogel and B. Wenderott, Arch.f.Eisenhüttenwesen 14, 1940, 279.

10. C. M. Craighead, O. W. Simmons, and L. W. Eastwood, Trans.AIME 188, 1950, 498-499.

11. D. J. McPherson and M. G. Fontana, Trans.ASM 43, 1951, 1098-1125.

12. M. K. McQuillan, J.Inst.Metals 79, 1951, 379-390.

13. P. Duwez and J. L. Taylor, ASM Preprint No. 3, 1951.

14. F. Laves and H. J. Wallbaum, Die Naturwissenschaften 27, 1939, 674-675.

15. H. J. Wallbaum, Arch.f.Eisenhüttenwesen 14, 1941, 521-526.

16. A. D. McQuillan, J.Inst.Metals 79, 1951, 73-88.

17. H. W. Worner, J.Inst.Metals 79, 1951, 173-188.

18. P. Duwez and J. L. Taylor, Trans.AIME 188, 1950, 1173-1176.

19. N. Karlsson, J.Inst.Metals 79, 1951, 391-405.

20. C. W. Carstens, Z.Kristallographie 67, 1928, 260.

21. P. Ehrlich, Z.Elektrochemie 45, 1939, 362-372.

22. P. Ehrlich, Z.anorg.allg.Chem. 247, 1941, 53-64.

23. P. Ehrlich, Z.anorg.allg.Chem. 259, 1949, 1-41.

24. R. I. Jaffee, H. R. Ogden, and D. J. Maykuth, Trans. AIME 188, 1950, 1261-1266.

25. R. I. Jaffee and I. E. Campbell, Trans. AIME 185, 1949, 646-654. Also J.Metals (Sept. 1949) T.P. 2681.

26. D. A. Sutcliffe, Royal Aircraft Establishment RAE Technical Note No. MET 141.

27. H. W. Worner, Australian Engineer 152, Nov. 1950.

28. A. E. Jenkins and H. W. Worner, J.Inst.Metals 80, 1951, 157-166(Dec.).

29. C. S. Smith, Trans. AIME 137, 1940, 313-333.

30. J. W. Hickman and E. A. Gulbransen, Anal.Chem. 20, 1948, 158-165.

APPENDIX I

A THEORETICAL ANALYSIS OF THE STRUCTURE OF TiO

by W. Rostoker

From density measurements, Ehrlich (1) has shown that the large range of miscibility may be interpreted in terms of titanium and oxygen vacant sites, respectively, on the high and low oxygen sides of the TiO composition. However, Ehrlich considered this phase to possess an ionic type of bonding and the vacant site phenomenon required the postulate of mixtures of mono- and divalent and of di- and trivalent titanium. Consideration of certain factors seems to indicate that the NaCl structure exhibited derives from factors other than ionic bonding.

From Pauling's (2) data, the diameter of the O^{--} ion is 2.80 Å. The diameter of the divalent titanium atom may be calculated from the expression (2)

$$D_{Ti}2+ = D_{Ti}4+ \cdot \frac{2^{-1/4}}{4^{-1/4}} = 3.45 \text{ Å}$$

The assumption has been made here that titanium in the pure state or in primary solid solutions is a tetravalent metal. Support has been found for this (3) from a consideration of the Brillouin Zone and lattice parameters of the alpha primary solid solution in the titanium-aluminum system. A calculation of the lattice parameter of the TiO phase, assuming ionic bonding, yields the value 6.25 Å, which is considerably in excess of that observed. On the other hand, using the diameter of tetravalent titanium and of the oxygen atom which can be derived from the alpha phase lattice parameters gives a value of 4.21 Å, which is very close to that observed.

As a further check on the hypothesis that the TiO phase has metallic bonding, a measurement was made of electrical resistivity. This measurement was made on a cast button of variable dimensions so that the results are likely to be in error on the high side by a factor of as much as two. The resistivity obtained was in the order of 3000 microhm-cm, which definitely excludes the possibility of either covalent or ionic bonding.

The magnitude of resistivity suggests a "full" Brillouin zone condition (in the sense of preceding an overlap). Because of the low scattering power of oxygen, the TiO structure may be considered as a face centered cubic lattice of titanium atoms. According to Raynor et al. (4), the second Brillouin zone for a face centered cubic structure can contain, on a volumetric estimate, four electrons per atom. An inscribed sphere corresponds to 2.49 electrons per atom but, as Raynor points out, the Fermi distribution within the second zone would be expected to be far from spherical. Accordingly, we may expect the full second zone

(electronic concentration prior to overlap) to contain 2.49-4 electrons per atom. From the deduction that the TiO structure is not ionic, it must be concluded that oxygen is a donor, rather than an acceptor, of electrons. Under these circumstances, the electron to atom ratio must reasonably lie between 2.5 and 4, assuming oxygen to yield 1-4 electrons, respectively.

Bibliography

1. P. Ehrlich, Z.anorg.allg.Chemie 247, 1941, 53.
    P. Ehrlich, Z.Elektrochemie, 45, 1939, 362.

2. L. Pauling, The Nature of the Chemical Bond, Cornell University Press.

3. W. Rostoker, Technical Note submitted to AIME.

4. R. L. Berry, M. B. Waldron and G. V. Raynor, Research 2, 1949, 195.